Constrained Connected Automated Vehicle Trajectory Planning: A Spatial Dynamics Perspective

by

Ran Yi

A dissertation submitted in partial fulfillment of

the requirements for the degree of

Doctor of Philosophy

(Civil and Environmental Engineering)

at the

University OF WISCONSIN-MADISON

2024

Date of final defense: 04/30/2024

The dissertation is approved by the following members of the Final Oral Committee:

Prof. Bin Ran, Advisor, Civil and Environmental Engineering, UW-Madison
Prof. David A. Noyce, Civil and Environmental Engineering, UW-Madison
Prof. Peter J. Jin, Civil & Environmental Engineering, Rutgers University
Prof. Sikai Chen, Civil and Environmental Engineering, UW-Madison
Prof. Xin Wang, Industrial and Systems Engineering, UW-Madison

ACKNOWLEDGEMENTS

Pursuing a Ph.D. has been a challenging yet unforgettable journey. I wish to express my deepest appreciation to the University of Wisconsin-Madison and the Department of Civil and Environmental Engineering for fostering an environment of academic growth and research excellence. The guidance, encouragement, and resources provided by the esteemed faculty, staff, and colleagues have been instrumental in the successful completion of this dissertation.

I am profoundly grateful to my advisor, Professor Bin Ran, for your unwavering guidance, support, and mentorship throughout my Ph.D. journey at the University of Wisconsin-Madison. Your extensive knowledge, passion for research, and commitment to academic excellence have continually inspired and motivated me. You have also been pivotal in helping me develop leadership, teamwork, and critical thinking skills. I deeply cherish the invaluable support you have provided throughout my Ph.D. journey.

My sincere thanks go to Professor Yang Zhou. Your selfless and patient guidance on my research has been critical to my academic and future career success. Completing this dissertation would not have been possible without your support. As a friend and mentor, you have taught me so much, and I am truly grateful for your encouragement during my Ph.D. journey. I would also like to extend my gratitude to my other dissertation committee members—Professor David Noyce, Professor Peter Jin, Professor Sikai Chen, and Professor Xin Wang—for their insightful advice that has greatly contributed to my growth. Additionally, I wish to thank Dr. Steven Parker for providing me with invaluable project experiences in the TOPS Lab, and Dr. Yang Cheng for his support within Professor Ran's group.

I appreciate the camaraderie and support from my lab mates: Dr. Shen Li, Dr. Zhen Zhang, Dr. Fan Ding, Dr. Xiaotian Chen, Dr. Xiaotian Li, Dr. Tianyi Chen, Dr. Shuoxuan Dong, Dr. Kunsong Shi, Dr. Haotian Shi, Dr. Keshu Wu, Dr. Yangxin Lin, Dr. Yuan Zheng, Yifan Yao, Sicheng Fu, Jingwen Zhu, Xiaodan Zhang, Han Cao, Sixu Li, Kexin Tian, and Junwei You. Your friendship has been invaluable.

Lastly, I would like to express my deepest gratitude to my parents. Thank you for your unwavering support and for believing in me, even when I doubted myself. I am eternally grateful for the love and guidance you have provided me throughout my life.

TABLE OF CONTENTS

LIST OF FIGURES

LIST OF TABLES

ABSTRACT

This dissertation introduces a comprehensive trajectory optimization method for connected automated vehicles (CAVs) operating on curved roads, augmented by infrastructure support. We offer detailed strategies for car-following and lane-changing, crafted specifically for intricate road structures. Specifically, this paper systematically formulates trajectory optimization in a spatial domain and on a curvilinear coordinate. This unique approach allows for a dynamic formulation that can adeptly accommodate spatially diverse road geometries, traffic regulations, road obstacles, and the dynamics of leading vehicles. The acquisition of this intricate data is facilitated through both vehicle-to-infrastructure (V2I) and vehicle-to-vehicle (V2V) communication channels. Our proposed strategies – encompassing trajectory optimization, car-following, and lane-changing – are underpinned by three foundational segments: i) An initial mathematical validation, confirming the controllability of our system and thereby ensuring its operational feasibility; ii) The employment of a multi-objective model predictive control (MPC) framework, devised to refine trajectories in a rolling horizon manner. This setup guarantees simultaneous adherence to collision avoidance, traffic regulations, and vehicular kinematic constraints; iii) To corroborate the efficacy of our approach, we undertook numerical simulations across a spectrum of scenarios. The derived results indicate that our method is adept at sculpting smooth vehicular trajectories, adeptly navigating around obstacles, and consistently complying with traffic regulations across varying circumstances. Notably, the method exhibits resilience against variations in road geometries and other potential disruptions. In essence, this paper presents a holistic solution for CAVs maneuvering on complex road topographies, ensuring safety, compliance, and efficiency in their operations.

KEYWORDS

Car-following, Connected Automated Vehicles, Mandatory Lane-changing, Model Predictive Control, Spatial Domain, Trajectory Optimization

1. INTRODUCTION

Advanced sensing and communication technologies integrated into vehicular and infrastructure systems have been experienced a fast development in very recent years (Cao et al., 2021; Wang et al., 2020a; Wang et al., 2020b). Automated vehicles (AVs) with advanced sensing technology provide the ability for the vehicle to take over its driving task from the human driver, which will eliminate all human errors and enable efficient microscopic control. Meanwhile, connected vehicles (CVs) incorporate communication technologies, such as V2V and V2I communication, to share information with each other. Although data privacy and security concerns may prevent AV and CV users from sharing data, Shi et al. (2021) showed that AV acceptability can be granted by providing a ride experience to people who are hesitant about AVs, and Acharya & Mekker (2022) showed that CV acceptability is affected by the reputation of the data manager. Through the integration of the advantages of both AV and CV technologies, CAVs are able to complete auto-driving tasks with a broader range of precise environment and vehicle dynamic information, which will assist them in obtaining current and future road situations, particularly the provision of information on previously unseen hazards in advance.

1.1 Background

Over the last decade, a large portion of all traffic accidents have been caused by inattention or fatigue of the driver. About 15 percent of all traffic accidents occurred due to unintended lane departure in German over the last 10 years, and 35 percent of those have been fatal (Pohl et al., 2007). In order to prevent these unintended lane departure types of accidents, many researches on LKAS or lane departure avoidance systems (LDAS) for human-driven vehicles has been performed, which tended to focus on the control algorithm considering the interaction of the human driver (Pilutti & Ulsoy, 1999; Raksincharoensak et al., 2008; Risack et al., 2000). The lane-keeping control without human driver

manipulation was less studied. Moreover, complex highway environments and unpredictable traffic conditions have set up higher requirements on accuracy and response time for CAVs to increase transportation safety and efficiency. Therefore, research on the management and avoidance of this problem has been carried out since the development of freeway roads.

Traffic oscillations, commonly referred to as "stop-and-go" driving in congested scenarios, represent a peculiar traffic phenomenon. In these situations, vehicles on highways continuously cycle between acceleration and deceleration rather than maintaining a consistent speed. This cyclic movement pattern can lead to a host of challenges related to highway traffic efficiency and sustainability, such as prolonged delays, potential safety hazards, driver discomfort, and increased fuel consumption. Given its significance and intricate nature, traffic oscillations have been the subject of extensive research. Both empirical observations and theoretical models have been employed to better understand the phenomenon. A considerable volume of literature posits that the genesis and spread of these oscillations largely stem from car-following behavior (Chen et al., 2014; Laval & Leclercq, 2010). This behavior pertains to a driver's reactions to the movements of the vehicle ahead based on their observations and perceptions. Equipped with insights into the formation and progression of traffic oscillations, several traffic control and management strategies have been devised to temper this phenomenon and mitigate its ramifications. Some notable methodologies, such as traffic policies and variable speed limit (VSL) control (Carlson et al., 2010a; Carlson et al., 2010b; Han & Ahn, 2018), aim to control and manage traffic on a macro scale, providing broader solutions to alleviate the challenges posed by these oscillations.

Over the past decade, there has been a marked progression in CAV technology. These advancements seamlessly meld connectivity with automation. As a result, CAVs are not only equipped to autonomously navigate using onboard systems but also have the ability to communicate inter-vehicularly through V2V interfaces or relay information to infrastructure elements via V2I channels. A particularly innovative application harnessed in CAVs is the Cooperative Adaptive Cruise Control (CACC). This technology elevates the traditional adaptive cruise control by introducing cooperative

vehicular maneuvers. Through communication mediums like Dedicated Short-Range Communications (DSRC), LTE, and 5G, CACC facilitates the exchange of essential vehicle data—acceleration, speed, and position, among others. The adoption of CACC brings several significant advantages for CAVs: 1) enhanced driving safety owing to reduced actuation times. 2) increased roadway capacity due to decreased headways between vehicles. 3) diminished energy consumption and environmental pollution as a result of fewer unnecessary speed fluctuations, as highlighted by (Zhou et al., 2017a). Over time, CACC technology has been explored, refined, and implemented across varied traffic contexts. A notable application is its role in streamlining cooperative merging of CAVs, especially in on-ramp scenarios. The innovative concept of employing a 'virtual vehicle' within the CACC system for on-ramp merging was broached by Lu et al. (2004). Their proposition involved preemptively positioning a virtual vehicle on the primary road prior to the actual merge. Elements of this pioneering concept have influenced aspects of our research, details of which will be elaborated upon in subsequent chapters.

In addition to the advancements made through V2V communication-based technologies, there's a burgeoning interest in harnessing infrastructure-centric solutions, notably through I2V communication. A standout example of an automated driving system utilizing this approach is the Connected and Automated Vehicle Highway (CAVH) (Ding et al., 2019). The CAVH system is a dual-layered construct, encompassing both the CAV subsystem and the Connected and Automated Highway (CAH) subsystem. The latter, as its name suggests, brings "intelligence" to the roadways by embedding Road Intelligent Units (RIUs). These units are armed with capabilities spanning sensing, predicting, decision-making, and controlling. With these RIUs in place, the CAH subsystem becomes an active participant in the transportation landscape. The synthesis of CAV and CAH within the CAVH system promises remarkable improvements across the board. This includes enhanced transportation efficiency, bolstered traffic safety, and optimized energy utilization. Delving into specifics, in an on-ramp context, the CAH subsystem actively dispatches data—covering road geometry, vehicle specifics, and control directives—to CAVs within its communication purview. What's noteworthy is that these stationary RIUs, strategically positioned along the roadways, act as computational relief for the CAVs. By

offloading certain tasks to these units, CAVs can focus on core functionalities. Furthermore, the presence of these RIUs elevates the stability and reliability of the overarching system, making it less susceptible to lapses or failures. In essence, such forward-thinking technologies pave the way for a new era of transportation, fostering a conducive environment for the development and deployment of intricate microscopic control algorithms.

1.2 Problem Statement

With the above discussion, the following issues and questions appear as part of the problem formulation:

- How to design a spatially formulated constrained CAV trajectory optimization strategy in a curvilinear coordinate?
- How to design a dynamic two-dimensional (2D) spatially formulated constrained CAV car-following algorithm in a curvilinear coordinate?
- How to combine the spatially formulated constrained CAV trajectory optimization strategy with a dynamic CAV car-following strategy?
- How to combine platoons within different lanes and form a new platoon when a mandatory lane-changing is required?

1.3 Research Objectives

- Design a CAV trajectory optimization strategy that can significantly simplify the formulation compared with ones formulated in the time domain and Cartesian coordinates.
- Design a CAV trajectory optimization strategy that can quickly converge to the desired vehicle operation state (e.g., target speed, following lane centerline) and robust to the spatial disturbances (e.g., lane curvature change) by the infrastructure communication and assistance.
- Provide a multi-objective optimization (e.g., smoothness of vehicle control, less deviation from the desired state) framework which explicitly incorporates the spatial characteristics (e.g., lane curvature) and constraints (e.g., speed limit, obstacles, and lane width) while avoiding obstacles.
- Fill the gap of no 2D CAV car-following in the literature by generating a state space combining

car-following and vehicle trajectory optimization.

- Design a CAV car-following strategy that can quickly converge to the desired car-following state with optimized vehicle trajectory by communicating with the infrastructure and the leading vehicle.
- Design a CAV car-following strategy that can maneuver a quick and smooth platooning obstacle avoidance without lane change.
- Design a spatially formulated mandatory lane-changing algorithm for CAVs using the curvilinear coordinate system and integrates lane-changing and car-following concerns.
- Design a spatially formulated mandatory lane-changing algorithm for CAVs integrating lane-changing and car-following concerns.

1.4 Scope and Assumption

In this study, we present an illustrative example underscoring the significance of trajectory planning, car-following, and lane-changing strategies. When a platoon of CAVs navigates a challenging traffic environment, such as a winding two-lane highway segment with right-hand traffic. This scenario, depicted in **FIG. 1-1**, features a potential obstacle and an outer lane that eventually merges into an inner lane which is denoted as the target lane. The expectation is for CAVs, especially those in the outer lane, to execute a lane-changing maneuver well before the outer lane concludes. To facilitate this, several strategies come into play. The lead CAV requires a trajectory optimization strategy ensuring both lane adherence and obstacle avoidance. Subsequent CAVs must implement a robust car-following strategy to maintain the platoon formation. Moreover, those positioned in the outer lane necessitate a prescriptive lane-changing approach to seamlessly and safely transition to the target lane prior to the outer lane's end. While a myriad of potential paths exist for these CAVs, the decision-making window is tight. It is assumed that all CAVs can collect sensing data from not only their sensors but also road attributes (road geometry, traffic control devices) communicated with roadside units through V2I communication (Ran et al., 2020) and other vehicles' dynamics, like speed and acceleration, through V2V communication, by which CAVs know exact traffic environment information in advance. The chief aim of our trajectory planning algorithm is to rapidly discern the optimal path among a plethora of choices. This optimal path

hinges on its leading CAV's trajectory and is designed to meet criteria concerning safety, efficiency, comfort, and adherence to traffic regulations. Once this optimal trajectory is determined by the leading CAV, it transmits its vehicular dynamics and control parameters to the following CAVs through V2V communication. This data then informs the car-following and lane-changing algorithms of the subsequent vehicles. It's imperative to note that our design framework is tailored exclusively for environments populated by CAVs and operating under CAVH systems.

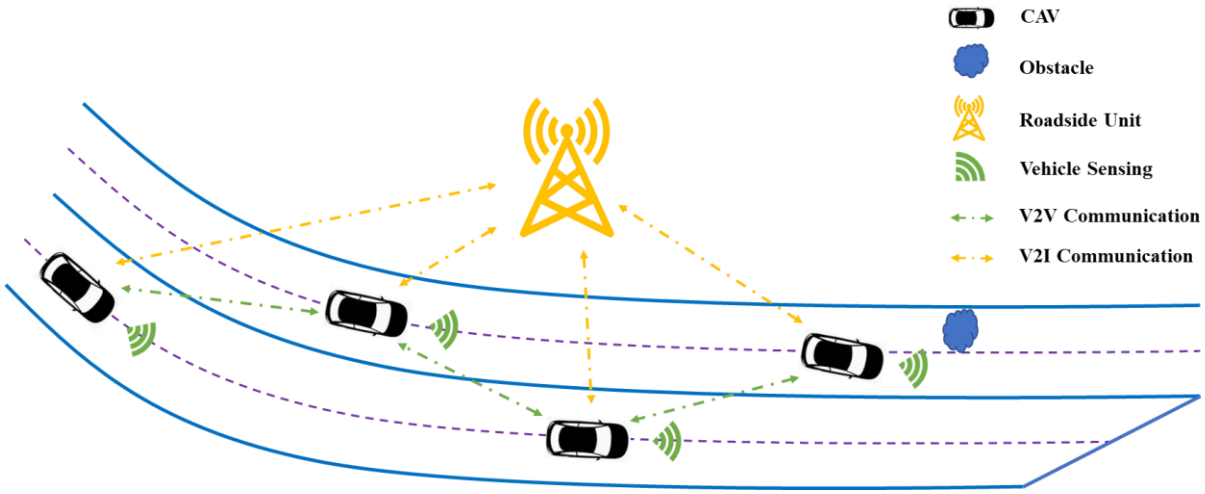

FIG. 1-1. Schematic Diagram of the Proposed Methods.

Ahead of detailed modeling, the following assumptions have been adopted:

- The infrastructure has “intelligence” (Ding et al., 2019) that can sense both vehicle information and road geometrics information.
- The vehicles are treated as points.
- The CAVs are fully automated, which (International, 2014) means the vehicle can control by themselves. Furthermore, they can communicate with each other and with infrastructure.
- All vehicle dynamics effects such as suspension movement, road inclination, and aerodynamic forces are negligible.
- All actuation and communication delays from other sensors through V2V and/or V2I communication are negligible due to the increasing maturity of 5G communication technologies (Akpakwu et al., 2017).

- The geometric features of roads (e.g., road curvature), traffic regulations (e.g., speed limit), obstacle shapes (e.g., lane boundaries), and vehicular data can be sensed in real-time by the infrastructure and leading CAV and transmitted to the following CAVs.

Note that our algorithm can be treated as an upper-level controller in a hierarchical framework, and the ignored factors are typically handled by lower level controllers, such as the controller proposed by Zhou & Ahn (2019).

1.5 Dissertation Organization

The rest of this paper is organized as follows. **Chapter 2** introduces the relevant studies of CAV. **Chapter 3** describes the vehicle trajectory optimization system by a state space and proves the controllability of our system. Based on that, we formulate a detailed MPC formulation and solve it using quadratic programming. **Chapter 4** provides numerical simulation experiments to show the practicality and effectiveness of our vehicle trajectory optimization algorithm. **Chapter 5** describes the CAV car-following system by a state space and proves the controllability of our system. Based on that, we formulate a detailed MPC formulation and solve it using the quadratic programming method. **Chapter 6** provides numerical simulation to show the practicality and effectiveness of our car-following algorithm. **Chapter 7** delves into the intricacies of the CAV lane-changing system by introducing the concept of 'virtual sequencing'. Building on this foundation, we formulate a mixed-integer programming based MPC, which is further enriched by incorporating a bi-directional communication topology, ensuring a holistic and interconnected design strategy. **Chapter 8** provides numerical simulation to show the practicality and effectiveness of our lane-changing and car-following algorithm. Last, we give the conclusion and point out future works in **Chapter 9**.

2. LITERATURE REVIEW

This chapter presents a literature review on research related to traditional CAV trajectory planning, car-following and lane-changing strategy.

2.1 CAVs Trajectory Planning Strategy

Due to the importance, CAVs trajectory planning algorithms have been widely researched in recent years (Bohren et al., 2008; Frazzoli et al., 2002; Gritschnede et al., 2018; Guo et al., 2018; Gutjahr et al., 2016; Manzinger et al., 2020; Mensing et al., 2011; Plessen, 2017; Werling et al., 2010). The state of art of CAV trajectory planning algorithms can be generally divided into four different approaches: (i) the graph search based approach (Bohren et al., 2008; Kala & Warwick, 2013); (ii) the interpolating curve planner (Fraichard & Scheuer, 2004; Labakhua et al., 2008; Reeds & Shepp, 1990); (iii) the sampling based approach (Karaman et al., 2011; Kuwata et al., 2009); and (iv) the function optimization approach (Cremean et al., 2006; Kogan & Murray, 2006). The graph search based approach divides the feasible vehicle travel region into multiple grids, and by that, finding the optimal trajectory can be equivalently treated as finding the shortest path among nodes of feasible grids. By the shortest path formulation, this type of approach (Wu et al., 2020a; Wu et al., 2020b) usually applied dynamic programming and A-star algorithm. By the nature of the shortest path problem, this type of approach can be slow depending on the number of lattices, and the resulting path may not continuous when the size of the grid is big. On the other hand, the interpolating curve planner, which uses predefined curve functions to generate reference points from the available space (Berglund et al., 2009; Labakhua et al., 2008; Pérez et al., 2013), is comparatively computational less expensive. The above-mentioned approaches largely ignore vehicle kinematics by assuming the physical positions are attainable regardless of vehicle speed and steering angle. The sampling based approach executes a random search over the vehicle feasible state space (e.g., position, speed, and acceleration) and finds an optimal sequence of state heuristically by comparing these randomly sampled state spaces according to a predefined objective function (e.g., minimize travel delay and intensive acceleration or brake). Though

effective, these approaches usually render suboptimal solutions suggested by (Elbanhawi & Simic, 2014) due to the searching heuristics nature. As an opposite, the function optimization approach formulates the trajectory planning of CAV as a constrained optimization problem that is flexible in handling constraints from the environment (Gritschneder et al., 2018; Guo et al., 2018; Heilmeier et al., 2019; Nolte et al., 2017), which can minimize a multi-objective cost function meanwhile satisfying the vehicle dynamics and hazard avoidances constraints. Further, the constrained optimization approach is usually implemented in a rolling horizon fashion to be against unexpected disturbances, and it is also known as MPC in the control theory field, which is widely applied in CAV car-following control (Gong et al., 2016; J. Wang et al., 2019; Zheng et al., 2016).

Though promising, the constrained optimization based CAVs trajectory planning still faces some challenges. One challenge is to describe the road geometries in the formulation explicitly. Differed in the utilized coordinates, they can be further categorized as (i) CAV trajectory constrained optimization on a Cartesian coordinate (Gritschneder et al., 2018; Guo et al., 2018; Heilmeier et al., 2019; Nolte et al., 2017) and (ii) CAV trajectory constrained optimization on a curvilinear coordinate (Barfoot & Clark, 2004; Khalifa et al., 2019; Manzinger et al., 2020; Plessen, 2017). As a most widely applied coordinate, the Cartesian coordinate is more suited to describe open spaces. However, road geometry is usually composed of complex and composite curves, which means using Cartesian coordinates will be technically challenging to formulate the road boundaries as constraints. On the other hand, the curvilinear coordinate system is born to describe geometries formed by curved lines (Héry et al., 2017). Especially for the road geometry description, one axle of the curvilinear coordinate can be the lane centerline, while the other axle can be perpendicular to the centerline tangent. By that, the road geometry and boundaries can be simply formulated, reducing a great formulation and computation complexity.

Nevertheless, most of the vehicle trajectory optimization in the literature is vastly built by a temporal formulation (Guo et al., 2018; Gutjahr et al., 2016; Manzinger et al., 2020; Mensing et al., 2011; Plessen, 2017; Werling et al., 2010), assuming that the road geometry characteristics (e.g., curvature, lane tangent directions) remain unchanged over time, have not fully exploited the potentials of the

curvilinear coordinate. The road geometries characteristics, traffic regulations (e.g., speed limit), and hazards are spatially varying rather than temporally varying, which serve as an unobservable exogenous disturbance impacting the performances further exert a negative impact on the desired planning objectives. Though the real-time information of road attributes can be conveyed to CAVs via V2I, with the increasing maturity of the V2I communication, explicitly incorporating these spatially varying characteristics in the temporal domain is still forbiddingly hard. However, the very recent works by Zhang et al., (2020) and Zhao et al., (2020), which utilize the spatial formulation for one-dimensional (1D) CAV car-following control and curvilinear coordinate based human-driven vehicles modeling in an intersection, respectively, provide a new angle to formulate the trajectory planning problems in a spatial domain. Inspired by their works, we found that the spatial domain formulation can explicitly incorporate the optimal formulation of spatially varying attributes on a curvilinear coordinate. Hence, an infrastructure-assisted spatially constrained optimal CAV trajectory planning algorithm based on a curvilinear coordinate is provided in this paper.

2.2 CAV Car-following Strategy

Among numerous algorithms comprising CAV technologies, the CAV car-following algorithm is a critical component that enhances control and traffic flow efficiency and decreases fuel consumption (e.g., Lu & Liu, 2021; Wei et al., 2019; Zeng et al., 2022). Due to its potential and significance, a vast number of notable CAV car-following control algorithms have been developed to increase the traffic flow's efficiency and stability. Despite the fact that numerous CAV car-following algorithms have been developed, the vast majority of the CAV car-following algorithms in the literature only apply to 1D CAV control, which prohibits their wide applications. In the urban environment or local street, incidents that can be detected by incident detection technology (e.g., Karim & Adeli, 2003) and the spatially varying road geometries can easily create bottlenecks for vehicle operation. Therefore, in the era of CAVs, the application of CAVs is not limited to an idealistic straight line, but the lateral vehicle dynamics are also essential to be considered (e.g., Attia et al., 2014). Moreover, the work zone area formed by the construction work in freeways or urban highways can affect the highway capacity and

lead to traffic delays and queueing problem (e.g., Jiang & Adeli, 2003, Jiang & Adeli, 2004a, Jiang & Adeli, 2004b). Even though literature has developed some algorithms to predict work zone areas (e.g., Adeli & Ghosh-Dastidar, 2004; Hooshdar & Adeli, 2004; Karim & Adeli, 2003) or applied lane change during congested areas (Li et al., 2021), how to cooperatively pass a narrowed lane as a CAV platoon is not researched. A cooperation CAV car-following control algorithm for such a complex scenario is needed to increase the automation level and CAV applicability.

The work related to the cooperative 2D CAV car-following control can be categorized into CAV car-following algorithms and 2D trajectory optimization. The state-of-the-art CAV car-following algorithms usually focus on 1D control, which can be generally classified into three streams: (i) state feedback control of a linear or nonlinear system (Morbidi et al., 2013; Zhang & Orosz, 2016; Zhang & Orosz, 2017), (ii) constrained optimization control (Hoogendoorn et al., 2012; Wang et al., 2014a; Wang et al., 2014b; Yang et al., 2017b) and (iii) deep reinforcement learning (DRL) approach (Qu et al., 2020; Shi et al., 2020). These three streams have advantages as well as disadvantages concerning constraint handling, trajectory forecasting, and stability assessment. For linear state feedback control or those reduced from simple nonlinear systems, while the string stability property can be mathematically proved, collision-free constraints imposed by reasonable vehicle dynamic limits and the environment cannot be explicitly incorporated. Additionally, it is not only challenging to create a multiple objective optimization scheme but also difficult to improve platooning control performance by incorporating the leading vehicle's predicted trajectory. In comparison, the constrained optimization control method, also referred to as MPC, is typically operative with a shifting horizon and is effective at dealing with exogenous uncertainties (e.g., work zones). The MPC method is adaptable to constraints imposed by the vehicle's physical limits (e.g., maximum steering angle and maximum acceleration/deceleration) and the environment (e.g., speed limit and lane boundaries), minimizing a cost function while satisfying multiple vehicle performance criteria (e.g., safety, comfort, and fuel consumption, etc.) in order to improve control performance. Additionally, the MPC approach can be classified as distributed MPC (Wang et al., 2015), consisting of only two vehicles in a platoon, or centralized MPC (Chen et al., 2018;

Zhou et al., 2017b), which involves all vehicles in a platoon. The distributed MPC has lower computational requirements than the central MPC, which makes it more practical. In contrast, the centralized control system increases the computational burden to achieve the best performance. Similar to the MPC controller, methodologies based on DRL have been increasingly used in constructing CAV controllers (Wang et al., 2015). The benefits of DRL approaches are primarily manifested in their model-free property for capturing the characteristics of complex systems and its quick decision can support CAV in real-time once the offline training is completed. However, as a learning-based method, DRL requires a large amount of data during its offline training phase, which can be difficult to collect or extremely expensive. Despite the fact that various algorithms mentioned above have been developed to enhance car-following performances, they are restricted to longitudinal movement. Seldom research addresses CAV car-following behaviors from a general 2D space.

On the other hand, the aforementioned CAV car-following and trajectory optimization approaches are largely constructed in the time domain (Guo et al., 2018; Gutjahr et al., 2016; Manzinger et al., 2020; Mensing et al., 2011; Plessen, 2017; Werling et al., 2010). However, the attributes and disturbances of the highway, such as the speed limit and work zones, are represented by coefficients that vary in space. Although real-time highway characteristics information can be transmitted to CAVs via V2V/V2I, converting from spatial to temporal information can still be difficult and quickly become a computational burden for the vehicles. In addition, the time domain based MPC assumes that the road geometry remains unchanged over time for each prediction horizon since there is no direct connection between each time step Δt and spatially varying road geometry, which can be easily solved by utilizing the nature of the space domain. Some cutting-edge research based on the space domain has been recently developed. For example, Zhang et al. (2020) proposed a 1D spatially formulated CAV car-following control that is robust to communication delay and better maintains equilibrium. Unlike the trajectory optimization problem which only considers the control of a single vehicle, the car-following problem is essentially a control problem for an interconnected system. The intricacy of the 2D car-following problem lies in that the interconnection between vehicles needs to be explicitly considered. This is due

to the fact that the leading vehicles continue to generate disturbances by accelerating and decelerating, and these disturbances can further propagate through the vehicular string. These changes bring the fundamental change of the control target as well as additional property analysis and guarantees. In particular, the controlled vehicle must maintain a distance and the same speed as the leading vehicle to ensure string stability (e.g., the disturbance will not get amplified through vehicular string). These concerns should also be alighted with other driving tasks in the real world (e.g., ensuring lane centering and avoiding obstacles), which requires a novel control algorithm to systematically solve the problems. Hence, in this paper, we aim to develop a new 2D spatially formulated constrained CAV car-following algorithm that is capable of (i) formulating a 2D CAV car-following policy based on a curvilinear coordinate in the spatial domain, extending from the simplified Newell's car-following model; (ii) developing optimally distributed CAV cooperative 2D-control through MPC-based trajectory planning; and (iii) achieving intelligent platoon behavior such as work zone avoidance without lane changes through the developed distributed policy.

2.3 CAV Lane-changing Strategy

Lane-changing, a pivotal element in vehicle operation, presents a challenging but common task for microscopic traffic control (Kesting et al., 2007; Sun & Elefteriadou, 2010; Zheng, 2014). Concerning drivers' reasons for lane changes, the literature classifies lane-changing research into two categories: discretionary lane-changing and mandatory lane-changing (Ali et al., 2020; Balal et al., 2016; Pan et al., 2016). Discretionary lane-changing refers to a driving maneuver where a vehicle's position is adjusted within the traffic flow out of preference or convenience, rather than out of necessity. On the other hand, mandatory lane-changing is necessitated by the conditions of the roadway or traffic rules. This can be due to an upcoming turn or exit that requires the driver to be in a specific lane, obstructions in the current lane, or lane closures. Comparatively, mandatory lane-changing is of more safety concerns due to the necessities and constraints. Further the act of lane-changing in traffic can induce abrupt alterations in both the distance maintained between vehicles and their relative speeds. These sudden shifts can have a cascading effect, contributing to the destabilization of the overall traffic flow (Chen

& Ahn, 2018; Wang et al., 2022; Zheng et al., 2013). Studies have empirically substantiated that lane-changing maneuvers are a principal catalyst for traffic oscillations (Shi et al., 2022; Sun et al., 2023; Wang et al., 2022). These oscillations manifest as waves of acceleration and deceleration that propagate through the traffic stream. Furthermore, this kind of congestion can lead to inefficient use of road space, known as traffic void, and increased travel time (Leclercq et al., 2011; Leclercq et al., 2016; Yuan et al., 2017). It not only exacerbates fuel consumption and emissions due to the stop-and-go nature of the traffic flow but also increases the risk of collisions as drivers react to the sudden changes in the speeds of vehicles around them (Qu et al., 2020a; Zheng et al., 2010).

Due to the importance, lane-changing planning has been widely investigated. One of the main approaches is curve interpolation method. For curve interpolation method, a vehicle's trajectory during a lane change is expected to conform to a predefined geometric curve (e.g., quantic polynomial curve (Papadimitriou & Tomizuka, 2003), cubic polynomial curve (Chu et al., 2012), and quadratic Bessel curve (Chen et al., 2013)). The parameters for this curve function are derived from the initial and terminal states of the lane-changing maneuver following certain polynomial types. For example, Luo et al. (2016) introduced a model that employed a time-dependent polynomial curve to sketch the lane-changing trajectory. Another instance is Yang et al. (2018), which proposed a model that used a cubic polynomial curve to trace the lane-changing trajectory. However, these approaches greatly limit the curve possibilities and render suboptimality. The strategy known as minimizing overall braking induced by lane changes (MOBIL) has been extensively applied for collaborative lane alterations in lane-changing (Nie et al., 2016; Treiber & Kesting, 2009; Zheng et al., 2020). However, this technique may not yield optimal mobility outcomes as a single lane change can potentially influence the progression of multiple vehicles behind it. Ali et al. (2019) proposed a game theory-based lane-changing approach. This approach assumes that CAVs continually share their individual utilities until they achieve a mutually beneficial decision that results in decreased travel times for all involved. Nevertheless, formulating this game involving numerous vehicles can become challenging, particularly in conditions of heavy traffic. Moreover, it might not always lead to a universally advantageous decision in real-

world timeframes. Wang et al. (2018) and Xu et al. (2020) implement deep reinforcement learning methods to determine lane changes. Nonetheless, the intricate driving behaviors typically observed in heavy traffic situations, along with the vast array of possible scenarios, could potentially limit the effectiveness of learning-based strategies. Differed from above approaches, the constrained optimization-based method proposed recently (Sun et al., 2023; Tajalli et al., 2022), brings a systematic angle by comprehensive consider the vehicle dynamics as well as corresponding constraints, and multi-objective functions, and make it excel other approaches. Another dimension of previous research is the consideration of lane-changing and car-following in a holistic manner. From the perspective of traffic flow theory, those researches which incorporate car-following considerations (Chen et al., 2021; Sun et al., 2023; Wang et al., 2022; Wang et al., 2015) are generally more advanced.

However, all these strategies are primarily constructed using the Cartesian coordinate system (Ren et al., 2011; Yang et al., 2018). While this system is ideal for describing open spaces, it proves challenging for accurately defining complex road geometries, which often consist of intricate curves (Chen et al., 2013; Zhang et al., 2012). Conversely, the curvilinear coordinate system was designed to describe geometries formed by curved lines. Within this system, one axis could correspond to the lane centerline while the other axis could be aligned perpendicular to the centerline tangent, which are optimally suited for describing road geometries. This approach simplifies the depiction of road boundaries, thereby reducing the complexity of formulating and calculating such models. Moreover, road geometric characteristics, traffic regulations (e.g., speed limits), and hazards are typically spatially rather than temporally variable. These factors can act as unobservable exogenous disturbances, negatively impacting planning objectives. Although CAVs can receive real-time road parameter updates via V2I and V2V communication, directly integrating these spatially variable aspects in the temporal domain remains a formidable challenge. However, real-time information is unnecessary for the spatial domain as vehicle dynamics and road geometries are constant in each spatial unit, allowing CAVs to use stored data. The employment of Spatial Formulation and curvilinear coordinates in the realm of car-following planning by Zhang et al. (2021) haves demonstrated remarkable success through the employment of

Spatial Formulation and curvilinear coordinates. Spatial Formulation in this context plays a critical role in elucidating the spatial relationships and interactions between vehicles longitudinally. This amalgamation of methodologies has proven to not only enhance the accuracy of car-following models but also foster a higher degree of safety and efficiency. However, despite the commendable strides in regular traffic conditions, the algorithms presented in both studies reveal limitations when it comes to handling conflict traffic scenarios such as mandatory lane changes. In such circumstances, where a vehicle must alter its lane due to external factors like road closures or diversions, the algorithms find it challenging to effectively navigate the complex interplay and potential conflicts between multiple vehicles. This indicates that the models still warrant further advancements to address the intricacies of conflict traffic environments adequately.

To address aforementioned challenges and inherit the merits of spatial formulation, constrained optimization as well as holistic lane change and car following treatment, this study aims to develop a spatially formulated mandatory lane-changing algorithm for CAVs using the curvilinear coordinate system. Specifically, we focused on developing a distributed trajectory planning policy for CAVs that integrates lane-changing and car-following concerns. In circumstances where vehicles are compelled to change lanes due to external exigencies such as road closures or diversions, it is crucial for the control algorithms to effectively deal with interactions and potential conflicts that may arise among multiple vehicles. By employing MPC in the trajectory planning process, our mandatory lane-changing algorithm is capable of ensuring safety and efficiency where complex scenarios are encountered.

3. SYSTEM MODELLING OF VEHICLE TRAJECTORY OPTIMIZATION

This chapter describes the design and formulation of the proposed vehicle trajectory optimization strategy for the scenario where the lane centerline may or may not straight to increase the application on all road geometries. A curvilinear coordinate system has been introduced to reduce modeling complexity. Specifically, **FIG 3-1** shows how to convert coordinates in a 2D Cartesian coordinate system into coordinates in a 2D curvilinear coordinate system as the x-axis deforms to x'-axis, where C and object w represent the road's centerline and an object on the road, respectively. As we can see, the distance between the object w and the road's centerline C in a 2D Cartesian coordinate is the distance between the object w and the point c as shown in **FIG 3-1** (a). In contrast, the distance between the object w and the road's centerline C in a 2D curvilinear coordinate is always the y-coordinate of the object w as shown in **FIG 3-1** (b).

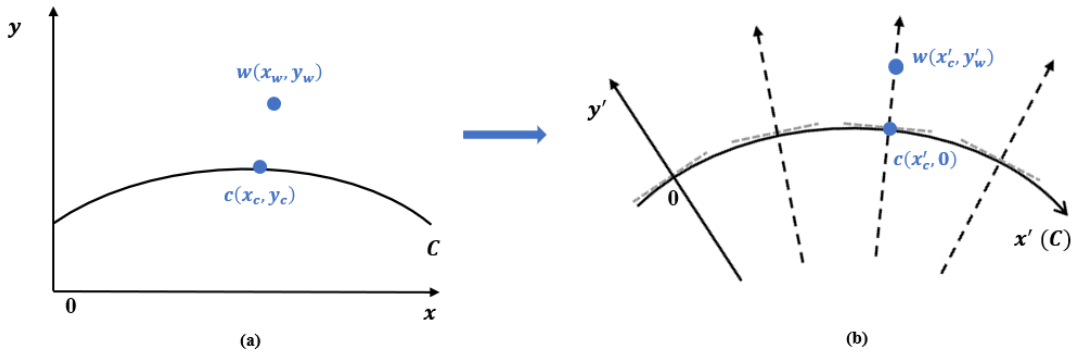

FIG. 3-1. Coordinate Transformation: (a) A 2D Cartesian Coordinate System; (b) A 2D Curvilinear Coordinate System.

3.1 State Space Formulation

Let C represents the centerline of the lane as shown in **FIG 3-2**. The lane centerline, with respect to the global frame, $\{G\}$, is represented by the $[x_{des}(s), y_{des}(s), \theta_{des}(s)]^T \in R^3$, where its position is given by $[x_{des}(s), y_{des}(s)]^T$ and its orientation in the global frame is represented by $\theta_{des}(s)$. Let s be the mapped length of the curvature along the lane centerline that vehicle has traveled. Based on that, we

define $\{V\}$ represents the vehicle body-fixed reference frame with its speed ($v(s)$) represents the vehicle's forward direction and its orientation in the global frame is represented by $\theta_v(s)$.

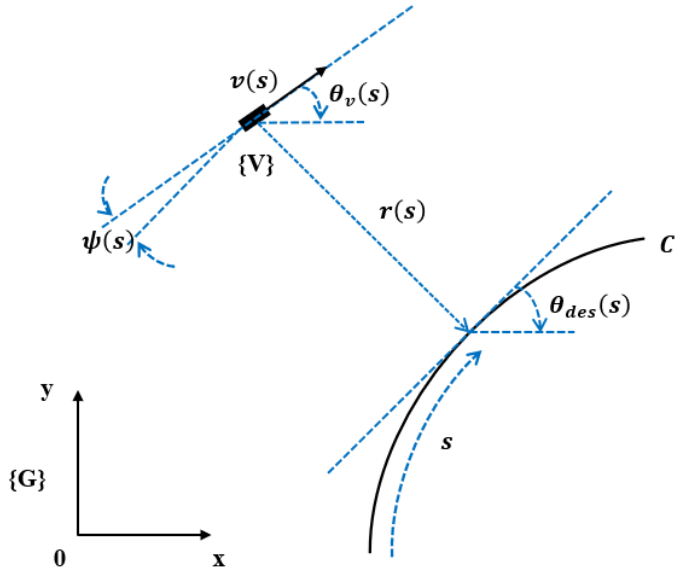

FIG. 3-2. Vehicle Modelling on the Defined Curvilinear Coordinate.

To describe the vehicle dynamics over the established curvilinear coordinate, we construct a state space system and define the system state $X(s)$ for each space s as:

$$X(s) = \begin{bmatrix} r(s) \\ \psi(s) \\ p(s) \end{bmatrix}, \tag{1}$$

where $r(s)$ is the lateral deviation, which equals to signed orthogonal distance from the CAV to the closest point on the lane centerline C, in meters; $\psi(s) = \theta_v(s) - \theta_{des}(s)$, where $\psi(s)$ is the angular deviation, θ_v is the angle between the CAV heading and the x-axis in the global frame $\{G\}$ and $\theta_{des}(s)$ is the angle between the tangent of the lane centerline and the x-axis in the global frame $\{G\}$, in radians; $p(s) = p_v(s) - p_{des}(s)$, where $p(s)$ is the pace deviation, $p_v(s)$ is the reciprocal of the vehicular velocity and $p_{des}(s)$ is the reciprocal of the road speed limit ($p_{des}(s)$ is a nondifferentiable function of s, which can be treated as a constant), in second per meter. Note that, $\theta_{des}(s)$ and $p_{des}(s)$ are spatially varying and got in a real-time manner by the infrastructure. Specifically, the vehicle dynamics are modeled as a nonlinear state space system as:

$$\frac{dX(s)}{ds} = \frac{d}{ds}\begin{bmatrix} r(s) \\ \psi(s) \\ p(s) \end{bmatrix} = \begin{bmatrix} sin(\psi(s)) \\ k(s) \\ \alpha(s) \end{bmatrix} = f[X(s), U(s)], \quad (2)$$

where $k(s) = k_v(s) - k_{des}(s)$, which is the relative angular spatial change rate that controlled by the steering wheel. $k_v(s)$ is the curvature of the vehicle trajectory; $k_{des}(s)$ is the curvature of the lane centerline, in radian per meter; and $\alpha(s)$ is relative moderation that indicates acceleration of the CAV, which can be treated as the control of the brake or throttle pedal (negative value indicates accelerating), in second per mater squared. $k(s)$ and $\alpha(s)$ compose our 'road characteristics compensated' control input $U(s)$, given as $U(s) = [k(s), \alpha(s)\ ]^T$.

However, the road speed limit can be changed based on geometric road design in a real-world situation, which means $p_{des}(s)$ cannot be treated as a spatially invariant constant when speed limit change occurs. Moreover, the speed limit change for the road is a unit jump and $p_{des}(s)$ is still a nondifferentiable function of s. To solve this problem, we introduce a "buffer zone" in front of the speed limit changing area where a changed speed limit is posted at the same length as our MPC model's prediction horizon. The "buffer zone" section divides the speed limit difference by the "buffer zone" length to smoothly form a discrete velocity transit. With Δs is sufficiently small, the velocity change in the "buffer zone" is close enough to be treated as a continuous system. Thus $p_{des}(s)$ becomes a differentiable function of $s$inside the "buffer zone", and $\alpha_{des}(s)$ which is the parameter indicating acceleration of the road is the derivative of $p_{des}(s)$, in second per mater squared. The new nonlinear function with the "buffer zone" introduced is $\frac{dX(s)}{ds} = \frac{d}{ds}\begin{bmatrix} r(s) \\ \psi(s) \\ p(s) \end{bmatrix} = \begin{bmatrix} sin(\psi(s)) \\ k(s) \\ \alpha(s) \end{bmatrix}$, where $\alpha(s) = \alpha_v(s) - \alpha_{des}(s)$, where $\alpha_v(s)$ is the parameter indicating acceleration of the CAV, in second per mater squared.

3.2 Controllability Check

Given the state space defined above, we first analyzed its controllability which describes the ability of any control variables that can move the state of a system from any initial state to any final state in a finite time interval. Hence, we applied the following definitions and theorems to approve the

controllability.

Theorem 1. Nonlinear system small-time locally controllability (Mahmoud, 2018): The linear test: If a nonlinear $\dot{y} = f(y,u)$, whose linearized control system over an equilibrium point (y_e, u_e): $\dot{y} = Ay + Bu$ is controllable, then it is small-time locally controllable at (y_e, u_e).

Definition 1. Equilibrium point: For a nonlinear differential equation $\frac{dX(s)}{ds} = f[X(s), U(s)]$, where f is a function mapping $R^n \times R^m \to R^n$. A point $\mathrm{X_e} \in \mathrm{R^n}$ is called an equilibrium point if there is a specific $U_e \in R^m$ such that $f(X_e, U_e) = 0_n$.

By the **Definition 1**, it is trivial to find that the equilibrium point of the system as Eq. (2) occurs if and only if $X_e = [0,0,0]^T$, $U_e = [0,0]^T$

Theorem 2. Linear time-invariant system controllability (Mahmoud, 2018): For a linear time-invariant system with the form $\dot{x} = Ax + Bu$, the controllability matrix can be written as:

$$G = G(A,B) = \underbrace{[B, AB, A^2B, \dots, A^{n-1}B]}_{n\times(mn)\ matrix}. \tag{3}$$

If $rank(G) = n$, this linear system is controllable.

Based on the **Definition 1**, **Theorem 1** and **2**, we can have the following Proposition:

Proposition 1: The state space formulated as Eq. (2) is small-time locally controllable at the equilibrium point $X_e = [0,0,0]^T$, $U_e = [0,0]^T$.

Proof:

With Taylor series, Eq. (2) at the equilibrium point (X_e, U_e) can be rewritten as:

$$\frac{dX(s)}{ds} = \sum_{i=1}^{n} \left[\frac{\frac{d^i f(X(s),U(s))}{d^i X(s)}_{X(s)=X_e} (X(s) - X_e)^n}{n!} + \frac{\frac{d^i f(X(s),U(s))}{d^i U(s)}_{U(s)=U_e} (U(s) - U_e)^n}{n!} \right]. \tag{4}$$

According to the Taylor series, a representation of a function as an infinite sum of terms that are

calculated from the values of the function's derivatives at a single point. In our case, only 1st order derivative needs to be considered for the linearized control system. Moreover, the equilibrium in our system occurs when the CAV drives along the lane centerline, which means there is no deviation between the CAV and the lane centerline. The 1st order derivative of Eq. (4) at the equilibrium point (X_e, U_e) can be written as:

$$\frac{dX(s)}{ds} = \begin{bmatrix} 0 & cos\,(\psi) & 0 \\ 0 & 0 & 0 \\ 0 & 0 & 0 \end{bmatrix}_{\psi=\psi_e} (X(s) - X_e) + \begin{bmatrix} 0 & 0 \\ 1 & 0 \\ 0 & 1 \end{bmatrix} (U(s) - U_e), \tag{5}$$

and Eq. (5) can be simplified as:

$$\frac{dX(s)}{ds} = AX(s) + BU(s), \tag{6}$$

where $A = \begin{bmatrix} 0 & 1 & 0 \\ 0 & 0 & 0 \\ 0 & 0 & 0 \end{bmatrix}$, $B = \begin{bmatrix} 0 & 0 \\ 1 & 0 \\ 0 & 1 \end{bmatrix}$.

Based on Eq. (3), the controllability matrix of Eq. (6) can be written as:

$$G(A, B) = [B, AB, A^2B] = \begin{bmatrix} 0 & 0 & 1 & 0 & 0 & 0 \\ 1 & 0 & 0 & 0 & 0 & 0 \\ 0 & 1 & 0 & 0 & 0 & 0 \end{bmatrix}, \tag{7}$$

which gives us the rank of the controllability matrix:

$$rankG(A, B) = 3. \tag{8}$$

Remark 1:

The above linearization process can also be proved by the small angle approximation. Specifically, when the angle is relevant small and $cos\,(\psi) \approx 1$, the small angle approximation can be applied. The same state-space model, as Eq. (6), can be derived based on the small angle approximation from Eq. (2).

To reflect control frequency in the real world, we applied the zeroth-order hold (ZOH) for control input for discretization. Specifically, the control input is assumed to be a constant during each update spatial

interval Δs, and when Δs is sufficiently small, the discretization process can be treated as a continuous system (B. M. Chen, Lin, & Shamash, 2004). The discrete version of Eq. (5), according to Eq. (6), is shown as below:

$$X_{(m+1)\Delta s} \approx A_d X_{m\Delta s} + B_d U_{m\Delta s} \; \forall m > 0, \tag{9a}$$

$s.t.$

$$A_d = e^{A\Delta s}, \tag{9b}$$

$$B_d = \int_0^{\Delta s} e^{A\gamma} d\gamma B. \tag{9c}$$

For notation brevity, we use X_m to represent $X_{m\Delta s}$ for the rest of the chapter.

3.3 Model Predictive Control Formulation

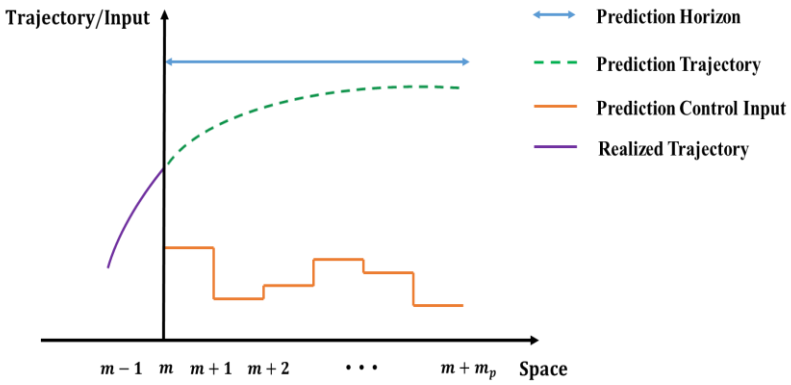

FIG. 3-3. Illustration of Model Predictive Control.

In this section, we provide an MPC formulation due to its great capability to systematically deal with system state and control constraints and meanwhile handling multi-objectives. Further, it is robust to be against system disturbances due to its rolling horizon implementation. Based on the discretized control Eq. (9a), a linear MPC formulation is formulated in our study. In our MPC framework, as illustrated by **FIG. 3-3**, at each current space step m, we solved a constrained trajectory optimization problem over a fixed finite prediction horizon with spatial length $\mathrm{m_p}$ to calculate the optimal control input and state

sequences within the horizon. The controller only implements the first step optimal control input at space step m, and the algorithm continues this process repetitively until the end of the algorithm, shown as **FIG. 3-3**.

To better illustrate the algorithm, we use $\mathcal{U}_m^p = \left[U_m^{p,m}, U_{m+1}^{p,m}, \dots, U_{m+m_p-1}^{p,m}\right]$ to denote the optimal control vectors for CAV obtained at space m for the prediction horizon, m to $m+m_p$; $\mathcal{X}_m^p = \left[X_m^{p,m}, X_{m+1}^{p,m}, \dots, X_{m+m_p}^{p,m}\right]$ to denote the predicted future states for CAV obtained at space m for the prediction space horizon, m to $m+m_p$; $\mathcal{X}_m^r = [X_0^r, X_1^r, \dots, X_m^r]$ to denote the realized states for CAV by space m, which can be seen as the optimal solution where X_0^r is the initial state when the control introduces.

By carefully considering the control efficiency and driving smoothness, an optimal control strategy can be obtained by solving the optimal control problem given as:

$$\left(\mathcal{X}_m^{p*}, \mathcal{U}_m^{p*}\right) = arg\,min\, F\left(X_{m+m_p}^{p,m}\right) + \sum_{i=m}^{m+m_p-1} L\left(X_i^{p,m}, U_i^{p,m}\right), \tag{10a}$$

$s.t.$

$$X_{i+1}^{p,m} = A_d X_i^{p,m} + B_d U_i^{p,m}\ \forall i \in \{m, m+1, m+2, \dots, m+m_p-1\}, \tag{10b}$$

$$X_m^{p,m} = X_m^r, \tag{10c}$$

$$X_i^{p,m} \in \mathbb{X}_i\ \forall i \in \{m, m+1, m+2, \dots, m+m_p\}, \tag{10d}$$

$$U_i^{p,m} \in \mathbb{U}_i\ \forall i \in \{m, m+1, m+2, \dots, m+m_p\}. \tag{10e}$$

where m_p is the prediction space horizon; $L\left(X_i^{p,m}, U_i^{p,m}\right)$ is the running cost consists of the CAV penalties on the deviation from equilibrium point and driving discomfort; $F\left(X_{m+m_p}^{p,m}\right)$ is the terminal cost which refers to the final stage of the prediction horizon. Eq. (10c) is the initial state for the prediction horizon at space step m, and Eq. (10d) is the state constraint used to guarantee the vehicle

states at each space point. Eq. (10e) is the control constraint used to regulate that the steering wheel rotation and acceleration/deceleration are within a reasonable range of $U(s)$.

For the objective function formulated in Eq. (10a), the running cost is specified as follows:

$$L\left(X_{m+n}^{p,m}, U_{m+n}^{p,m}\right) = \left(X_{m+n}^{p,m}\right)^T P X_{m+n}^{p,m} + \left(U_{m+n}^{p,m}\right)^T Q U_{m+n}^{p,m} + 2q_1 k_{v,m+n} k_{des,m+n} - q_1 k_{des,m+n}^2, \tag{11a}$$

where P and Q are diagonal positive definite matrices, usually designed as the diagonal matrix below:

$$P = \begin{bmatrix} p_1 & & \\ & p_2 & \\ & & p_3 \end{bmatrix}, p_1, p_2, p_3 > 0, \tag{11b}$$

$$Q = \begin{bmatrix} q_1 & \\ & q_2 \end{bmatrix}, q_1, q_2 > 0. \tag{11c}$$

Especially, if we want to regulate that the vehicles stick to the lane centerline for safety concerns, we can predefine p_1 and p_2 with large values, while on the other hand, if we are willing to provide the trajectories with flexibility, we can set $\mathrm{p}_{1,2} \to 0$.

We further specify the terminal cost as:

$$F\left(\mathrm{X}_{\mathrm{m+m_p}}^{\mathrm{p,m}}\right) = \left(\mathrm{X}_{\mathrm{m+m_p}}^{\mathrm{p,m}}\right)^T \mathrm{S}\mathrm{X}_{\mathrm{m+m_p}}^{\mathrm{p,m}}, \tag{12}$$

In Eq. (10d) and (10e), by considering vehicle's physical limits, CAV's state constraint determined at space m is formulated as:

$$r_{m+n}^L \le C X_{m+n}^{p,m} \le r_{m+n}^U \; \forall n \in \{0,1,2,\dots,m_p\}, \tag{13a}$$

$$\psi_{min} \le D X_{m+n}^{p,m} \le \psi_{max} \; \forall n \in \{0,1,2,\dots,m_p\}, \tag{13b}$$

$$0 \le T X_{m+n}^{p,m} \le +\infty \; \forall n \in \{0,1,2,\dots,m_p\}, \tag{13c}$$

$$-\frac{1}{R_{min}} - k_{des}(m+n) \le E U_{m+n}^{p,m} \le \frac{1}{R_{min}} - k_{des}(m+n) \; \forall n \in \{0,1,2,\dots,m_p - 1\}, \tag{13d}$$

$$\alpha_{min} \le I U_{m+n}^{p,m} \le \alpha_{max} \; \forall n \in \{0,1,2,\dots,m_p - 1\}. \tag{13e}$$

Eq. (13a) is the constraint to make sure that the CAV drives within the drivable lane, where $C = [1,0,0]$, and $r_{m+n}^{L} = \begin{cases} r_{m+n}^{-}, & if\ O_b \le m+n \le O_e \\ -r_{max}, & Otherwise \end{cases}$ and $r_{m+n}^{U} = \begin{cases} r_{m+n}^{+}, & if\ O_b \le m+n \le O_e \\ r_{max}, & Otherwise \end{cases}$. Where r_{m+n}^{-} and r_{m+n}^{+} are lower bound and upper bound that CAV can pass through within the obstacle zone, respectively; O_b and O_e are spatial positions where obstacle start and end; r_{max} is the half of the lane width; Eq. (13b) is the constraint that the physical limits of allowable angular deviation for CAV, where $D = [0,1,0]$, ψ_{min} and ψ_{max} indicates the lower and upper bound of allowable angular deviation; Eq. (13c) is the constraint to make sure that the CAV does not exceed the speed limit, where $T = [0,0,1]$; Eq. (13d) is the constraint that the realized moving path of CAV is bounded by a given minimum turning radius, where $E = [1,0]$, R_{min} is the minimum turning radius of the CAV; Eq. (13e) is the constraint based on the physical limits of the vehicle's acceleration/deceleration rate a, where $I = [0,1]$, α_{min} is CAV's deceleration and α_{max} is CAV's acceleration limits.

To be noted that, the above formulation can be expanded in the scenario with speed limit change or stop sign by introducing the concept of "buffer zone", and correspondingly, Eq. (13e) changes to $\alpha_{min} - \alpha_{des} \le IU_{m+n}^{p,m} \le \alpha_{max} - \alpha_{des}\ \forall n \in \{0,1,2,\dots,m_p - 1\}$.

3.4 Quadratic Programming

To solve the proposed MPC, we reformulated the above formulation as quadratic programming by introducing an auxiliary variable $y = [X_m^{p,m}; X_{m+1}^{p,m}; \dots; X_{m+m_p}^{p,m}; U_m^{p,m}; U_{m+1}^{p,m}; \dots; U_{m+m_p-1}^{p,m}]$. The optimization framework is given by Eqs. (10a) to (10e), can be reformulated as follows:

$$minf(y) = y^T H y + y^T K, \tag{14a}$$

$s.t.$

$$F_{eq} y = g_{eq}, \tag{14b}$$

$$y_{min} \le y \le y_{max}, \tag{14c}$$

where

$$H = \begin{bmatrix} \overbrace{\begin{matrix} P & & \\ & \ddots & \\ & & P \end{matrix}}^{3m_p} & S & \overbrace{\begin{matrix} & & \\ Q & & \\ & \ddots & \\ & & Q \end{matrix}}^{2m_p} \end{bmatrix}, \tag{15a}$$

$$K = \begin{bmatrix} \overbrace{0 \quad 0 \quad 0 \quad \cdots}^{3m_p+3} & \overbrace{2q_1 k_{des,m} \quad 0 \quad 2q_1 k_{des,m+1} \quad \cdots}^{2m_p} \end{bmatrix}^T, \tag{15b}$$

$$F_{eq} = \begin{bmatrix} \overbrace{\begin{matrix} M & O & O & \cdots & O & O \\ A_d & N & O & \cdots & O & O \\ O & A_d & N & \cdots & O & O \\ \vdots & \vdots & \vdots & \vdots & \vdots & \vdots \\ O & O & O & \cdots & A_d & N \end{matrix}}^{3m_p+3} & \overbrace{\begin{matrix} R & R & R & \cdots & R \\ B_d & R & R & \cdots & R \\ o & B_d & R & \cdots & R \\ \vdots & \vdots & \vdots & \vdots & \vdots \\ R & R & R & \cdots & B_d \end{matrix}}^{2m_p} \end{bmatrix}, \tag{15c}$$

$$g_{eq} = \begin{bmatrix} r_m^r & \psi_m^r & p_m^r & \overbrace{0 \quad 0 \quad \cdots}^{5m_p} \end{bmatrix}^T, \tag{15d}$$

with $M = \begin{bmatrix} 1 & 0 & 0 \\ 0 & 1 & 0 \\ 0 & 0 & 1 \end{bmatrix}$; $N = \begin{bmatrix} -1 & 0 & 0 \\ 0 & -1 & 0 \\ 0 & 0 & -1 \end{bmatrix}$; $O = \begin{bmatrix} 0 & 0 & 0 \\ 0 & 0 & 0 \\ 0 & 0 & 0 \end{bmatrix}$; $R = \begin{bmatrix} 0 & 0 \\ 0 & 0 \\ 0 & 0 \end{bmatrix}$.

Differed in the existence of buffer zone, the bound constraint y_{min} and y_{max} without a "buffer zone" can be defined as follows:

$$y_{min} = \begin{bmatrix} \overbrace{-r_{max} \quad -\frac{\pi}{6} \quad 0 \quad \ldots}^{3m_p+3} & \overbrace{-k_{max} - k_{des,m+n} \quad \alpha_{min} \quad \ldots}^{2m_p} \end{bmatrix}^T, \tag{16a}$$

$$y_{max} = \begin{bmatrix} \overbrace{r_{max} \quad \frac{\pi}{6} \quad +\infty \quad \ldots}^{3m_p+3} & \overbrace{k_{max} - k_{des,m+n} \quad \alpha_{max} \quad \ldots}^{2m_p} \end{bmatrix}^T, \tag{16b}$$

For the buffer zone case, $y_{min} = \begin{bmatrix} \overbrace{-r_{max} \quad -\frac{\pi}{6} \quad 0 \quad \ldots}^{3m_p+3} & \overbrace{-k_{max} - k_{des,m+n} \quad \alpha_{min} - \alpha_{des} \quad \ldots}^{2m_p} \end{bmatrix}^T$

and $y_{max} = \begin{bmatrix} \overbrace{r_{max} \quad \frac{\pi}{6} \quad +\infty \quad \ldots}^{3m_p+3} & \overbrace{k_{max} - k_{des,m+n} \quad \alpha_{max} - \alpha_{des} \quad \ldots}^{2m_p} \end{bmatrix}^T$.

4. NUMERICAL SIMULATION RESULT OF VEHICLE TRAJECTORY OPTIMIZATION STRATEGY

This chapter presents numerical simulations to validate the efficiency and stability of our proposed control strategy. To test our optimal control model, we create a one-lane road segment with a series of curves as the numerical simulation environment shown in **FIG. 4-1**. The road comprises three continuous curves with a total length of 1600 m and 3.6 m lane width which means a 1.8 m width from lane centerline to left/right lane boundary. The first two curves have the same radius of 300 m, and the radius of the third curve is 200 m. The speed limit of the road is set as 54 km/h (15 m/s).

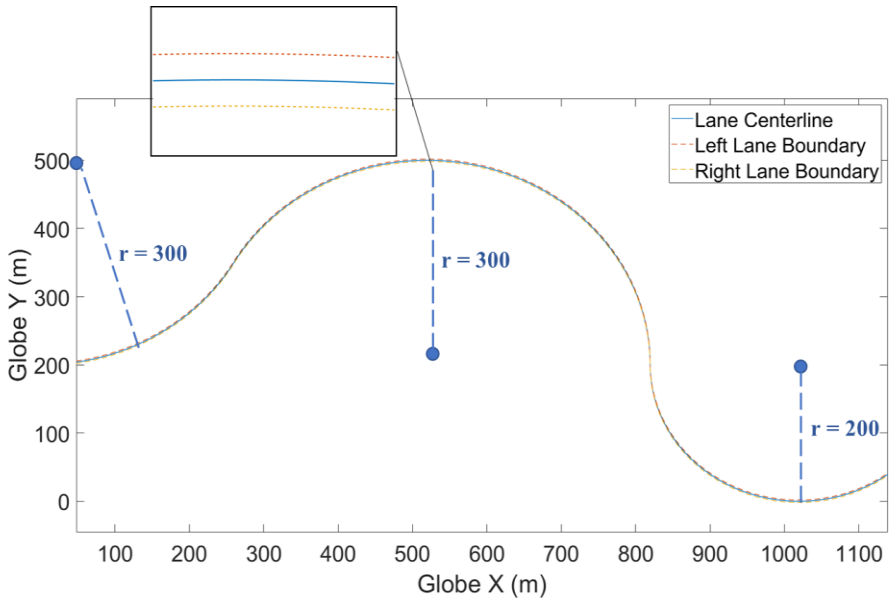

FIG. 4-1. Illustration of Road Trajectory.

To validate our proposed method, a simulation experiment is performed on MATLAB since the field test is expensive and beyond the scope of this paper. The parameter setting for the CAV trajectory optimization as Eq. (10a) to (10e) is given in **Table 4-1**, according to (Zhao et al., 2020) and (Y. Zhou, Ahn, Wang, & Hoogendoorn, 2020).

Table 4-1. Default Value Setting for the Vehicle Trajectory Optimization.

Parameters	Value
ψ_{min} and ψ_{max}	$-\pi/6\ rad$ and $\pi/6\ rad$
a_{min} and a_{max}	-5 m/s^2 and 3 m/s^2
r_{max}	1.8 m
p_1, p_2 and p_3	0.33, 0.1 and 10
q_1 and q_2	1 and 500
s_1, s_2 and s_3	$5p_1$, $5p_2$ and $5p_3$
Δs	2 m
m_p	80 m

4.1 Scenario I: A continuous curvy road segment with the constant speed limit

For the initial condition, we set the vehicle's lateral deviation from the lane centerline to be 1 m, the angular deviation to be $-\frac{\pi}{6}\ rad$ and the pace deviation to be $\frac{1}{30}\ s/m$ (equivalently desired speed difference 5 m/s in our case). To better analyze the convergence behavior of the proposed algorithm, we plot the proposed controller performance of the first 50 m in **FIG. 4-2**, which demonstrates the proposed trajectory optimization method's performance without the "buffer zone" introduced. To be noted that system states and control inputs maintain very closely to the system equilibrium point with nearly no oscillation from 50 m to 1600 m. **FIG. 4-2** (a)-(c) and **FIG. 4-2** (d)-(e) indicate the system state evolution, including lateral deviation, angular deviation, and pace deviation, and how the control inputs change in the space domain as the CAV moves by our control, respectively. As can be seen, similar trends are observed for different system states and the control input values. To be more specific, the lateral deviation exhibits some reasonable fluctuation initially: CAV moves 1.386 m laterally from lane centerline's left side to the right side in the first 6 m along the road, where the positive sign indicates

that the CAV has been off the track and is at the left side of the lane centerline and the negative sign indicates that the CAV has off the track and is at the right side of the lane centerline. Then it quickly turns back from the right side to the lane centerline in the next 6 m and keeps driving on the lane centerline afterward. Angular deviation and relative angular spatial change rates converge in a nearly similar fashion as lateral deviation. As for the pace deviation and relative moderation converges to zero gradually. These results show that the algorithm quickly finds the difference between the vehicle states and the lane centerline and calculates the optimal control inputs to achieve the system equilibrium dynamically. Moreover, even though the $\theta_{des}(s)$ and $k_{des}(s)$ evolve spatially, the proposed controller shows great robustness to these disturbances mentioned above. Rather than the time domain approach (B. C. Chen, Luan, & Lee, 2014), the proposed method can better handle the space varying $\theta_{des}(s)$ and $k_{des}(s)$, which shows the superiority of proposed algorithm by incorporating the road geometric attributes via infrastructure to vehicle communication.

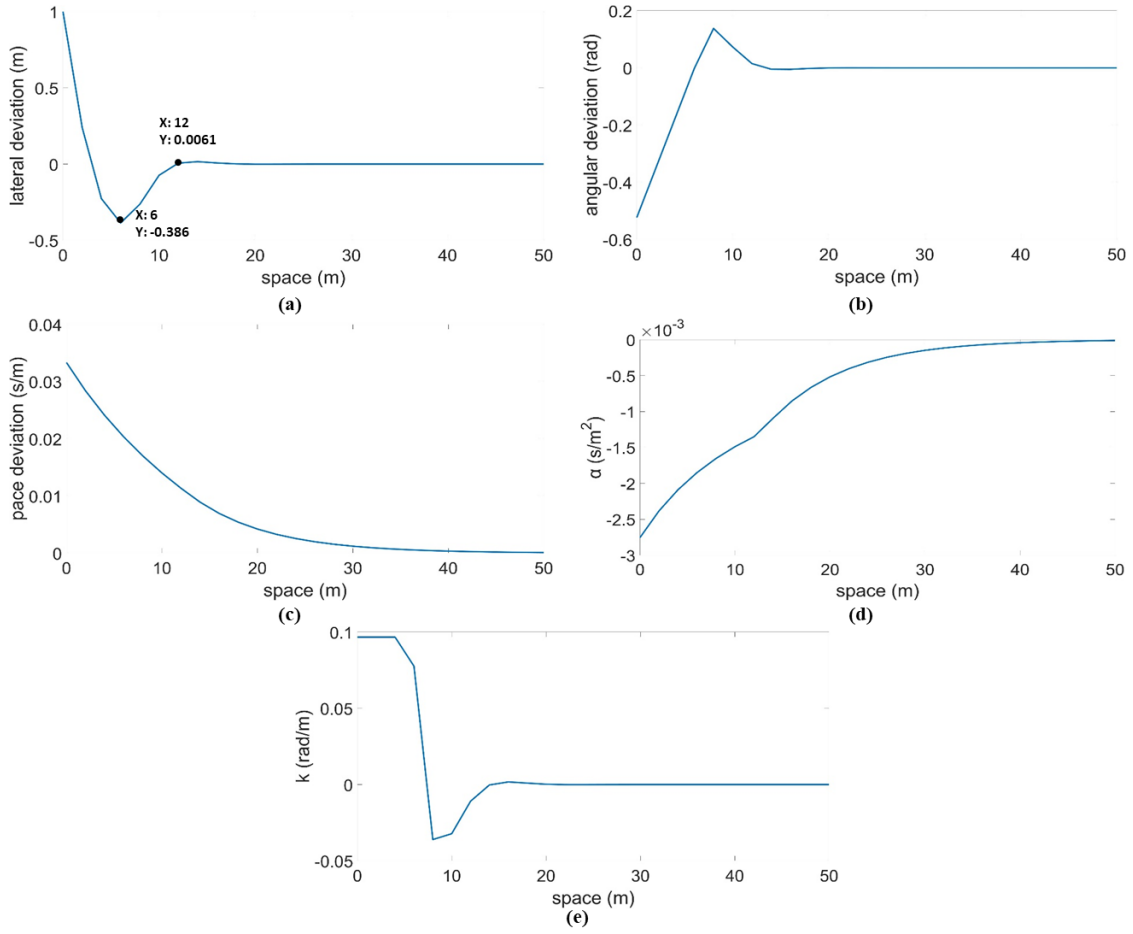

FIG. 4-2. CAV State and Control Results of the first 50 Meters: (a) Lateral Deviation $r(s)$; (b) Angular Deviation $\psi(s)$; (c) Pace Deviation $p(s)$; (d) Relative Moderation $\alpha(s)$; (e) Relative Angular Spatial Change Rate $k(s)$.

To gain further insight into the proposed trajectory optimization method, we convert $p_v(s)$, $\alpha(s)$ and $k_v(s)$ in the spatial domain into speed, acceleration, and angular deviation rate in the time domain, as shown in **FIG. 4-3**. The CAV starts with and keeps a high acceleration for the first 15 m, and then it decreased gradually until it achieves equilibrium points, as shown in **FIG. 4-3** (a). These acceleration changes lead to a speed increase in the first 50 m, and make the speed converge to the desired speed, as shown in **FIG. 4-3** (b). We can also find that the angular deviation rate is within a reasonable range initially and gradually converges to zero.

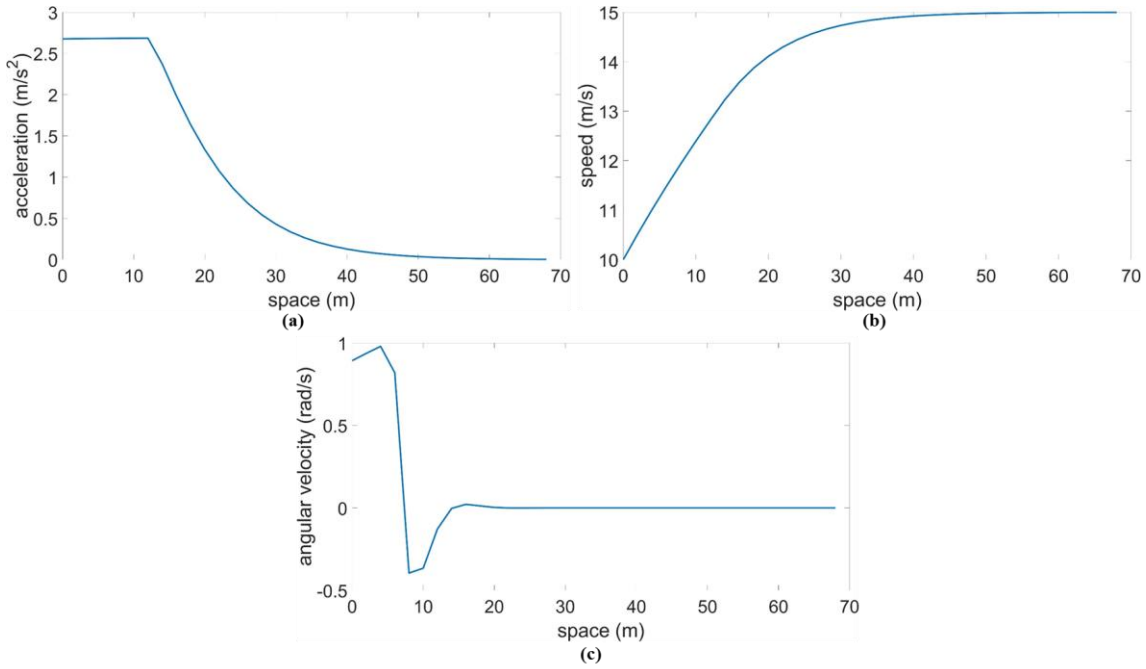

FIG. 4-3. Speed, Acceleration, and Angular Deviation Rate of CAV without the "buffer zone": (a) Acceleration; (b) Speed; (c) Angular Deviation Rate.

4.2 Scenario II: A curved road with two different desired driving behaviors

The previous sections demonstrated the performance of our proposed trajectory optimization method.

In this section, we further conduct a comparison to see the p_1 and p_2 weight impact on the obedience to the lane centerline. To see the flexibility of CAV's decision, we set an obedient driving behavior with p_1 and p_2 as the default case, and a flexible one with weights approaches to zero. To better visualize, we create a new one-lane 150 m curvy road with the same CAV initial conditions and adjust the reference line's weight. The dash-dotted line in **FIG. 4-4** shows the result with original weight, and the dotted line shows the result of all q_1, q_2, s_1 and s_2 changed to 0, which means that there is no reference line to follow.

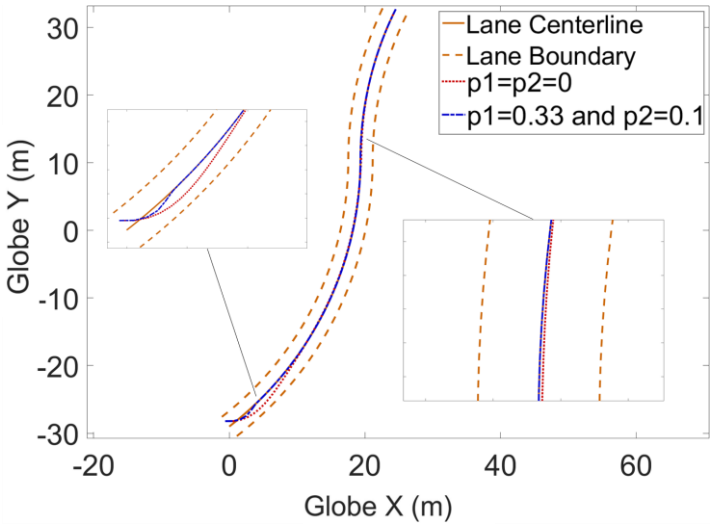

FIG. 4-4. Comparison of Different p_1 and p_2 Values.

The results shown in **FIG. 4-4** illustrate that CAV makes much more aggressive decisions with the obedient driving behavior than those with flexible driving behavior. As we can see, CAV, with the obedient driving behavior, makes sharp turning decisions and quickly turns back to the lane centerline. In contrast, CAV makes smooth turning decisions and needs more time to reach the lane centerline with the flexible driving behavior. Moreover, unlike CAV with obedient driving behavior tightly follows the reference line as long as it reaches the reference line, CAV with the flexible driving behavior can deviate from the reference line when the curve occurs.

4.3 Scenario III: A curved road with an obstacle

We further conduct a simulation experiment using the same initial condition and one-lane road as shown in **FIG. 4-4** to test our proposed trajectory optimization method with a 10 m obstacle created. The $r_{m+n}^{L} = 0.5\ m$ and $r_{m+n}^{U} = 1.8\ m$ during the obstacle section. To meet both safety and driving comfort requirements, a joint driving mode is designed, which means a flexible driving behavior before and during the obstacle and an obedient driving behavior afterward.

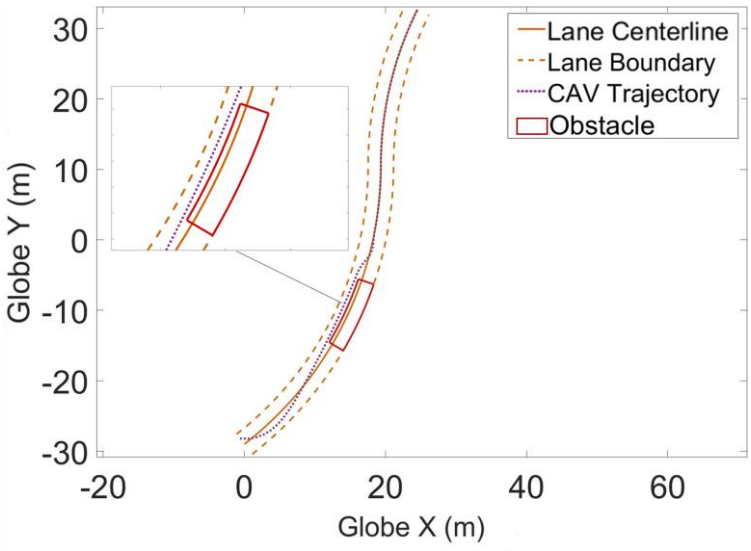

FIG. 4-5. CAV Trajectory with Obstacle introduced.

As we can see from **FIG. 4-5**, the CAV quickly detects the obstacle and makes smooth and comfortable control decisions to avoid the obstacle. The flexible driving behavior makes the CAV drive in the center to prevent any potential collision between the CAV and the obstacle during the obstacle section. In contrast, the obedient driving behavior lets the CAV quickly turn back and keep to the lane centerline after the CAV passes the obstacle section.

4.4 Scenario IV: A continuous curvy road segment with speed limit change

The results in the previous sections show that the proposed trajectory optimization method is efficient and stable without speed limit change to be considered. However, in order to test how the proposed trajectory optimization method works in a real-world situation, we change the speed limit of the road

segment from 1104 m to 1600 m to be 10 m/s and create a "buffer zone" of the same length as m_p. In other words, we now pay our attention to a new situation where the road segment from 1024 m to 1104 m is replaced by the "buffer zone" with α_{des} equals $\frac{1}{1200}$ s/m^2. The illustration for the road trajectory with a "buffer zone" is given in **FIG. 4-6**.

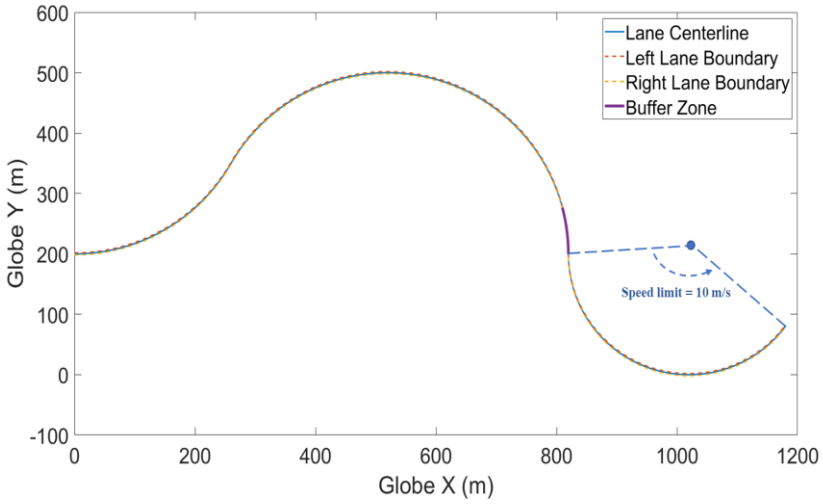

FIG. 4-6. Illustration of Road Trajectory with a "buffer zone".

The results in **FIG. 4-7** give us a generalized illustration of how the proposed trajectory optimization method performs with the "buffer zone". Although the "buffer zone" is introduced, the system state evolution and how the control inputs change in the space domain, as shown in **FIG. 4-7** (a)-(c) and **FIG. 4-7** (d)-(e) respectively, is stable and shows great robustness to the real-world disturbance. The change of angular deviation rate that indicates the relative turning speed and direction of the CAV shown in **FIG. 4-7** (h) shows a similar trend as that in **FIG. 4-3** (c). Furthermore, as expected, CAV's speed and acceleration oscillate around the "buffer zone".

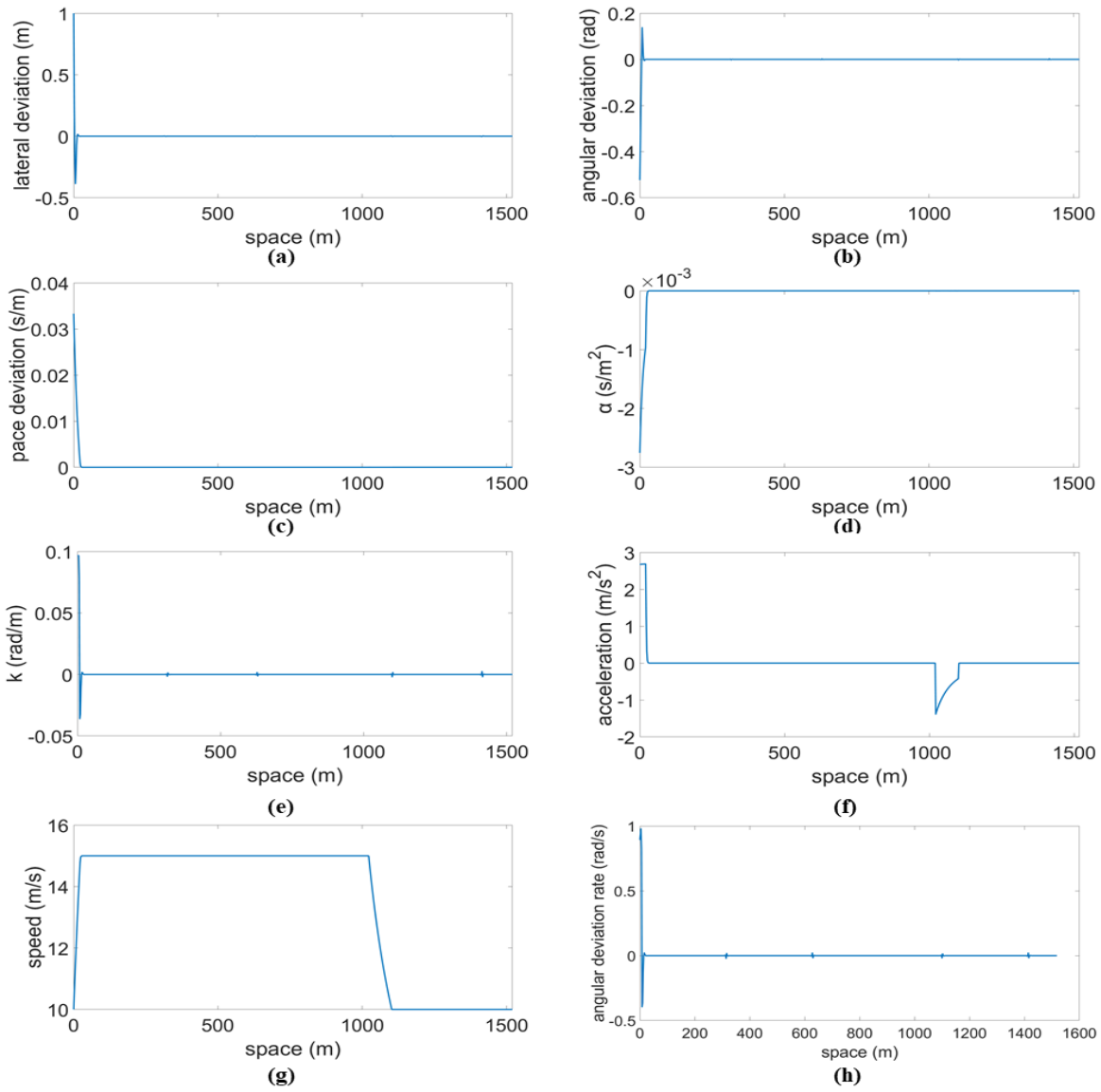

FIG. 4-7. CAV State and Control Results with the "buffer zone": (a) Lateral Deviation $r(s)$; (b) Angular Deviation $\psi(s)$; (c) Pace Deviation $p(s)$; (d) Relative Moderation $\alpha(s)$; (e) Relative Angular Spatial Change Rate $k(s)$; (f) Acceleration; (g) Speed; (h) Angular Deviation Rate.

FIG. 4-8 gives us a detailed illustration of CAV's speed and acceleration changes inside the "buffer zone". **FIG. 4-8** (a) shows that the algorithm quickly detects the speed limit change in the "buffer zone" and makes the deceleration decision to achieve the system equilibrium dynamically, which leads to a smooth speed transition, as shown in **FIG. 4-8** (b).

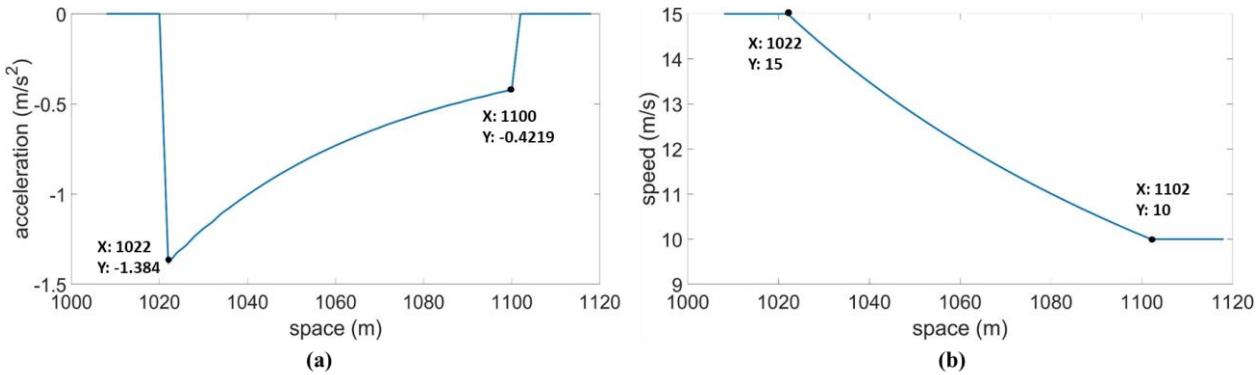

FIG. 4-8. Speed and Acceleration inside the "buffer zone": (a) Acceleration; (b) Speed.

5. SYSTEM MODELLING OF CAV CAR-FOLLOWING STRATEGY

This chapter delves into the design and formulation of the advanced CAV car-following strategy we propose. Contrary to existing CAV car-following algorithms in the literature, which primarily concentrate on the longitudinal driving aspect, our model integrates both lane-keeping and car-following behaviors. For instance, in complex traffic scenarios like a curved lane with potential obstacles, following CAVs must manage not only longitudinal force to tail the lead CAV but also the lateral force to fine-tune their trajectory for obstacle evasion. We operate under the assumption that the following CAV can garner road attributes from RIUs and grasp the dynamics of the leading vehicle directly from the lead CAV. This enables subsequent CAVs to possess comprehensive knowledge of the traffic environment and the dynamics of the lead vehicle in advance. The ultimate goal of our 2D CAV car-following algorithm is to determine the optimal trajectory for a CAV platoon, ensuring safety, efficiency, and comfort even in the face of unforeseen hazards.

5.1 State Space Formulation

For demonstration convenience, notations are illustrated in **FIG. 5-1**. Let $\{V_{i-1}\}$ represents the leading vehicle with its speed $(v_{i-1}(s))$ represents the vehicle's forward direction, we first characterize the location of a vehicle $\{V_i\}$ by curvilinear coordinates. Suppose vehicles aim to travel along a predetermined curved road, with a centerline C. Let s be the projected vehicle travel distance along C. The corresponding signed perpendicular deviation from C is denoted by $r(s)$, and the arrival time is $t(s)$. The mapping from the curvilinear coordinates to a fixed Cartesian coordinates is denoted by $\hat{x}\big(s, r(s)\big), \hat{y}\big(s, r(s)\big)$, and the corresponding moving direction referenced by a fixed horizontal line (e.g., $\hat{y} = 0$) is represented by $\theta(s)$. Note that if indexed by time t, the trajectory of vehicle is determined by a current location $\big(\hat{x}(t), \hat{y}(t)\big)$ and its velocity $(\theta(t), q(t))$, where $q(t)$ is the speed. In a curvilinear coordinates system indexed by distance s, we only need three dimensions $(s, r(s), \theta(s))$

to determine the trajectory. The speed information is decomposed with the trajectory information, which is given by pace, or inverse of speed, $p(s)$, i.e., the travel time needed to go through one unit distance at location s. Therefore, a trajectory of vehicle can be expressed by a fixed Cartesian coordinates $[\hat{x}(s), \hat{y}(s), \theta(s)]^T \in \mathbb{R}^3$ parameterized by $s \in \mathbb{R}_+$.

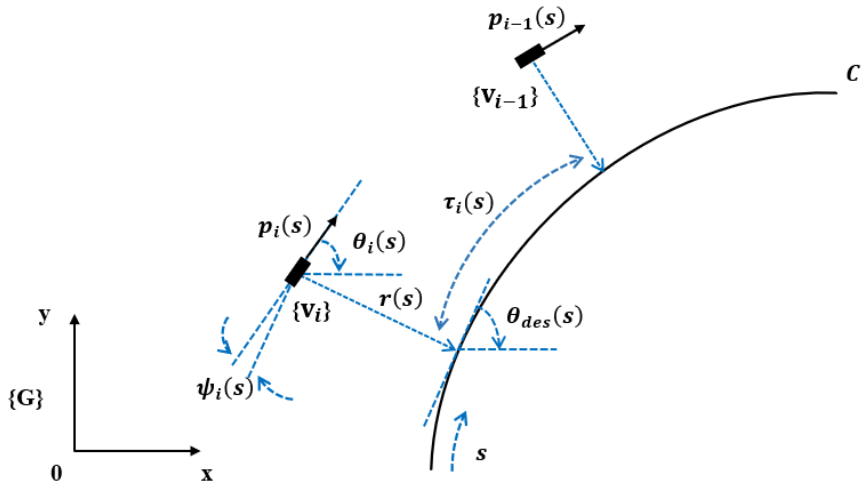

FIG. 5-1. Vehicle Modelling on the Defined Curvilinear Coordinate.

Suppose a platoon of vehicles indexed by $i = 1,2, ...$, and the head vehicle is indexed by 1. The notation with subscript i will indicate the corresponding characterization for Vehicle i. We establish the car-following behavior for each vehicle in 2D given the leading vehicle information. For vehicle i, let $\tau_i(s) = t_i(s) - t_{i-1}(s - l_s)$ be the headway to its leading vehicle i $-$ 1, where $t_i(s)$ is the time when vehicle i arrives at point s and l_s is the standstill length. The primary principle of Newell's car-following model is to maintain a constant time gap between a vehicle and its preceding vehicle similar to the constant time gap policy that's widely adopted. We further modified the original Newell's model to a 2D version, as shown in **FIG. 5-2**. To describe the vehicle dynamics, we define a system state X_i for vehicle i which can be represented by $[\Delta\tau_i, \Delta p_i, r_i, \psi_i]^T$, which contains the headway deviation $\Delta\tau_i(s)$ between vehicle i and its leading vehicle $i - 1$, the pace deviation $\Delta p_i(s)$ between vehicle i and its leading vehicle $i - 1$, the lateral deviation $r_i(s)$ between vehicle i and road centerline, and the angular deviation $\psi_i(s)$ between vehicle i and road centerline. Then, the vehicle state X_i is represented by:

$$X_i(s) = \begin{bmatrix} \Delta\tau_i(s) \\ \Delta p_i(s) \\ r_i(s) \\ \psi_i(s) \end{bmatrix}, \tag{17}$$

where $\Delta\tau_i(s) = \tau_i(s) - \tau^*$, where τ^* is the desired headway, in s; $\Delta p_i(s) = p_{i-1}(s - l_s) - p_i(s)$, where $p_{i-1}(s)$ is the reciprocal of the vehicular velocity of its leading vehicle $i-1$ and $p_i(s)$ is the reciprocal of the vehicular velocity of the vehicle i, in s/m; $r_i(s)$ is the signed orthogonal distance from the vehicle i to the closest point on the road centerline, in m; $\psi_i(s) = \theta_i(s) - \theta_{des}(s)$, where $\theta_i(s)$ is the angle between the vehicle i heading and the x-axis in the global frame {G} and $\theta_{des}(s)$ is the angle between the tangent of the road centerline and the x-axis in the global frame {G}, in rad.

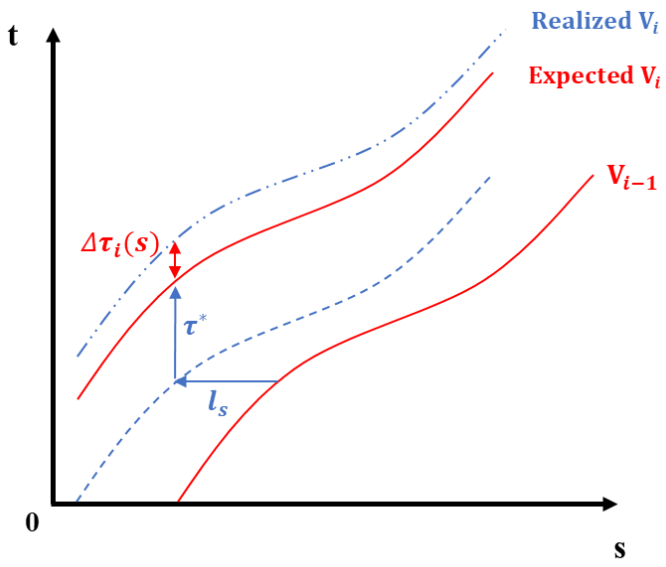

FIG. 5-2. Illustration of Extended 2D Newell's Car-following Model.

Specifically, the vehicle dynamics are modeled as a nonlinear state space system as:

$$\frac{dX_i(s)}{ds} = \frac{d}{ds}\begin{bmatrix} \Delta\tau_i(s) \\ \Delta p_i(s) \\ r_i(s) \\ \psi_i(s) \end{bmatrix} = \begin{bmatrix} p_i(s) - p_{i-1}(s - l_s) \\ \alpha_{i-1}(s - l_s) - \alpha_i(s) \\ \sin(\psi_i(s)) \\ k_i(s) \end{bmatrix} = f[X_i(s), U_i(s)]. \tag{18}$$

Here, $\alpha_i(s)$ is the derivative of pace (on the contrary to the acceleration as the derivative of speed, $\alpha_i(s) > 0$ indicates the vehicle is decelerating). $k_i(s) := k_{i,v}(s) - k_{\text{des}}(s)$, where $k_{i,v}(s)$ is the curvature (reciprocal of vehicle turning radius) of the vehicle trajectory and $k_{\text{des}}(s)$ is the curvature of

the centerline. Since $k_{\mathrm{des}}(s)$ is given by the road geometry in advance, we do not explicitly write it out for $k_i(s)$ due to model convenience. Note that $\alpha_i(s)$ and $k_i(s)$ are the decomposed control of the system (one dimension is for the pace and the other one is for turning), represented as $U_i(s) = [\alpha_i(s) - \alpha_{i-1}(s - l_s), k_i(s)\ ]^T$, which shows the beauty of our curvilinear coordinate system indexing by s.

However, unlike the information that is needed for the time domain is time sensitive, our model formulates based on s. As the leading vehicle passes point s, its state $p_{i-1}(s)$, and time arriving at s, $t_{i-1}(s)$, are measured and recorded by leading vehicle. During the communication, this information will be delivered to the following vehicle. Since $t_{i-1}(s)$ has been contained in the communication information, even there is communication delay, vehicles can still know exact $t_{i-1}(s)$, based on which the following vehicle can compute $\tau_i(s)$ and $\Delta\tau_i(s)$. Under this mechanism, the communication delay will exert minor impacts.

5.2 Controllability Check

The vehicle control system is formulated as a state space system. Specifically, the system state is defined as $X_i(s)$ and the input state is defined as $U_i(s)$. The controllability check is needed to ensure the system must be controllable to do whatever we want with the state space defined above using control variables.

Based on the **Theorem 2** and **Remark 1**, we can have the following Proposition:

Proposition 2: The state space formulated as Eq. (18) is controllable if the change rate of the angular deviation is relevant small.

Proof:

The state-space model of Eq. (18) can be derived based on the small-angle approximation as follows:

$$\frac{dX_i(s)}{ds} = AX_i(s) + BU_i(s), \tag{19}$$

where $A = \begin{bmatrix} 0 & -1 & 0 & 0 \\ 0 & 0 & 0 & 0 \\ 0 & 0 & 0 & 1 \\ 0 & 0 & 0 & 0 \end{bmatrix}$, $B = \begin{bmatrix} 0 & 0 \\ -1 & 0 \\ 0 & 0 \\ 0 & 1 \end{bmatrix}$.

Based on Eq. (3), the controllability matrix of Eq. (19) can be written as:

$$G(A,B) = [B, AB, A^2B, A^3B] = \begin{bmatrix} 0 & 0 & 1 & 0 & 0 & 0 & 0 & 0 \\ -1 & 0 & 0 & 0 & 0 & 0 & 0 & 0 \\ 0 & 0 & 0 & 1 & 0 & 0 & 0 & 0 \\ 0 & 1 & 0 & 0 & 0 & 0 & 0 & 0 \end{bmatrix}, \tag{20}$$

which gives us the rank of the controllability matrix:

$$rankG(A,B) = rank \begin{bmatrix} 0 & 0 & 1 & 0 & 0 & 0 & 0 & 0 \\ -1 & 0 & 0 & 0 & 0 & 0 & 0 & 0 \\ 0 & 0 & 0 & 1 & 0 & 0 & 0 & 0 \\ 0 & 1 & 0 & 0 & 0 & 0 & 0 & 0 \end{bmatrix} = 4. \tag{21}$$

5.3 Model Predictive Control Formulation

In this section, we present a nonlinear MPC formulation in this section to manage system state and control constraints efficiently as illustrated by **FIG. 5-3**. Different from traditional MPC defined on time domain, we formulate based on the space domain instead. For each vehicle, we consider a space window $s \in [m, m + m_p]$, where the vehicle's projected location at the centerline is at m and our prediction horizon covers a distance m_p. Given the leading vehicle's trajectory input/prediction (derivative of pace in particular), the controller solves an optimal control problem over the space window, and only implement the control at m. Such calculation and control are conducted sequentially with a moving prediction window with length m_p.

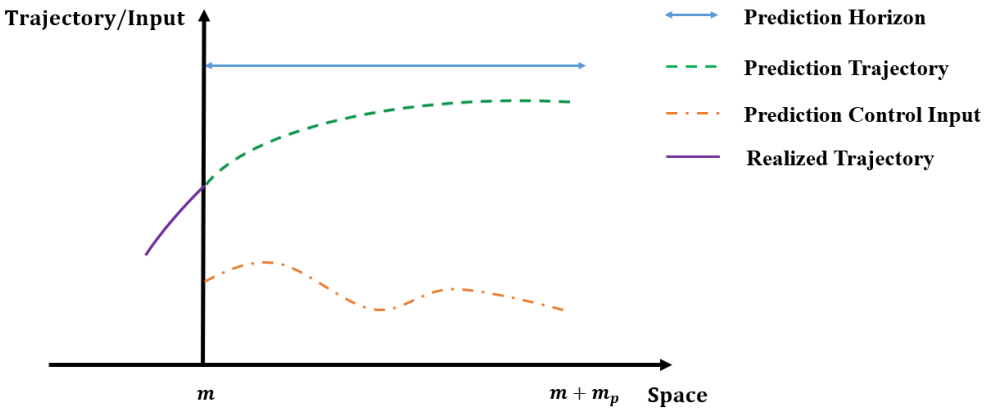

FIG. 5-3. Illustration of Nonlinear Model Predictive Control.

To better illustrate the MPC algorithm, we introduce serval additional notations. First, we use superscript (p, m) to represent the variables predicted at moving window starting from m. In addition, superscript r is used to represent those variables already realized. For example, $X_i^{p,m}(m)$ indicates the predicted system state at location m, with a moving window starting from m. Therefore, we can define the predicted control set $\mathcal{U}_i^p(m) = \{U_i^{p,m}(s) | m \le s \le m + m_p\}$ to denote the predicted control sequences for Vehicle i at location m with moving window $[m, m + m_p]$. In addition, we define the realized control set $\mathcal{U}_i^r(m) = \{U_i^r(s) | 0 \le s \le m\}$ to denote the realized control sequences for Vehicle i at location m. In particular, $U_i^r(0)$ is the initial control inputs, and $U_i^r(s) = U_i^{p,s}(s)$ always holds. Similarly, we have $\mathcal{X}_i^p(m) = \{X_i^{p,m}(s) | m \le s \le m + m_p\}$ to be the predicted future states for Vehicle i obtained at location m, and $\mathcal{X}_i^r(m) = \{X_i^r(s) | 0 \le s \le m\}$ to be its realized states, where X_0^r is the initial state and $X_i^r(s) = X_i^{p,s}(s)$.

Then, given the leading vehicle information $\hat{\alpha}_{i-1}$ (can be already realized or be predicted), we can formulate an optimal control problem incorporating the control efficiency and driving smoothness, which is given as:

$$J = arg\ min\ F\left(X_i^{p,m}(m + m_p)\right) + \int_m^{m+m_p} L\left(X_i^{p,m}(s), U_i^{p,m}(s)\right) ds, \tag{22a}$$

$s.t.$

$$\frac{dX_i^{p,m}(s)}{ds} = f[X_i(s), U_i(s), \alpha_{i-1}(s - l_s)] \; \forall s \in [m, m + m_p], \tag{22b}$$

$$X_i^{p,m}(m) = X_i^r(m), \tag{22c}$$

$$U_i^{p,m}(m) = U_i^r(m), \tag{22d}$$

$$X_i^{p,m}(s) \in \mathbb{X}_i(s) \; \forall s \in [m, m + m_p], \tag{22e}$$

$$U_i^{p,m}(s) \in \mathbb{U}_i(s) \; \forall s \in [m, m + m_p]. \tag{22f}$$

where m_p is the prediction space horizon; $L\left(X_i^{p,m}(s), U_i^{p,m}(s)\right)$ is the running cost consists of the vehicle i travel distance and driving smoothness before reaching the equilibrium point X_e; and $F\left(X_i^{p,m}(m + m_p)\right)$ is the terminal cost that penalizes a deviation from the equilibrium point X_e from the desired final state (i.e., the end of the prediction horizon). Eq. (22c) and Eq. (22d) are the initial condition at space step m; and Eq. (22e) is the state constraint to regulate the transition vehicle states at each space point. The constraint in Eq. (22f) is used to guarantee that the commanded steering wheel rotation and acceleration are within a reasonable range of $U_i(s)$.

For the optimal control formulated in Eq. (22a), we specify the running cost and the terminal cost as follows:

$$L\left(X_i^{p,m}(s), U_i^{p,m}(s)\right) = \left(X_i^{p,m}(s)\right)^T W X_i^{p,m}(s) + \left(U_i^{p,m}(s)\right)^T Q U_i^{p,m}(s) \; \forall s \in [m, m + m_p], \tag{23a}$$

$$F\left(X_i^{p,m}(m + m_p)\right) = \left(X_i^{p,m}(m + m_p)\right)^T S X_i^{p,m}(m + m_p), \tag{23b}$$

where W, Q and S are positive definite diagonal coefficients matrices, which are usually designed as the diagonal matrix below:

$$W = \begin{bmatrix} w_1 & & & \\ & w_2 & & \\ & & w_3 & \\ & & & w_4 \end{bmatrix}, w_1, w_2, w_3, w_4 > 0, \tag{24a}$$

$$Q = \begin{bmatrix} q_1 & \\ & q_2 \end{bmatrix}, q_1, q_2 > 0, \tag{24b}$$

$$S = \begin{bmatrix} s_1 & & & \\ & s_2 & & \\ & & s_3 & \\ & & & s_4 \end{bmatrix}, s_1, s_2, s_3 > 0. \tag{24c}$$

For Eq. (22e) and Eq. (22f), by considering collision-free constraints, steering wheel, and acceleration/deceleration limits, CAV's state constraint determined at space m is formulated in detail as follows:

$$-\tau_{dev} \leq DX_i^{p,m}(s) \; \forall s \in [m, m_p], \tag{25a}$$

$$EX_i^{p,m}(s) \leq p_{i-1}(s - l_s) - p_{min} \; \forall s \in [m, m_p], \tag{25b}$$

$$r_i^L(s) \leq FX_i^{p,m}(s) \leq r_i^U(s) \; \forall s \in [m, m_p], \tag{25c}$$

$$\psi_{i,min} \leq IX_i^{p,m}(s) \leq \psi_{i,max} \; \forall s \in [m, m_p], \tag{25d}$$

$$\alpha_{i,min}(s) - \alpha_{i-1}(s - l_s) \leq MU_i^{p,m}(s) \leq \alpha_{i,max}(s) - \alpha_{i-1}(s - l_s) \; \forall s \in [m, m_p), \tag{25e}$$

$$-\frac{1}{R_{i,min}} - k_{des}(s) \leq NU_i^{p,m}(s) \leq \frac{1}{R_{i,min}} - k_{des}(s) \; \forall s \in [m, m_p). \tag{25f}$$

Eq (25a) is a constraint to make sure that the headway between the vehicle i and its preceding vehicle along the road centerline does not deviate from equilibrium headway significantly for the safety concern, where $D = [1,0,0,0]$. To be noted that, τ_{dev} can be picked according to the safety requirement. For the extreme case (e.g., a vehicle suddenly cut in the front of controlled vehicle), we can set $\tau_{dev} = \tau^*$, to increase feasible region while guaranteeing collision avoidance; Eq (25b) is used to ensure that vehicle i will never surpass the road's speed limit, where p_{min} indicates the reciprocal of the maximum speed limit and $E = [0,1,0,0]$; Eq (25c) is the constraint imposed on the vehicle i to ensure that it stays within

the lane, where $F = [0,0,1,0]$, and $r_i^L(s) = \begin{cases} r_i^-(s), & if\ O_b \le s \le O_e \\ -r_{max}, & Otherwise \end{cases}$ and $r_i^U(s) = \begin{cases} r_i^+(s), & if\ O_b \le s \le O_e \\ r_{max}, & Otherwise \end{cases}$. Where $r_i^-(s)$ and $r_i^+(s)$ are the lower and upper bounds of the work zone through which vehicle i may pass, respectively; O_b and O_e are starting and ending positions of the work zone; r_{max} is equal to a half the width of the lane; Eq (25d) is used to impose the vehicle's permissible angular deviation's physical restrictions, where $I = [0,0,0,1]$, $\psi_{i,min}$ and $\psi_{i,max}$ specify the allowable angular deviation's lower and upper bounds; Eq (25e) is used to ensure the actual acceleration/deceleration of the vehicle is within the vehicle's physical limits, where $M = [1,0]$, $\alpha_{i,min}(s) = -a_{i,max}p_i^3(s)$ and $\alpha_{i,max}(s) = -a_{i,min}p_i^3(s)$ with $a_{i,max}$ is the vehicle i's maximum acceleration and $a_{i,min}$ is the vehicle i's maximum deceleration limits; Eq (25f) is the constraint that the vehicle i's actual moving path is constrained by a specified minimum turning radius, where $N = [0,1]$, $R_{i,min}$ is the minimum turning radius of the vehicle i.

String stability is a critical property of vehicle platoons because it ensures that system state disturbances do not propagate along the string of vehicles (Dunbar & Caveney, 2011; Kianfar et al., 2015). However, due to the complexity of MPC caused by state and control constraints, analyzing the string stability of MPC based car-following control is typically difficult. Hence, we conducted an approximated linear stability analysis for our proposed control, as suggested by Liu et al. (2021) and Zhou et al. (2019).

5.4 Discretization and linearization

The stability analysis is important for a vehicle control model that could introduce system-level impacts on traffic. String stability signifies disturbances (e.g., $\alpha_i(s)$) dampening performance as it propagates through a platoon of vehicles.

Due to the non-analytical form of MPC, we simplify the proof by assuming that the constraints are inactive and m_p is large enough, which describes the MPC's long-term control behaviors given disturbances are small. By which, the MPC given by Eqs (25) can be reduced to a linear quadratic regulator, whose control law is analytical. The linear quadratic regulator is as follows:

$$J = \int_0^{+\infty} \left(\left(X_i(s)\right)^T W X_i(s) + \left(U_i(s)\right)^T Q U_i(s) \right) ds, \tag{26a}$$

$s.t.$

$$\frac{d}{ds} X_i(s) = A X_i(s) + B U_i(s). \tag{26b}$$

As can be found that, the constrained control problem above is a linear quadratic regulator (LQR), which gives linear control law as below:

$$U_i(s) = K_i X_i(s), \tag{26c}$$

where K_i is the continual feedback gain of vehicle i, which is resolved using Algebraic Riccati Equation as below:

$$K_i = Q^{-1} B^T Y, \tag{27a}$$

$$YA + A^T P - YBQ^{-1}B^T Y + W = 0. \tag{27b}$$

To simplify the calculation, we use block matrix to illustrate matrix A, A^T, B, B^T, W, and Y as below:

$$A = \begin{bmatrix} \widetilde{A_{11}} & 0^{2\times 2} \\ 0^{2\times 2} & \widetilde{A_{22}} \end{bmatrix}, \tag{28a}$$

$$A^T = \begin{bmatrix} 0 & 0 & 0 & 0 \\ -1 & 0 & 0 & 0 \\ 0 & 0 & 0 & 0 \\ 0 & 0 & 1 & 0 \end{bmatrix} = \begin{bmatrix} \widetilde{A_{11}^T} & 0^{2\times 2} \\ 0^{2\times 2} & \widetilde{A_{22}^T} \end{bmatrix}, \tag{28b}$$

$$B = \begin{bmatrix} \widetilde{B_{11}} & 0^{2\times 1} \\ 0^{2\times 1} & \widetilde{B_{22}} \end{bmatrix}, \tag{28c}$$

$$B^T = \begin{bmatrix} 0 & -1 & 0 & 0 \\ 0 & 0 & 0 & 1 \end{bmatrix} = \begin{bmatrix} \widetilde{B_{11}^T} & 0^{1\times 2} \\ 0^{1\times 2} & \widetilde{B_{22}^T} \end{bmatrix}, \tag{28d}$$

$$W = \begin{bmatrix} \widetilde{W_{11}} & 0^{2\times 2} \\ 0^{2\times 2} & \widetilde{W_{22}} \end{bmatrix}, \tag{28e}$$

$$Y = \begin{bmatrix} \widetilde{Y_{11}} & \widetilde{Y_{12}} \\ \widetilde{Y_{21}} & \widetilde{Y_{22}} \end{bmatrix}. \tag{28f}$$

Based on that, Eq. (27b) can be calculated as:

$$\begin{cases} \widetilde{Y_{11}}\widetilde{A_{11}} + \widetilde{A_{11}^T}\widetilde{Y_{11}} - \widetilde{Y_{11}}\widetilde{B_{11}}\dfrac{1}{q_1}\widetilde{B_{11}^T}\widetilde{Y_{11}} + \widetilde{W_{11}} = 0^{2\times 2} \\ \widetilde{Y_{12}}\widetilde{A_{22}} + \widetilde{A_{11}^T}\widetilde{Y_{12}} - \widetilde{Y_{12}} \times 0^{1\times 2} \times \dfrac{1}{q_2}\widetilde{B_{11}^T}\widetilde{Y_{12}} = 0^{2\times 2} \\ \widetilde{Y_{21}}\widetilde{A_{11}} + \widetilde{A_{22}^T}\widetilde{Y_{21}} - \widetilde{Y_{21}}\widetilde{B_{11}}\dfrac{1}{q_1}\widetilde{B_{22}^T}\widetilde{Y_{21}} = 0^{2\times 2} \\ \widetilde{Y_{22}}\widetilde{A_{22}} + \widetilde{A_{22}^T}\widetilde{Y_{22}} - \widetilde{Y_{22}} \times 0^{1\times 2} \times \dfrac{1}{q_2}\widetilde{B_{22}^T}\widetilde{Y_{22}} + \widetilde{W_{22}} = 0^{2\times 2} \end{cases}. \tag{29}$$

Based on Eq (29), we can get $\begin{cases} \widetilde{Y_{12}}\widetilde{A_{22}} + \widetilde{A_{11}^T}\widetilde{Y_{12}} = 0^{2\times 2} \\ \widetilde{Y_{21}}\widetilde{A_{11}} + \widetilde{A_{22}^T}\widetilde{Y_{21}} = 0^{2\times 2} \end{cases}$, which suggests $\widetilde{Y_{12}} = \widetilde{Y_{21}} = 0^{2\times 2}$. Hence, Y and K_i should follow the form as:

$$Y = \begin{bmatrix} \widetilde{Y_{11}} & 0^{2\times 2} \\ 0^{2\times 2} & \widetilde{Y_{22}} \end{bmatrix} = \begin{bmatrix} y_{11} & y_{12} & 0 & 0 \\ y_{21} & y_{22} & 0 & 0 \\ 0 & 0 & y_{33} & y_{34} \\ 0 & 0 & y_{43} & y_{44} \end{bmatrix}, \tag{30a}$$

$$K_i = Q^{-1}B^T Y = \begin{bmatrix} -\frac{y_{21}}{q_1} & -\frac{y_{22}}{q_1} & 0 & 0 \\ 0 & 0 & \frac{y_{43}}{q_2} & \frac{y_{44}}{q_2} \end{bmatrix}. \tag{30b}$$

By applying Eq (30b) into Eq (26c), we can get that:

$$\alpha_i(s) - \alpha_{i-1}(s - l_s) = -\frac{y_{21}}{q_1}(t_i(s) - t_{i-1}(s - l_s) - \tau^*) - \frac{y_{22}}{q_1}\big(p_{i-1}(s - l_s) - p_i(s)\big). \tag{31}$$

By applying the Laplacian transformation on Eq (31), we have

$$\alpha_i(z) - \alpha_{i-1}(z)e^{-l_s z} = -\frac{y_{21}}{q_1} \times \frac{\alpha_i(z) - \alpha_{i-1}(z)e^{-l_s z}}{z^2} - \frac{y_{22}}{q_1} \times \frac{\alpha_{i-1}(z)e^{-l_s z} - \alpha_i(z)}{z}, \tag{32}$$

where $\alpha_i(z)$ is the Laplacian transformation of $\alpha_i(s)$; $z = j\omega$, where j is the imaginary unit and ω denotes the frequency of the signal. After simplification, we have

$$\frac{\alpha_i(z)}{\alpha_{i-1}(z)} = \left|\frac{\alpha_i(z)}{\alpha_{i-1}(z)}\right| \measuredangle \frac{\alpha_i(z)}{\alpha_{i-1}(z)}, \tag{33a}$$

where $\left|\frac{\alpha_i(z)}{\alpha_{i-1}(z)}\right|$ represents the acceleration amplification magnitude, and $\measuredangle \frac{\alpha_i(z)}{\alpha_{i-1}(z)}$ represents the phase shift of acceleration. In our case, we have:

$$\left|\frac{\alpha_i(z)}{\alpha_{i-1}(z)}\right| = 1, \tag{33b}$$

$$\measuredangle \frac{\alpha_i(z)}{\alpha_{i-1}(z)} = l_s. \tag{33b}$$

Based on the above analysis, we can conclude that our spatial formulation can greatly pertain to the 2D Newell's car-following model, as the acceleration after reaching equilibrium is not affected by the choice of W and Q. Compared with the time domain method (e.g., Zhou et al., 2019), which requires careful W and Q design, our MPC in spatial domain simplifies the weighting matrix tuning procedure. Additionally, compared with works suffering from continuous deviation from equilibrium, our design is capable of sticking to equilibrium in a straightforward manner.

The reason why we prove an approximated linear string stability is due to the non-analytical form of MPC makes it challenging to conduct theoretical string stability analysis. we further simplify the proof by considering the case that the constraints are inactive and $\mathrm{m_p}$ is large enough, which describes the MPC's long-term control behaviors given disturbances are small. There are currently no mature mathematical tools to conduct theoretical string stability analysis for non-analytical control law such as MPC. One approach is to adding constraints such as Zhou et al. (2019), whereas this approach may render infeasibility due to the extra constraints. Another approach is to evaluate the string stability empirically.

5.5 Discretization and linearization

We divide the prediction horizon into N steps and discretize the optimal control problem on the s-axis. To accurately represent control frequency in the real world, we used the ZOH technique for control

input discretization. To be more precise, the control input is assumed to be constant during each update spatial interval Δs, and when Δs is small enough, the discretization process can be treated as a continuous system.

$$X_{i,s+\Delta s}^{p,m} \approx A_d X_{i,s} + B_d U_{i,s} \; \forall s \in \{m, m+1, \dots, m+N-1\}, \tag{34a}$$

$s.t.$

$$A_d = e^{As}, \tag{26b}$$

$$B_d = \int_0^s e^{A\gamma} d\gamma B. \tag{26c}$$

with $\Delta s = \frac{m_p}{N}$.

The objective function in Eqs. (22) can be transformed into

$$J = arg\ min\, F\left(X_{i,m+N}^{p,m}\right) + \sum_{s=m}^{m+N-1} L\left(X_{i,s}^{p,m}, U_{i,s}^{p,m}\right), \tag{35a}$$

$s.t.$

$$X_{i,s+\Delta s}^{p,m} \approx A_d X_{i,s} + B_d U_{i,s} \; \forall s \in \{m, m+1, \dots, m+N-1\}, \tag{27b}$$

$$X_{i,m}^{p,m} = X_{i,m}^{r}, \tag{27c}$$

$$U_{i,m}^{p,m} = U_{i,m}^{r}, \tag{27d}$$

$$X_i^{p,m} \in \mathbb{X}_i \; \forall i \in \left\{m, m+\Delta s, \dots, m+m_p\right\}, \tag{27e}$$

$$U_i^{p,m} \in \mathbb{U}_i \; \forall i \in \left\{m, m+\Delta s, \dots, m+m_p\right\}. \tag{27f}$$

With the optimization framework becoming a discretized linear quadratic equation, quadratic programing can be applied. we specialize the result in Eqs. (27) to the fundamental quadratic programing problem.

5.6 Online Vehicle Control Scheme

The proposed algorithm uses the most recent information from the leading vehicle, and therefore, control of CAVs in a platoon is performed sequentially. This setting enhances the performance of the controller by utilizing the most recent information and is shown in **Algorithm 1**.

Algorithm 1 Online Vehicle Control Scheme

1: initialization: Without losing generality, CAV $i = 1$ start with the space $s_{1,0} = 0$, at global time frame $t = 0$.

2: at time point t, if $i = 1$, Update and Record $s_{i,t}^r$;

3: if $i = 1$, Compute $\mathcal{U}_{i,t}^p, \mathcal{X}_{i,t}^p$ by solving the leading vehicle trajectory problem and record $\mathcal{X}_i^r$, $\mathcal{U}_i^r$; else Compute $\mathcal{U}_{i,t}^p, \mathcal{X}_{i,t}^p$ by solving the CF problem and record $\mathcal{X}_i^r$, $\mathcal{U}_i^r$;

4: check whether $s_{i,t}^r + l_s \geq s_{i+1,t}^r + m_p$, if yes, transmit $\mathcal{X}_i^r$, $\mathcal{U}_i^r$ to vehicle $i+1$; else calculate $\widetilde{\mathcal{X}}_i^p = [x_{i,s_{i+1,t}^r - l_s}^r, x_{i,s_{i+1,t}^r - l_s+1}^r \ \dots, x_{i,s_{i,t}^r}^r, x_{i,s_{i,t}^r+1}^p, \dots, x_{i,s_{i+1,t}^r+m_p-l_s}^p]$, $\widetilde{\mathcal{U}}_i^p = [u_{i,s_{i+1,t}^r - l_s}^r, u_{i,s_{i+1,t}^r - l_s+1}^r \ \dots, u_{i,s_{i,t}^r}^r, u_{i,s_{i,t}^r+1}^p, \dots, u_{i,s_{i+1,t}^r+m_p}^p]$.

5: implement $u_{i,s_{i,t}^r}^r$;

6: if $i < N$, update CAV number: $i = i + 1$, and go to Step 2; Else, go to Step 7;

7: update time point: t = t + 1. Set i = 1; Go to Step 2.

FIG. 5-4 illustrates two cases described in step 4. If the leading vehicle i is $m_p - l_s$ meters ahead of its following vehicle $i+1$ when vehicle $i+1$ arrives at s_{i+1}, the leading vehicle i will transmit its realized states sequences from $s_{i+1} - l_s$ to $s_{i+1} + m_p - l_s$ to its following vehicle $i+1$, as shown in **FIG. 5-4** (a). Otherwise, the leading vehicle i will send a total of m_p meters of joint state sequences that combine realized state sequences and predicted state sequences of its current space s_{i+1}, as shown in **FIG. 5-4** (b). To be noted that, in comparison to the time domain approach that comprises entirely

of predicted state sequences, as shown in **FIG. 5-4** (c), we believe that these predicted state sequences will never be realized because they will be out of date once they are realized. Additionally, communication delay is a significant concern for the time domain approach, as the following vehicle $i+1$ will use the most recently received information from its leading vehicle i as the current information due to the nature of the time domain approach. However, the information that CAV uses in the spatial domain does not have to be real-time. Because road geometries are fixed in space, the CAV can even use saved information, which means that our model can be implemented properly as long as the CAV receives road information in advance.

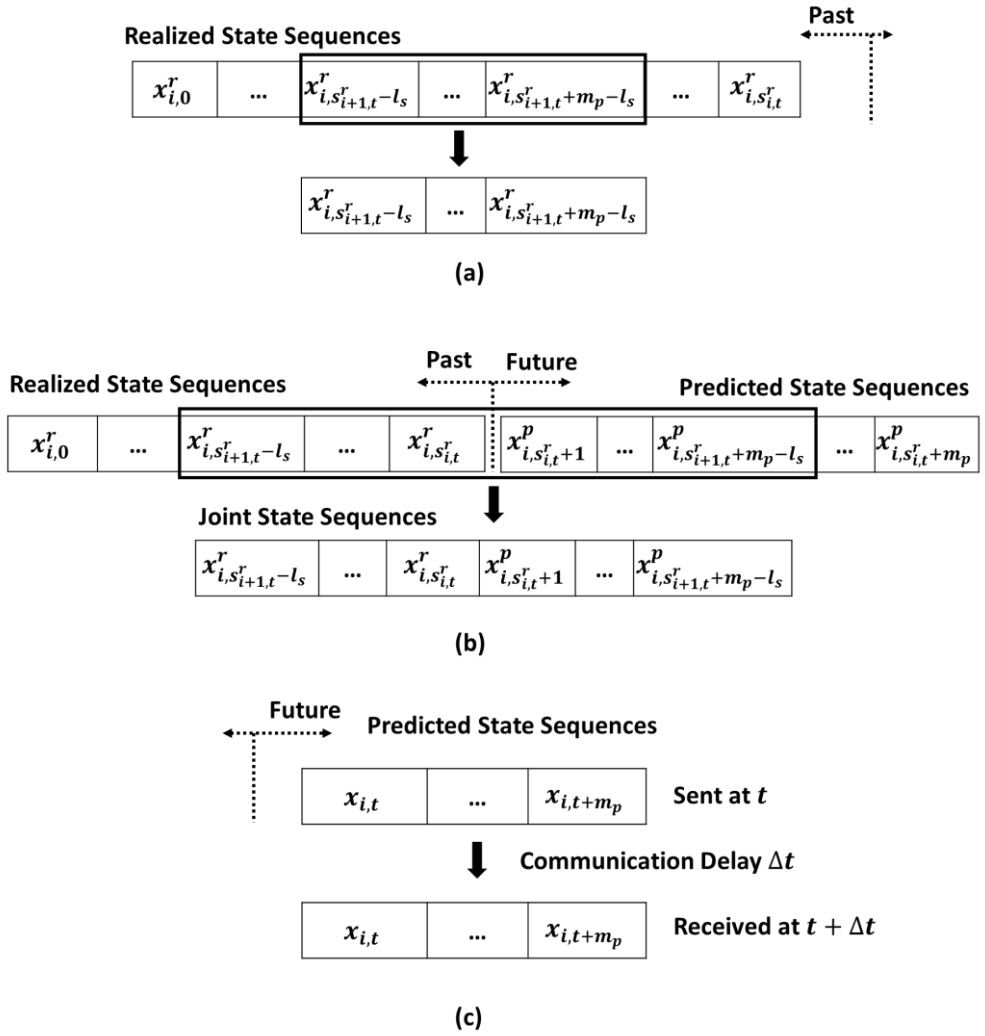

FIG. 5-4. Illustration of State Sequences transmission for Different Cases: (a) The Distance between Vehicles is Greater than or Equal to Prediction Horizon in Space Domain; (b) The Distance between

Vehicles is Smaller than Prediction Horizon in Space Domain; (c) State Sequences transmission in Time Domain.

6. NUMERICAL SIMULATION RESULT OF CAV CAR-FOLLOWING STRATEGY

We conducted a numerical simulation experiment using MATLAB to validate the efficiency of our proposed method. Vehicle 1, which is the leading vehicle, has its dynamics calculated using our CAV trajectory optimization strategy. **Table 6-1** contains the parameter settings for the CAV trajectory optimization as Eqs (25a) to (25f).

Table 6-1. Default Parameters for Car-following Model

Parameters	Value
l_s	$2\ m$
τ^*	$1\ s$
τ_{dev}	$0.5\ s$
m_p	$80\ m$
p_{min}	$1/15\ s/m$
ψ_{min} and ψ_{max}	$-\frac{\pi}{6} rad$ and $\pi/6\ rad$
α_{min} and α_{max}	$-5\ m/s^2$ and $3\ m/s^2$
R_{min}	$10\ m$
w_1, w_2, w_3, and w_4	1, 10, 0.33, and 0.1
q_1 and q_2	5000 and 1
s_1, s_2, s_3, and s_4	5, 50, 1.65, and 0.5

6.1 Scenario I: A continuous curvy road segment without an obstacle

To validate our optimal control model, we create a numerical simulation environment consisting of an 800 m one-lane road segment with a series of curves as shown in **FIG. 6-1**. The road is divided into two continuous curves with the same radius of 300 meters and lane width of 3.6 meters. The leading

vehicle is designed to drive at varying speeds in order to simulate our car-following strategy in real-world situations, which means that the leading vehicle's speed limit changes. The road's speed limit is set at 15 m/s for the first 200 meters, 10 $\mathrm{m/s}$ between 250 and 350 meters, and 15 $\mathrm{m/s}$ between 400 and 800 meters, with the remainder of the road designated as a "buffer zone." We set the leading vehicle's lateral deviation from the lane centerline to 1 m, its angular deviation to $-\frac{\pi}{6}$ rad, and its pace deviation to $\frac{1}{30}$ $\mathrm{s/m}$ (equivalently desired speed difference of 10 m/s in our case). Additionally, we add three vehicles as car-following vehicles: vehicle 2 begins with the majority of its states at equilibrium points but with a -0.2 s headway deviation, while vehicles 3 and 4 begin at equilibrium states.

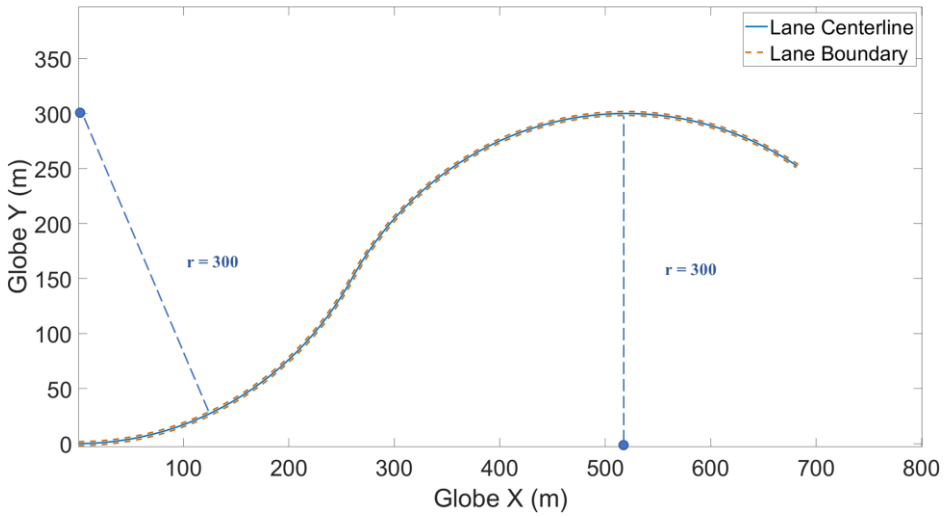

FIG. 6-1. Illustration of Road Trajectory.

To better understand the proposed algorithm's convergence behavior, we plot the proposed controller's performance in **FIG. 6-2** (a)-(d) and **FIG. 6-2** (e)-(f), which demonstrates the system state evolution, including headway deviation, pace deviation, lateral deviation, and angular deviation, as well as how the control inputs change in the space domain as CAVs move under our control. To gain a better understanding of the proposed car-following method, we convert $p_{i,v}(s)$, $\alpha_i(s)$ in the spatial domain to speed and acceleration in both the spatial and temporal domains, as illustrated in **FIG. 6-2** (g)-(j). The initial headway deviation of vehicle 2 is -0.2 s, indicating that the initial headway between vehicles 1 and 2 is smaller than expected. To achieve headway equilibrium, vehicle 2 begins with a deceleration phase followed by an acceleration phase, which accounts for the vehicle's inevitable fluctuation in pace

deviation during the initial stage. As can be seen, analogous trends exist for vehicles 2, 3, and 4, with the lateral deviation, the angular deviation, and the relative angular spatial change rate remaining nearly constant. The relative moderation for vehicles 2, 3, and 4 fluctuates slightly during both acceleration processes of the leading vehicle, then quickly returns to equilibrium, and the fluctuation wave decreases as the order of platoon vehicles increases. To be more precise, while vehicle 1's speed changes as it moves, car-following vehicles 2, 3, and 4 rapidly detect these speed changes and dynamically adjust their acceleration/deceleration to maintain system equilibrium. This explains why the speed and acceleration of car-following vehicles are nearly identical to those of the leading vehicle in the space domain and imperatively shift right in the time domain, as shown in **FIG. 6-2** (g)-(j). These results demonstrate that the algorithm rapidly determines the difference between the leading and following vehicles and calculates the optimal control inputs required to dynamically achieve system equilibrium. Additionally, the infinitesimal oscillation demonstrates our proposed controller's high robustness to disturbances such as the leading vehicle's speed change and road curvature. Rather than using a time-domain approach, the proposed method can better handle disturbances that vary in space, demonstrating the proposed algorithm's superiority by incorporating road geometric attributes and leading vehicle dynamics via V2V communication.

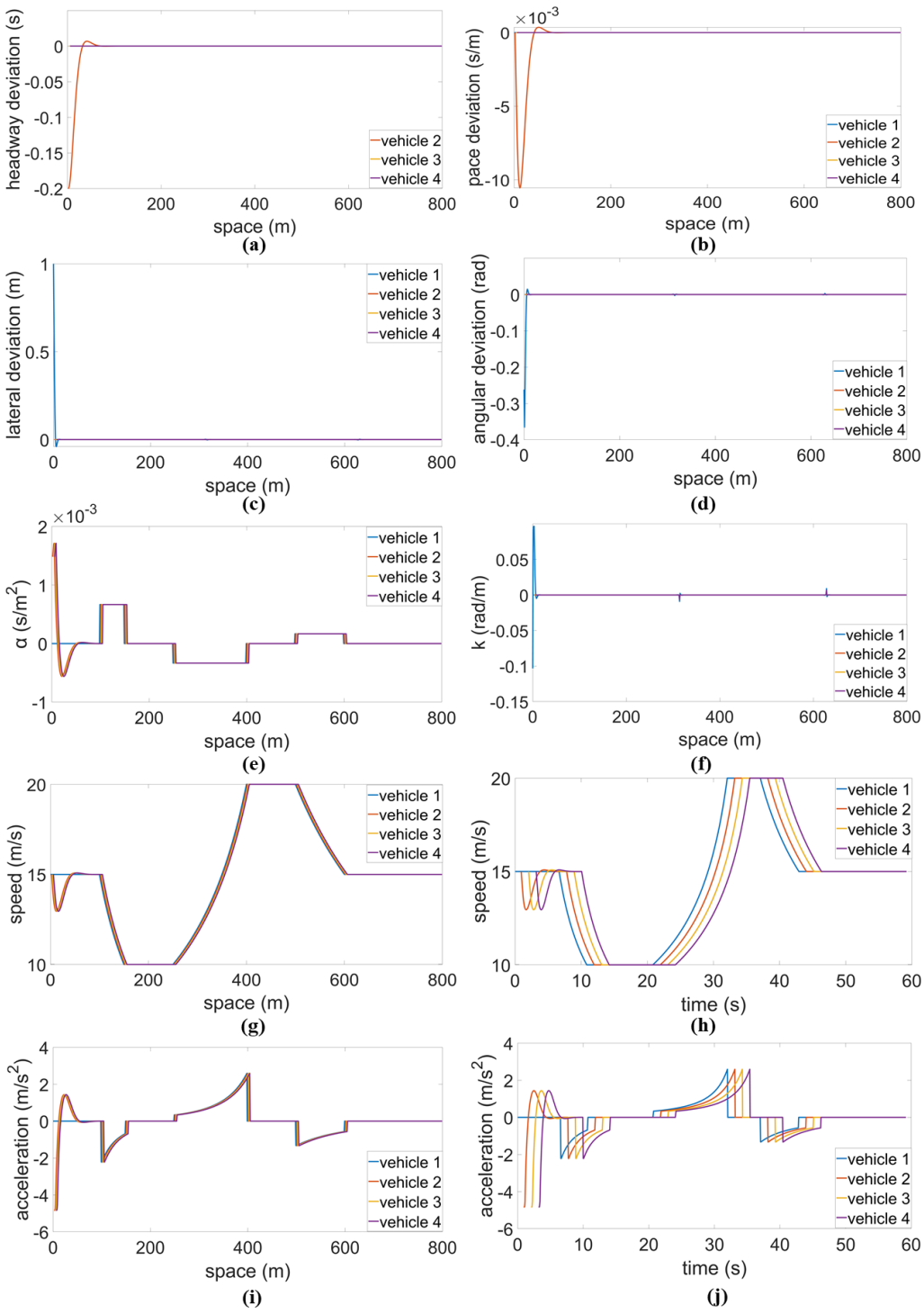

FIG. 6-2. CAVs States and controls Results with no Obstacle: (a) Headway Deviation $\Delta\tau_i(s)$; (b) Pace Deviation $\Delta p_i(s)$; (c) Lateral Deviation $r_i(s)$; (d) Angular Deviation $\psi_i(s)$; (e) Relative Moderation $\alpha_i(s)$; (f) Relative Angular Spatial Change Rate $k_i(s)$; (g) Speed in Space Domain; (h) Speed in Time Domain; (i) Acceleration in Space Domain; (j) Acceleration in Time Domain.

6.2 Scenario II: A curved road with an obstacle

The results in the preceding section demonstrate that the proposed CAV car-following strategy is efficient and stable in the absence of an obstacle. Therefore, to validate the proposed CAV car-following strategy in the presence of an obstacle, we conduct a simulation experiment using a 155 m one-lane road as shown in **FIG. 6-3** to evaluate our proposed trajectory optimization method in the presence of a 10 m obstacle located between 50 m and 60 m. During the obstacle section, $r_{m+n}^{L} = 0.5$ m and $r_{m+n}^{U} = 1.8$ m. To meet both safety and driving comfort requirements, a combined driving mode is designed that combines an obstacle avoidance driving behavior 5 meters before and during the obstacle section with an obedient driving behavior during the non-obstacle sections. The default weights are used for obedient driving, whereas the weights for obstacle avoidance driving with g_3 and g_4 are approaching zero. For the initial condition, we set the leading vehicle's lateral deviation from the lane centerline to 1 m, its angular deviation to $-\frac{\pi}{12}$ rad, and its pace deviation to 0 $\mathrm{s/m}$ (driving at a speed of 15 $\mathrm{m/s}$). Vehicle 2 starts with the majority of its states at equilibrium points except for a 0.2 s headway deviation, and vehicles 3 and 4 both start at an equilibrium state.

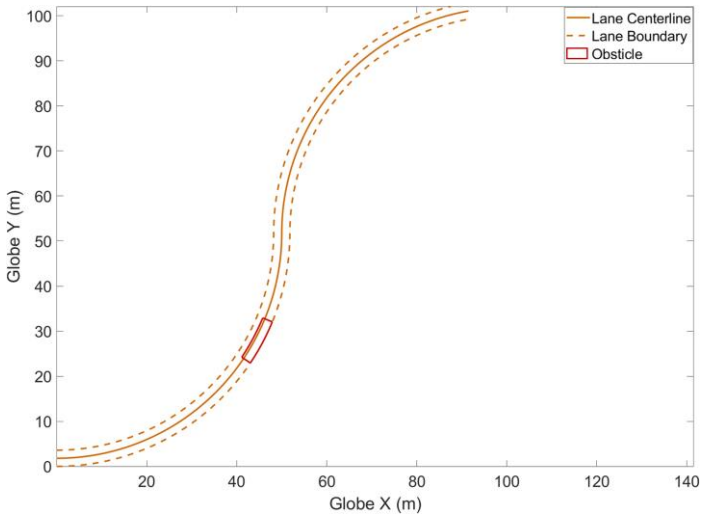

FIG. 6-3. Illustration of Road Trajectory with the Obstacle.

The results in **FIG. 6-4** clearly demonstrate how the proposed CAV car-following strategy addresses the situation that arises when an obstacle is observed. Albeit the obstacle is introduced, how the

evolution of the system state and control input change in the spatial domain, as illustrated in **FIG. 6-4** (a)-(d) and **FIG. 6-4** (e)-(f), respectively, is stable and demonstrates exceptional robustness to the obstacle. Additionally, **FIG. 6-4** (g)-(j) illustrates the evolution of speed and acceleration in both the spatial and temporal domains. Vehicle 2's initial headway deviation is 0.2 seconds, indicating that the initial headway difference between vehicles 1 and 2 is 0.2 seconds greater than expected. **FIG. 6-4** (a), (b) and (e) show that during the initial stage of achieving headway equilibrium, vehicle 2 goes through an acceleration phase followed by a deceleration phase, which accounts for the vehicle's inevitable fluctuations in pace deviation and corresponding relative moderation changes that occur during the initial stage and explains the acceleration and speed change shown in **FIG. 6-4** (g)-(j). **FIG. 6-4** (c), (d) and (f) illustrate how CAV reacts when the obstacle avoidance driving behavior is applied, the vehicles 2, 3, and 4 quickly rotate left and continue driving on the left side of the lane throughout the obstacle section, then return to the center of the lane once the obstacle section is passed. These results demonstrate that the algorithm quickly determines the difference between the obstacle section and the non-obstacle section and calculates the optimum control inputs necessary to achieve dynamic system balance. The proposed method can, instead of using a time-domain approach, manage obstacles that vary spatially and demonstrate the superiority of the proposed algorithm through the integration of the geometric road attributes and leading vehicle dynamics via V2V communication.

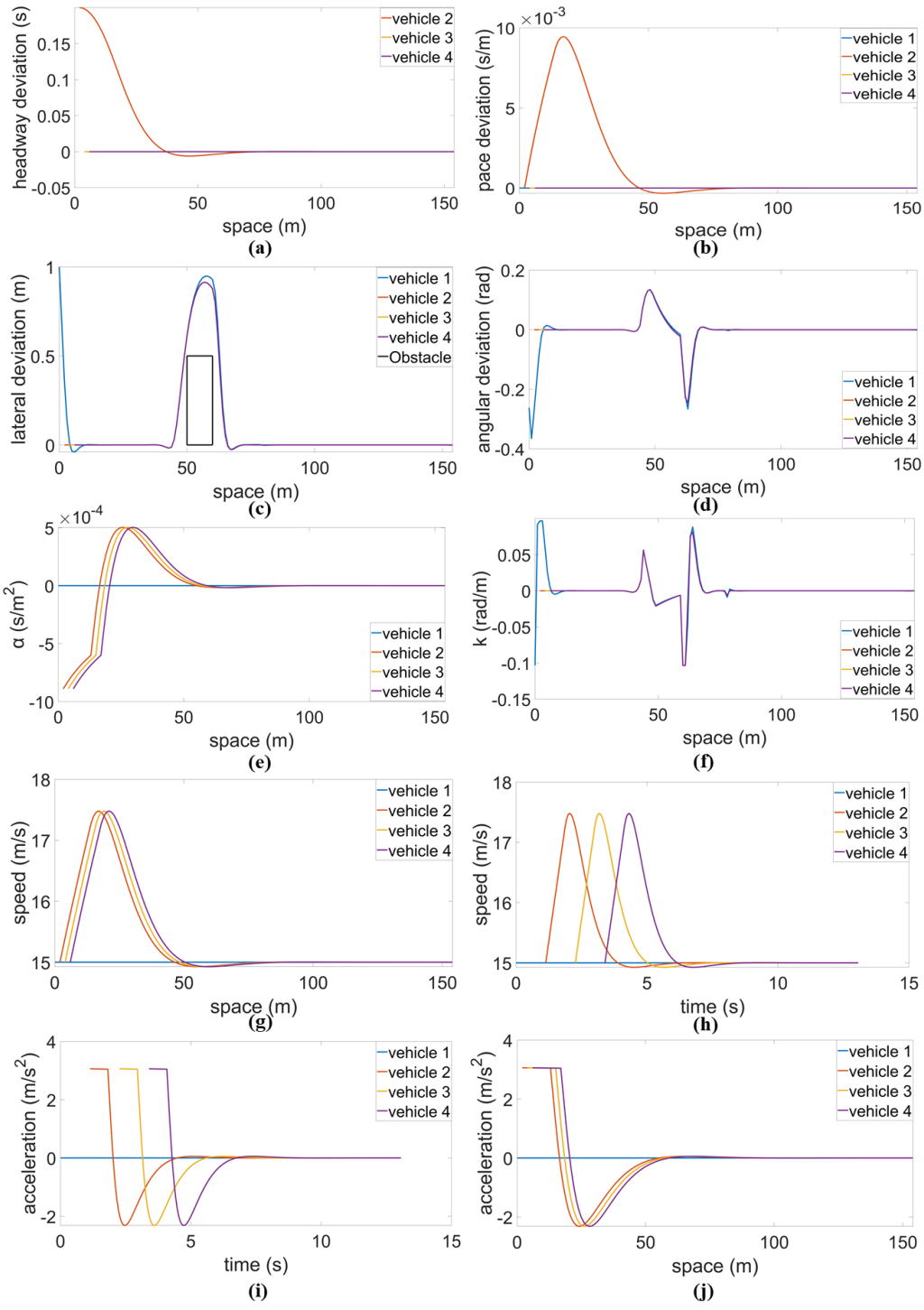

FIG. 6-4. CAVs States and controls Results with an Obstacle: (a) Headway Deviation $\Delta\tau_i(s)$; (b) Pace Deviation $\Delta p_i(s)$; (c) Lateral Deviation $r_i(s)$; (d) Angular Deviation $\psi_i(s)$; (e) Relative Moderation $\alpha_i(s)$; (f) Relative Angular Spatial Change Rate $k_i(s)$; (g) Speed in Space Domain; (h) Speed in Time Domain; (i) Acceleration in Space Domain; (j) Acceleration in Time Domain.

6.3 Scenario III: Comparison with Temporal LQR

The preceding section's results establish that the proposed CAV car-following strategy is both efficient and stable in dealing with the road situation whether a work zone exists or not. To validate the proposed CAV car-following strategy against a time-domain CAV car-following strategy, we compared our method with a temporal LQR trajectory optimization method mentioned by Chen et al. (2021). Specifically, we conduct a simulation experiment with 6 continuous curves, which all have the same radius of $\frac{60}{\pi}\ m$, as illustrated in **FIG. 6-5**. The result of the temporal LQR trajectory optimization method is the joint results of the temporal lane-keeping algorithm and temporal car-following algorithm.

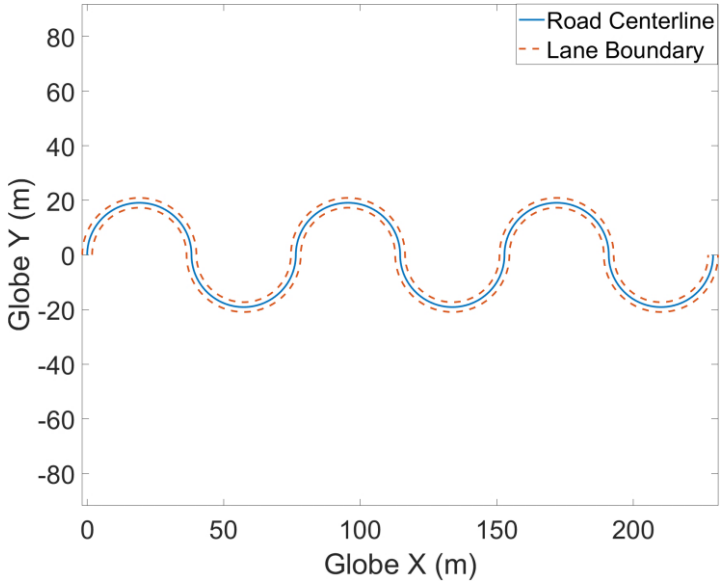

FIG. 6-5. Illustration of Road Trajectory.

To facilitate the comparison of the results of two distinct strategies, the results were transformed into the time domain, as illustrated in **FIG. 6-6**. As can be seen, both algorithms perform admirably when driving on this curvy road at a relatively low speed. However, when the vehicle speed approaches 20 m/s, the temporal LQR model's lateral and angular deviations begin to degrade, indicating that the angular speed is too fast and exceeds the angular speed boundary. Additionally, when the CAV transits from curve 3 to curve 4 at 11 seconds, the temporal LQR model's reaction lags, resulting in sharp turning decisions, thus leading to lateral control oscillation, as illustrated in **FIG. 6-6** (b)-(d), resulting in further

control failure and a 0.5 m lateral deviation. When the CAV's speed is reduced to 18 m/s, the lateral and angular control oscillations begin to subside.

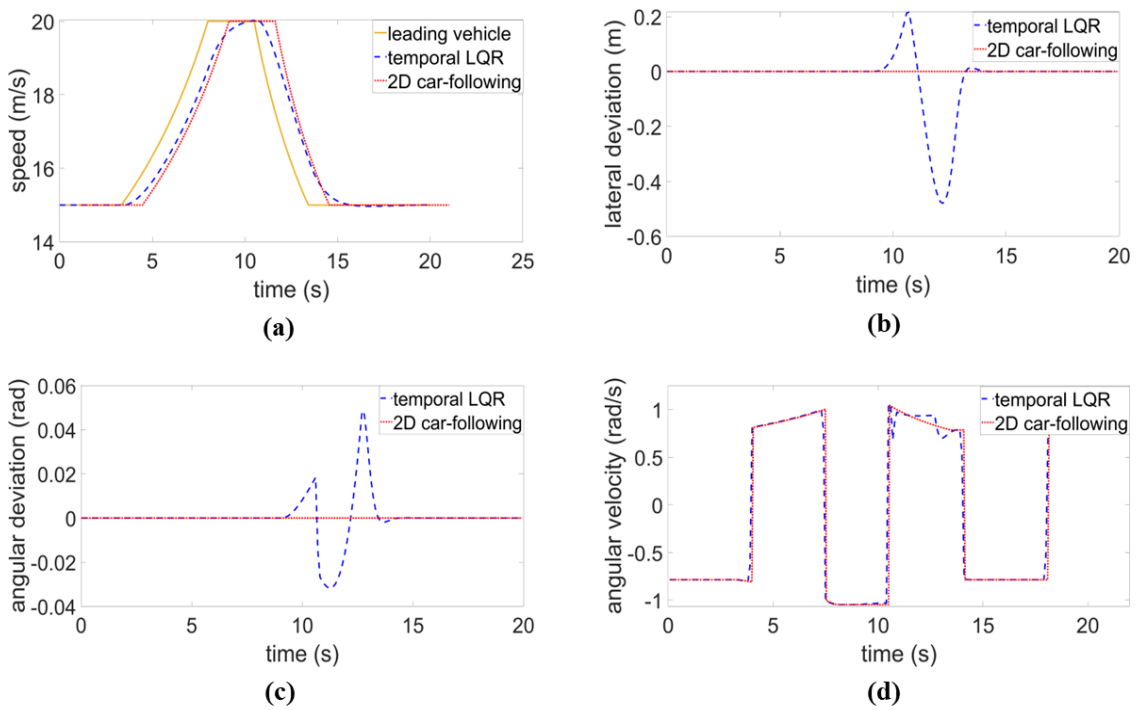

FIG. 6-6. Comparison of 2D Car-following Strategy and Temporal LQR Trajectory Optimization Method: (a) Speed; (b) Lateral Deviation $r_i(t)$; (c) Angular Deviation $\psi_i(t)$; (d) angular velocity.

In addition, we evaluate the effectiveness of our model by comparing the processing time of three different MPC horizon lengths. The proposed model runs on a 64-bit Intel i7-11800H with a 2.30 GHz CPU and 32G RAM. The calculation time is about 0.03 s/m, 0.016 s/m, and 0.007 s/m for MPC horizon lengths 80 m, 60 m, and 40 m, respectively, which suggests that our method meets real-time computation needs.

7. SYSTEM MODELLING OF LANE CHANGE STRATEGY

This chapter centers on a segment of a two-lane highway with right-hand traffic. The outer lane eventually ends over a specified distance, merging into the inner lane, which is referred to as the target lane. Vehicles, especially CAVs, are anticipated to perform a lane-changing maneuver before the outer lane terminates. We postulate that CAVs can collect data regarding traffic and road geometry from their onboard sensors, RIUs, and other CAVs. This means that CAVs possess detailed and accurate knowledge of both the road and prevailing traffic conditions. Notably, this CAV lane-changing strategy is an integration of the CAV trajectory optimization algorithm and the advanced CAV car-following strategy we proposed in the previous chapters.

7.1 State Space Formulation

In this section, we present a formulation that capitalizes on employing a spatial domain state space to articulate vehicle kinematics within a curvilinear coordinate framework drawing from the assumptions delineated above. This approach is paramount in rendering a more flexible representation of vehicle kinematics, particularly when navigating through trajectories that are not strictly linear.

The vehicle state $X_{i,m}(\mathrm{s})$ for vehicle $V_{i,w}$ at each space s as $X_{i,m}(s) = \left[t_{i,w}(s), p_{i,w}(s), r_{i,w}(s), \psi_{i,w}(s)\right]^T$. i is the lane index, $i = 1,2$; m is the vehicle index in each lane, $w = 1,2,\dots,W_i$ and W_i is the total number of vehicles in lane i; $t_{i,w}(s)$ is the time when the w^{th} vehicle in lane i arrives space s; $p_{i,w}(s)$ is the reciprocal of the vehicular speed of the w^{th} vehicle in lane i; $r_{i,w}(s)$ is the lateral deviation of the w^{th} vehicle in lane i, which equals to signed orthogonal distance from the CAV to the closest point on the lane centerline; $\psi_{i,w}(s) = \theta_{i,w}(s) - \theta_{des}(s)$, where $\psi_{i,w}(s)$ is the angular deviation of the m^{th} vehicle in lane i, $\theta_{i,w}(s)$ is the angle between the CAV heading and the x-axis in the global frame and $\theta_{des}(s)$ is the angle between the tangent of the lane centerline and the x-axis in the global frame as **FIG. 7-1**.

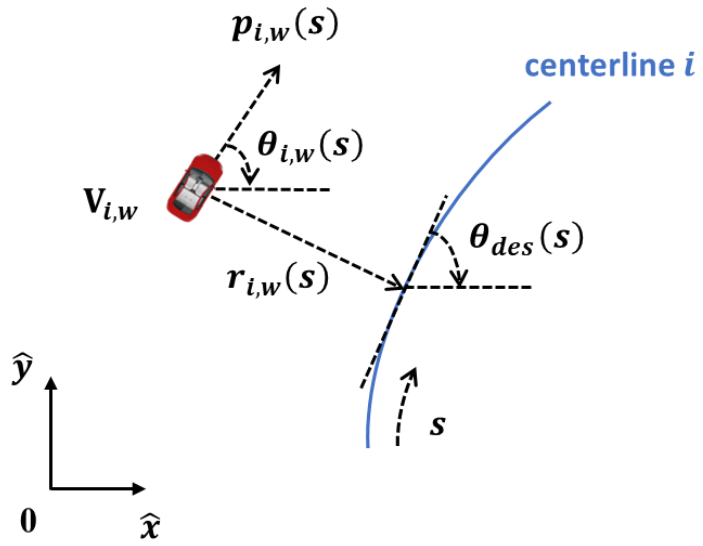

FIG. 7-1. Illustration of Vehicles Kinematics on the Curvilinear Coordination.

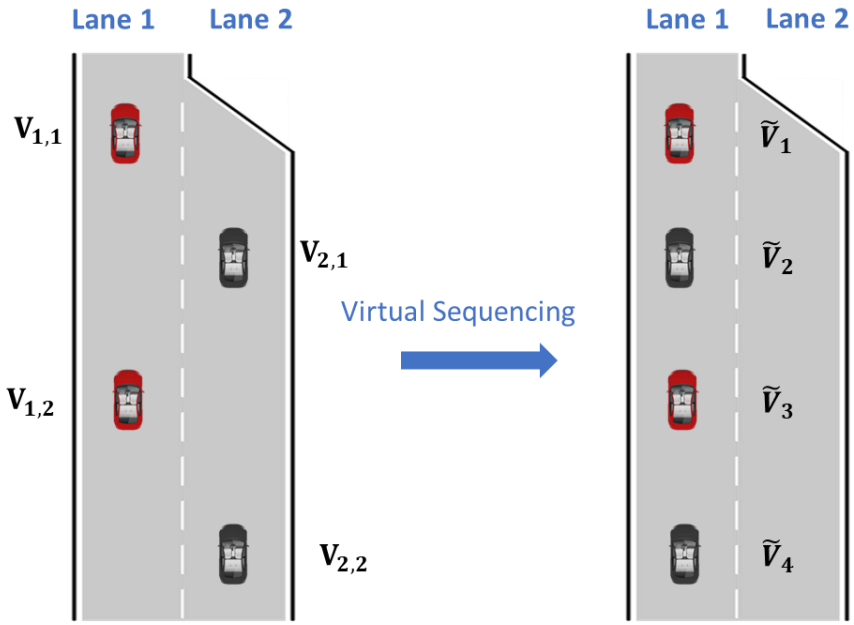

FIG. 7-2. Illustration of Virtual Sequencing.

Leveraging the state information of the vehicles, we introduce the concept of 'virtual sequencing'. This process, crucial for defining the sequence of lane-changing vehicles, can be conceptualized as identifying the optimal car-following order within a virtual lane guided by a predefined law. The key benefit of this maneuver is the significant reduction in modeling complexity it offers, essentially transforming the mandatory lane-changing problem into a 'virtual' car-following problem as **FIG. 7-2**. A notably simple yet effective strategy within this framework involves sorting the car-following

sequence based on the vehicles' arrival time to the point s. Adopting this approach facilitates a more efficient and streamlined lane-changing process.

Let $I_1 = \begin{bmatrix} 1 \\ \vdots \\ W_1 \end{bmatrix}$ and $I_2 = \begin{bmatrix} 1 \\ \vdots \\ W_2 \end{bmatrix}$, we can combine and number all vehicle in the virtual lane and get new vehicle states at point s in the virtual lane as

$$\tilde{X}_j(s) = f\left[X_{I_1}(s), X_{I_2}(s)\right]. \tag{36}$$

According to the arrival time of the CAVs at point s, we can swiftly determine the virtual car-following and lane-changing sequences on the virtual lane. This is achieved by the sorting function f that sorts the variable $t_j(s)$ in a monotonically descending order. To be noted that, in cases where two vehicles reach point s simultaneously, the function would sequence them based on their pace. This precision ensures the method retains its efficacy even in the face of such potential coincidences.

Consider a virtual platoon of vehicles indexed by $j = 1, 2, \dots, K$ with the lead vehicle indexed by 1. The notation with subscript j will denote the vehicle j after sequencing. On the basis of the aforementioned assumptions, we give a formulation by a spatial domain state pace to describe the vehicle kinematics of the cooperative lane-changing and car-following behavior in the virtual lane, given information about the leading vehicle. For any vehicle j, we define its adjusted system state for each space s as $\tilde{Y}_j(s) = \left[\tilde{\tau}_j(s) + \tau^*,\ \tilde{p}_{j-1}(s - l_s) - \tilde{p}_j(s),\ \tilde{r}_j(s),\ \tilde{\psi}_j(s)\right]^T$, where $\tilde{\tau}_j(s) = \tilde{t}_{j-1}(s - l_s) - \tilde{t}_j(s)$ is the headway between vehicle j and vehicle $j-1$ and l_s is the safe distance when vehicles are standstill and τ^* is the desired headway.

By above definition, the vehicle dynamics can be modeled as a nonlinear system with respect to distance s as

$$\frac{d\tilde{Y}_j(s)}{ds} = \begin{bmatrix} \tilde{p}_{j-1}(s-l_s) - \tilde{p}_j(s) \\ \tilde{\alpha}_{j-1}(s-l_s) - \tilde{\alpha}_j(s) \\ sin\left(\tilde{\psi}_j(s)\right) \\ \tilde{k}_j(s) \end{bmatrix}. \quad (37)$$

Here, $\tilde{\alpha}_j(s)$ is the derivative of pace (on the contrary to the acceleration as the derivative of speed, $\tilde{\alpha}_j(s) < 0$ indicates the vehicle is accelerating). $\tilde{k}_j(s) = \tilde{k}_{j,v}(s) - \tilde{k}_{des}(s)$, where $\tilde{k}_{j,v}(s)$, $\tilde{k}_{des}(s)$ is the curvature of the CAV's path and the centerline, respectively. Since $\tilde{k}_{des}(s)$ is given by the road geometry in advance, we do not explicitly write it out for $\tilde{k}_j(s)$ due to model convenience. Note that $\tilde{\alpha}_j(s)$ and $\tilde{k}_j(s)$ are the decomposed control of the system (one dimension is for the pace and the other one is for turning), represented as $\tilde{U}_j(s) = \left[\tilde{\alpha}_{j-1}(s-l_s) - \tilde{\alpha}_j(s),\ \tilde{k}_j(s)\right]^T$.

To be note that for the leading vehicle lane-changing problem, which is when vehicle *j* is the leading vehicle without any preceding vehicle, the system state becomes $\tilde{Y}_j(s) = \begin{bmatrix} \tilde{p}_{des}(s) - \tilde{p}_j(s) \\ \tilde{r}_j(s) \\ \tilde{\psi}_j(s) \end{bmatrix}$ with control state $\tilde{U}_j(s) = \begin{bmatrix} \tilde{\alpha}_{des}(s) - \tilde{\alpha}_j(s) \\ \tilde{k}_j(s) \end{bmatrix}$. Where $\tilde{p}_{des}(s)$ is the reciprocal of the road speed limit and $\tilde{\alpha}_{des}(s)$ is the parameter indicating acceleration of the road speed limit.

When $\psi_i(s)$ is small, we have $sin(\psi_i(s)) \approx \psi_i(s)$ according to small angle approximation, and the state-space model of Eq. (37) can be approximated as

$$\frac{d\tilde{Y}_j(s)}{ds} = A\tilde{Y}_j(s) + B\tilde{U}_j(s), \quad (38)$$

where $A = \begin{bmatrix} 0 & 1 & 0 & 0 \\ 0 & 0 & 0 & 0 \\ 0 & 0 & 0 & 1 \\ 0 & 0 & 0 & 0 \end{bmatrix}$, $B = \begin{bmatrix} 0 & 0 \\ 1 & 0 \\ 0 & 0 \\ 0 & 1 \end{bmatrix}$.

7.2 Mixed-integer Programming Based MPC Formulation and Implementation

In this section, we present the MPC formulation of our approach. This choice is motivated by the

inherent capabilities of MPC to handle system state and control constraints in a systematic manner. Further, its rolling horizon implementation offers robustness against system disturbances. This balance between predictive modeling and real-time adjustments allows the MPC approach to perform effectively in dynamic and uncertain environments.

7.3 Mixed-integer programming based MPC

We introduce several additional notations to enhance the understanding of the MPC algorithm. First, we use superscript (c, m) to denote variables computed at the moving window starting from m. Additionally, superscript r is used to represent variables that have already been realized. For example, $\tilde{Y}_j^{c,m}(m)$ denotes the system state to be computed at location m, with a moving window initiating from m.

To realistically represent control frequency as experienced in the real world, we segment the prediction horizon into N steps and discretize the optimal control problem along the s-axis. To discretize control inputs, we employ the ZOH technique. Specifically, at each spatial update interval Δs, the control input is assumed to remain constant. When Δs is sufficiently small, this discretization process can be approximated as a continuous system.

$$\tilde{Y}_{j,s+\Delta s}^{c,m} \approx A_d \tilde{Y}_{j,s}^{c,m} + B_d \tilde{U}_{j,s}^{c,m} \; \forall s \in \{m, m+\Delta s, \dots, m+N-\Delta s\}, \tag{39}$$

where, $A_d = e^{A\Delta s} = \begin{bmatrix} 1 & \Delta s & 0 & 0 \\ 0 & 1 & 0 & 0 \\ 0 & 0 & 1 & \Delta s \\ 0 & 0 & 0 & 1 \end{bmatrix}$, $B_d = \int_0^{\Delta s} e^{A\gamma} d\gamma B = \begin{bmatrix} \frac{\Delta s^2}{2} & 0 \\ \Delta s & 0 \\ 0 & \frac{\Delta s^2}{2} \\ 0 & \Delta s \end{bmatrix}$, and Δs is the discretization step.

Thus, we define the state set to be computed $\mathcal{Y}_{j,m}^c = \left\{ \tilde{Y}_{j,s}^{c,m} \middle| s \in \{m, m+\Delta s, \dots, m+N\} \right\}$ to be the predicted future states for vehicle j obtained at location m with a moving window spanning from m to $m+N$. Furthermore, we define the realized state set $\mathcal{Y}_{j,m}^r = \left\{ \tilde{Y}_{j,s}^r \middle| s \in \{0, \Delta s, \dots, m\} \right\}$ to capture all the realized states of vehicle i at location m. Particularly, $\tilde{Y}_{j,0}^r$ signifies the initial state inputs, and $\tilde{Y}_{j,s}^r =$

$\tilde{Y}_{j,s}^{c,s}$ is always maintained. In a similar manner, we define the predicted control set $\mathcal{U}_{j,m}^{c} = \left\{\tilde{U}_{j,s}^{c,m} \middle| s \in \{m, m+\Delta s, \dots, m+N-\Delta s\}\right\}$ to be the computed future control sequences for vehicle j obtained at location m, and $\mathcal{U}_{j,m}^{r} = \left\{\tilde{U}_{j,s}^{r} \middle| s \in \{0, \Delta s, \dots, m\}\right\}$ to be its realized control sequences, where $\tilde{U}_{j,s}^{r} = \tilde{U}_{j,s}^{c,s}$.

We can define the discretized optimal control problem that includes both control efficiency and driving smoothness as follows:

$$J = min\left\{\begin{array}{c}\left(\tilde{Y}_{j,m+N}^{c,m}\right)^{T} Q_{m+N} \tilde{Y}_{j,m+N}^{c,m} + \\ \sum_{s=m}^{m+N-1}\left(\left(\tilde{Y}_{j,s}^{c,m}\right)^{T} G_s \tilde{Y}_{j,s}^{c,m} + \left(\tilde{U}_{j,s}^{c,m}\right)^{T} L_s \tilde{U}_{j,s}^{c,m}\right)\end{array}\right\} \tag{40a}$$

$s.t.$

$$\tilde{Y}_{j,s+\Delta s}^{c,m} \approx A_d \tilde{Y}_{j,s}^{c,m} + B_d \tilde{U}_{j,s}^{c,m} \; \forall s \in \{m, m+1, \dots, m+N-1\}, \tag{40b}$$

$$\tilde{Y}_{j,m}^{c,m} = \tilde{Y}_{j,m}^{r}, \tag{40c}$$

$$\tilde{U}_{j,m}^{c,m} = \tilde{U}_{j,m}^{r}, \tag{40d}$$

$$\tilde{Y}_{j,s}^{c,m} \in \tilde{\mathbb{Y}}_{j,s} \; \forall s \in \{m, m+\Delta s, \dots, m+N\}, \tag{40e}$$

$$\tilde{U}_{j,s}^{c,m} \in \tilde{\mathbb{U}}_{j,s} \; \forall s \in \{m, m+\Delta s, \dots, m+N-\Delta s\}. \tag{40f}$$

Eq. (40c) is the initial condition and Eq. (40e) is the state constraint applied to each space point regulating the transition between states of a vehicle. The constraint in Eq. (40f) is the constraint ensuring that the steering wheel and acceleration/deceleration commanded by the algorithm remain within a suitable range of $\tilde{U}_{j,s}$. The diagonal coefficients matrices G_s, L_s, and Q_{m+N} are all positive definite, and they are typically designed in the manner of the diagonal matrix below:

$$G_s = \begin{bmatrix} g_1 & & & \\ & g_2 & & \\ & & g_{3,s} & \\ & & & g_4 \end{bmatrix}, g_1, g_2, g_{3,s}, g_4 > 0, \tag{41a}$$

$$L_s = \begin{bmatrix} l_1 & \\ & l_2 \end{bmatrix}, l_1, l_2 > 0, \tag{41b}$$

$$Q_{m+N} = \begin{bmatrix} q_1 & & & \\ & q_2 & & \\ & & q_{3,m+N} & \\ & & & q_4 \end{bmatrix}, q_1, q_2, q_{3,m+N}, q_4 > 0. \tag{41c}$$

It should be noted that all diagonal coefficient matrices are set to a fixed coefficient, except for $g_{3,s}$ and $q_{3,m+N}$, which are dynamically determined by a function as below:

$$g_{3,s} = e^{\alpha\left(s - \frac{O_b + O_e}{2}\right)}, \tag{42a}$$

$$q_{3,m+N} = \beta e^{\alpha\left(m+N - \frac{O_b + O_e}{2}\right)}. \tag{42b}$$

O_b is the spatial point where the merging lane physically starts shrinking, O_e is the spatial point where the merging lane fully ends. Eqs. (42) are adopted to balance the merge lane utilization by α and β. We assign less weight to lane-changing decisions when vehicles are farther from the lane ending point, to maintain passenger comfort. Conversely, as vehicles approach the lane ending point, we assign more weight to lane-changing decisions, to prioritize safety.

Considering collision-free limitations, steering wheel rotation, and acceleration/deceleration limits, the state constraints for the CAV at location m are as follows:

$$C\tilde{Y}_{j,s}^{c,m} \leq h_{min,s} \; \forall s \in \{m, m + \Delta s, \dots, m + N\}, \tag{43a}$$

$$D\tilde{Y}_{j,s}^{c,m} \leq \tilde{p}_{j-1,s-l_s} - \tilde{p}_{des,s} \; \forall s \in \{m, m + \Delta s, \dots, m + N\} \tag{43b}$$

$$\tilde{r}_{j,s}^{L} \leq E\tilde{Y}_{j,s}^{c,m} \leq \tilde{r}_{j,s}^{R} \; \forall s \in \{m, m + \Delta s, \dots, m + N\}, \tag{43c}$$

$$\tilde{\psi}_{j,min} \leq F\tilde{Y}_{j,s}^{c,m} \leq \tilde{\psi}_{j,max} \; \forall s \in \{m, m + \Delta s, \dots, m + N\}, \tag{43d}$$

$$\tilde{\alpha}_{j-1,s-l_s} + \tilde{a}_{j,min}\tilde{p}_{j,s}^3 \le M\tilde{U}_{j,s}^{c,m} \le \tilde{\alpha}_{j-1,s-l_s} + \tilde{a}_{j,max}\tilde{p}_{j,s}^3 \ \forall s \in \{m, m+\Delta s, \dots, m+N-\Delta s\}, \tag{43e}$$

$$-\frac{1}{\tilde{R}_{j,min}} - k_{des,s} \le N\tilde{U}_{j,s}^{c,m} \le \frac{1}{\tilde{R}_{j,min}} - k_{des,s} \ \forall s \in \{m, m+\Delta s, \dots, m+N-\Delta s\}. \tag{43f}$$

Eq.(43a) is the constraint to make sure that there will be no collision between vehicle j and its virtual lane preceding vehicle (not necessary for leading vehicle lane changing problem), where $h_{min,s}$ is the minimum headway allowed at point s and $C = [1,0,0,0]$; Eq. (43b) is the constraint that the vehicle j does not exceed the speed limit, $\tilde{p}_{des,s}$ is the reciprocal of the road speed limit and $D = [0,1,0,0]$; Eq. (43c) is the constraint imposed on the vehicle j to ensure that it stays within the proper lane, where $E = [0,0,1,0]$, and $\tilde{r}_{j,s}^R$ is the maximum right lateral deviation following $\tilde{r}_{j,s}^R = \begin{cases} \frac{3}{2}r_{max}, & s \le O_b \\ \frac{r_{max}}{2} + L_w, & O_b \le s \le O_e \\ \frac{r_{max}}{2}, & s \ge O_e \end{cases}$. $\tilde{r}_{j,s}^L$ is the maximum left lateral deviation, following $\tilde{r}_{j,s}^L = -\frac{r_{max}}{2}$. r_{max} is the lane width and L_w is the actual lane width while lane shrinking; Eq. (43d) is used to impose the vehicle's permissible angular deviation's physical restrictions, where $F = [0,0,0,1]$, $\tilde{\psi}_{j,min}$ and $\tilde{\psi}_{j,max}$ specify the allowable angular deviation's lower and upper bounds; Eq. (43e) is the constraint to ensure that the vehicle's actual acceleration/deceleration is within the vehicle's physical limits, where $M = [1,0]$, $\tilde{a}_{j,max}$ is the vehicle j's maximum acceleration and $\tilde{a}_{j,min}$ is the vehicle j's maximum deceleration limits; Eq. (43f) is the constraint that the vehicle j's actual moving path is constrained by a specified minimum turning radius, where $N = [0,1]$, $R_{i,min}$ is the minimum turning radius of the vehicle j.

In fact, many constraints in Eqs. (43) are not explicit due to their nonlinearity. We will provide reformulations for them so that the resulted programming problem can be solved by solvers.

There are two different situations for Eq.(43a), depending on whether two vehicles are within the same lane: (i) If two vehicles are within the same lane, the headway deviation between two vehicles will follow car-following constraint; (ii) Otherwise, the headway deviation will not be constrained as long

as vehicle j does not exceed vehicle $j-1$ to ensure the sequencing consistency. These two different situations are shown as:

i If $\left(E\tilde{Y}^{r}_{j-1,s-l_s}-\frac{r_{max}}{2}\right)*\left(E\tilde{Y}^{c,m}_{j,s}-\frac{r_{max}}{2}\right)\geq 0$, we have $h_{min,s}=\tau_{min}$.

ii Otherwise, we have $h_{min,s}=\tau^{*}$.

τ_{min} is the minimum car-following headway. To formulate these two different situations more canonically, we introduce indicator binary variable $b_s\in\{0,1\}$ and V be a positive big number:

Suppose $b_s=1$ requires $\left(E\tilde{Y}^{r}_{j-1,s-l_s}-\frac{r_{max}}{2}\right)*\left(E\tilde{Y}^{c,m}_{j,s}-\frac{r_{max}}{2}\right)\geq 0$, which can be expressed as

$$\left(E\tilde{Y}^{r}_{j-1,s-l_s}-\frac{r_{max}}{2}\right)*\left(E\tilde{Y}^{c,m}_{j,s}-\frac{r_{max}}{2}\right)\geq (b_s-1)*V, \tag{44a}$$

Furthermore, suppose $b_{1,s}=0$ requires $\left(E\tilde{Y}^{r}_{j-1,s-l_s}-\frac{r_{max}}{2}\right)*\left(E\tilde{Y}^{c,m}_{j,s}-\frac{r_{max}}{2}\right)\leq 0$, which can be expressed as

$$\left(E\tilde{Y}^{r}_{j-1,s-l_s}-\frac{r_{max}}{2}\right)*\left(E\tilde{Y}^{c,m}_{j,s}-\frac{r_{max}}{2}\right)\leq b_s*V, \tag{44b}$$

By combining Eqs. (44a) and (44b), Eq.(43a) can be reformulated as

$$C\tilde{Y}^{c,m}_{j,s}\leq b_s*\tau_{min}+(1-b_s)*\tau^{*}. \tag{44c}$$

There are three different situations for vehicle j under Eq. (43c): (i) If vehicle $j-1$ is at target lane and meanwhile the headway deviation of vehicle j exceeds the maximum car-following headway deviation, vehicle j cannot change lane; (ii) If vehicle $j+1$ is at target lane and the headway deviation of vehicle $j+1$ exceeds the maximum allowance of car-following headway deviation, then vehicle j cannot change lane; (iii) Otherwise, vehicle j can make lane change. These three different situations are shown as:

i If $E\tilde{Y}^{r}_{j-1,s-l_s}-\frac{r_{max}}{2}\leq 0, C\tilde{Y}^{c,m}_{j,s}-\tau_{min}\geq 0$, we have $\tilde{r}^{L}_{j,s}=\frac{r_{max}}{2}$.

ii If $E\tilde{Y}^{c,m}_{j+1,s+l_s}-\frac{r_{max}}{2}\leq 0, C\tilde{Y}^{c,m}_{j+1,s+l_s}-\tau_{min}\geq 0$, we have $\tilde{r}^{L}_{j,s}=\frac{r_{max}}{2}$.

iii Otherwise, $\tilde{r}_{j,s}^{L} = -\frac{r_{max}}{2}$.

To further formulate the problem as a canonical format, we introduce binary variables $z_{1,s}, z_{2,s}, z_{3,s}, z_{4,s}, z_{5,s}, z_{6,s}$, and $z_s \in \{0,1\}$, by defining:

$z_{1,s} = 1$ if $E\tilde{Y}_{j-1,s-l_s}^{r} - \frac{r_{max}}{2} \leq 0$ and $z_{2,s} = 1$ if $C\tilde{Y}_{j,s}^{c,m} - \tau_{min} \geq 0$, which can be expressed as:

$$-z_{1,s} * V \leq E\tilde{Y}_{j-1,s-l_s}^{r} - \frac{r_{max}}{2} \leq (1 - z_{1,s}) * V, \tag{45a}$$

$$(z_{2,s} - 1) * V \leq C\tilde{Y}_{j,s}^{c,m} - \tau_{min} \leq z_{2,s} * V, \tag{45b}$$

$z_{3,s} = 1$ if $z_{1,s} = z_{2,s} = 1$.

$z_{4,s} = 1$ if $E\tilde{Y}_{j-1,s-l_s}^{r} - \frac{r_{max}}{2} \leq 0$ and $z_{5,s} = 1$ if $C\tilde{Y}_{j,s}^{c,m} - \tau_{min} \geq 0$, which can be expressed as:

$$-z_{4,s} * V \leq E\tilde{Y}_{j+1,s+l_s}^{c,m} - \frac{r_{max}}{2} \leq (1 - z_{4,s}) * V, \tag{45c}$$

$$(z_{5,s} - 1) * V \leq C\tilde{Y}_{j+1,s+l_s}^{c,m} - \tau_{min} \leq z_{5,s} * V, \tag{45d}$$

$z_{6,s} = 1$ if $z_{4,s} = z_{5,s} = 1$ and $z_s = 1$ for either $z_{3,s} = 1$ or $z_{6,s} = 1$.

Based on that, Eq. (43c) can be reformulated as:

$$z_s * \frac{r_{max}}{2} + (z_s - 1) * \frac{r_{max}}{2} \leq E\tilde{Y}_{j,s}^{c,m}. \tag{45e}$$

7.4 Bi-directional communication topology and MPC implementation scheme

To ensure the robustness of trajectory planning against the disturbance, we designed a bi-directional communication topology as well as an implementation scheme by modifying the work before. As depicted in **FIG. 7-3**, each vehicle utilizes information from its leading and (virtually) following vehicles to perform sequential CAV control within the virtual platoon. Note that, the mixed integer based MPC is formulated in spatial domain, whereas we need to implement it in the time domain since we cannot utilize the information that either not known or not computed. At a given time point t, vehicle

j utilizes recorded data from its following vehicle $j+1$ received at time $t-1$ and real-time data from its leading vehicle $j-1$. Then vehicle j will transmit its anticipated movement to both vehicles $j-1$ and $j+1$. This process is repeated until the end of the platooning.

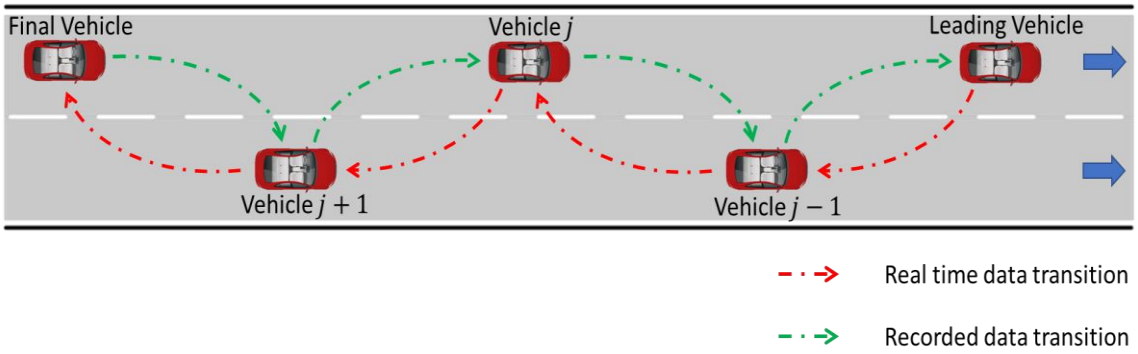

FIG. 7-3. Bi-directional Information Topology.

The proposed algorithm leverages the most recent data from both its leading and following vehicles, enabling sequential CAV control within the platoon. By utilizing the latest data, the algorithm enhances the efficiency of the lane-changing planning, as exemplified in **Algorithm 2**.

Algorithm 2 Bi-directional Vehicle Control Scheme for Each Vehicle

---

1: at space point m_j, for vehicle j update and record the time t

2: if $j=1$, compute and record $\mathcal{U}^c_{j,m_j}, \mathcal{Y}^c_{j,m_j}$ using the predicted information of its following vehicle $[\tilde{Y}^c_{j+1,m_j+l_s}, \dots, \tilde{Y}^c_{j+1,m_{j+1}+N}]$; If $1<j<K$, find m_{j-1} at time t, for $m_j \le m_{j-1}+l_s-N$: compute and record $\mathcal{U}^c_{j,m_j}, \mathcal{Y}^c_{j,m_j}$ using the predicted information of its following vehicle $[\tilde{Y}^c_{j+1,m_j+l_s}, \dots, \tilde{Y}^c_{j+1,m_{j+1}+N}]$ and the realized information of its leading vehicle $[\tilde{Y}^r_{j-1,m_j-l_s}, \dots, \tilde{Y}^r_{j-1,m_j+N-l_s}]$; otherwise: compute and record $\mathcal{U}^c_{j,m_j}, \mathcal{Y}^c_{j,m_j}$ using the predicted information of its following vehicle $[\tilde{Y}^c_{j+1,m_j+l_s}, \dots, \tilde{Y}^c_{j+1,m_{j+1}+N}]$ and the realized information of its leading vehicle $[\tilde{Y}^r_{j-1,m_j-l_s}, \dots, \tilde{Y}^c_{j-1,m_j+N-l_s}]$; If $j=K$, find m_{j-1} at time t, for $m_j \le m_{j-1}+l_s-N$: compute and record $\mathcal{U}^c_{j,m_j}, \mathcal{Y}^c_{j,m_j}$ using the realized information of its leading

vehicle $[\tilde{Y}^r_{j-1,m_j-l_s}, \dots, \tilde{Y}^r_{j-1,m_j+N-l_s}]$; otherwise: compute and record $\mathcal{U}^c_{j,m_j}, \mathcal{Y}^c_{j,m_j}$ the realized information of its leading vehicle $[\tilde{Y}^r_{j-1,m_j-l_s}, \dots, \tilde{Y}^c_{j-1,m_j+N-l_s}]$;

3: Update $\hat{\mathcal{Y}}^c_{j,s_j} = [\tilde{Y}^r_{j,0}, \dots, \tilde{Y}^r_{j,m_j}, \tilde{Y}^c_{j,m_j+\Delta s}, \dots, \tilde{Y}^c_{j,m_j+N}]$, $\hat{\mathcal{U}}^c_{j,s_j} = [\tilde{U}^r_{j,0}, \dots, \tilde{U}^r_{j,m_j}, \tilde{U}^c_{j,m_j+\Delta s}, \dots, \tilde{U}^c_{j,m_j+N-\Delta s}]$;

4 if $j > 1$, transmit $\mathcal{Y}^c_{j,m_j}$ to vehicle $j-1$;

5: if $j < K$, transmit $\hat{\mathcal{Y}}^c_{j,m_j}, \hat{\mathcal{U}}^c_{j,m_j}$ to vehicle $j+1$;

6: implement $\tilde{U}^r_{j,m_j}$;

Our implementation scheme together with spatial formulation, distinct from the traditional real-time based approach (Zhou et al., 2017; Zhou et al., 2019), uses spatial formulation. The control, as per Eqs. (40), relies on both recorded and predicted leading vehicle information according to real-time distance. The leading vehicle always sends its realized and predicted state sequences to its following vehicle and the following vehicle will auto detect which information it needs. If the leading vehicle is less than $N - l_s$ meters ahead, the following vehicle will use a total of N meters of joint state sequences. The following vehicle calculates its trajectory using these and shares its future predicted states (**FIG. 7-4** (a)). If the leading vehicle is more than $N - l_s$ meters ahead, the following vehicle will use all realized state sequences to calculate its trajectory and share predicted states (**FIG. 7-4** (b)). The time domain MPC system (**FIG. 7-4** (c)) transmits recent lead vehicle data, potentially causing communication delay issues leading to inaccurate control and accidents. The spatial domain approach proves more robust against communication failures (Zhang et al., 2021) and is preferable for platoons negotiating curvy roads.

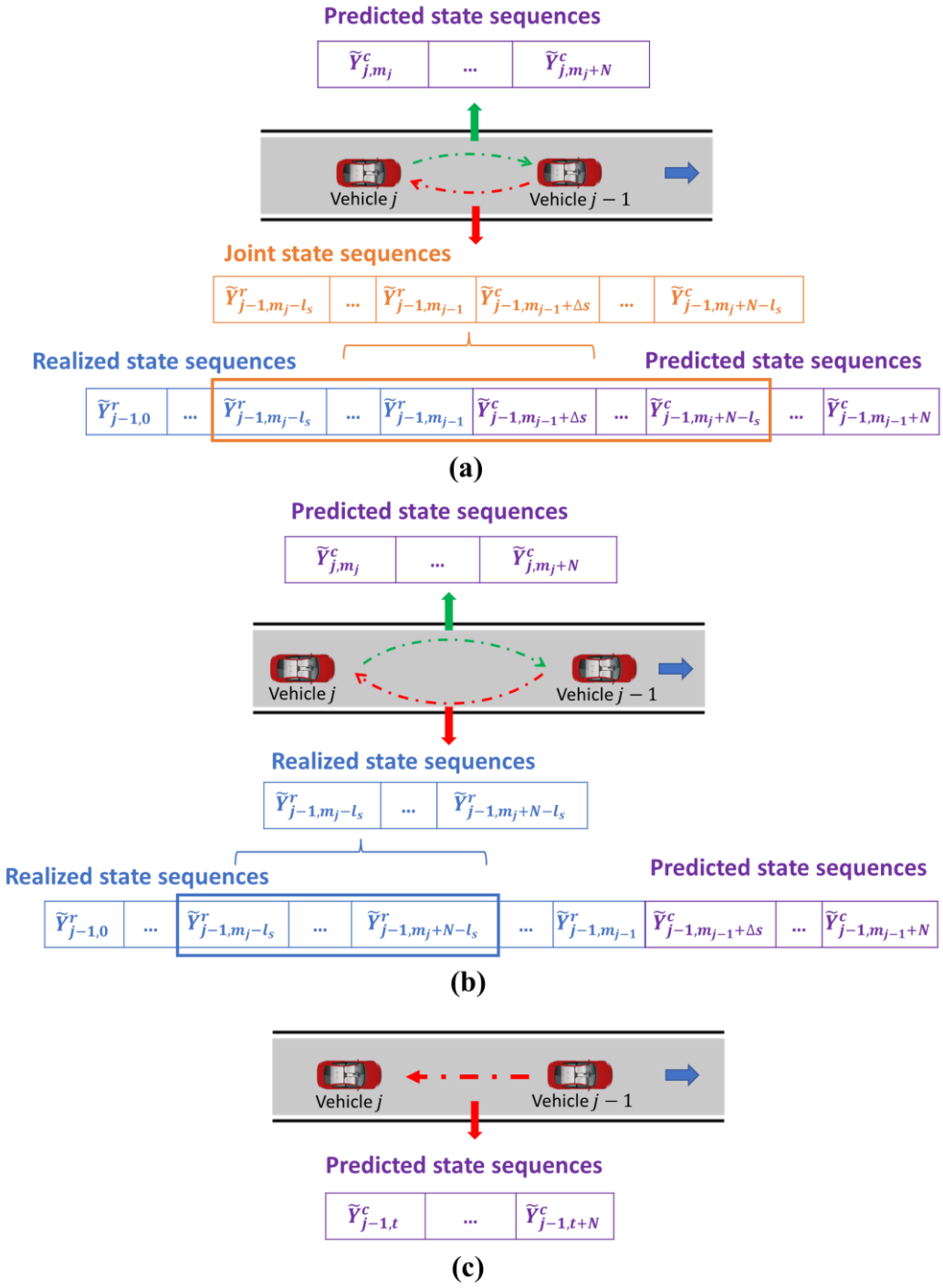

FIG. 7-4. V2V Information Transmission and Selection: (a) Close Distance under Space Domain; (b) Far Distance under Space Domain; (c) Under Time Domain.

8. NUMERICAL SIMULATION RESULT OF LANE-CHANGING STRATEGY

To demonstrate the effectiveness of the proposed method, a series of numerical simulation experiments were carried out using the Python programming language. Given the spatially dependent nature of our algorithm, each following vehicle requires data of its leading vehicle extending l_s meters ahead of the starting point for safety concerns (if vehicle 1 starts from point 0 m, vehicle 2 starts from point l_s meters). The parameters utilized for the trajectory planning of the CAVs are comprehensively detailed in **Table 8-1**. These settings were carefully chosen to optimize the performance of our algorithm and represent a comprehensive set of realistic driving conditions. We have designed three distinct traffic scenarios: uncongested traffic, uncongested traffic with obstacle presence, and congested traffic. These scenarios aim to evaluate the efficiency of our proposed trajectory planning algorithm in managing mandatory lane-changing, addressing unexpected disruptions, and minimizing collision risks.

Table 8-1. Default Parameters for Vehicle Lane-changing

Parameters	Value
τ^*	$1\ s$
τ_{min}	$0.5\ s$
l_s	$2\ m$
$\tilde{p}_{des,s}$	$1/20\ s/m$
$\tilde{\alpha}_{des,s}$	$0\ s/m^2$
r_{max}	$3.6\ m$
Δs	$1\ m$
N	20
$\tilde{R}_{j,min}$	$10\ m$

$\tilde{\psi}_{j,min}$ and $\tilde{\psi}_{j,max}$	$-\pi/6\ rad$ and $\pi/6\ rad$
$\tilde{a}_{j,min}$ and $\tilde{a}_{j,max}$	$-5\ m/s^2$ and $3\ m/s^2$
$l_{1,s}$ and $l_{2,s}$	10000 and 1
α	0.1
β	5
$g_{3,s}$ for car-following	0.0001
g_1, g_2, and g_4	1, 10, and 0.1
$q_{3,m+N}$ for car-following	0.03
q_1, q_2, and q_4	5, 50, and 0.5

8.1 Scenario I: Uncongested Mandatory Lane-changing

To evaluate the performance of the optimized control model, a numerical simulation environment is constructed, which features a 180 meters long section of a two-lane road with an outer/right lane merging from 126 meters to 146 meters, as illustrated in **FIG. 8-1**. The inner lane, with a width of 3.6 meters, has a curvature corresponding to a radius of $360/\pi$ meters. Similarly, the outer lane has a width of 3.6 meters, but with a slightly larger curvature radius of $360/\pi + 3.6$ meters, to account for its position. The section designated for lane-changing section from 30 meters to 146 meters shown as magenta dashed line. A speed limit of $20\ m/s$ is imposed on this road. The leading vehicle is initialized with a pace deviation of $-1/180\ s/m$, no lateral and no angular deviation, corresponding to an initial speed of $18\ m/s$ (note that the leading vehicle's speed is capped at $18\ m/s$ to avert any potential gap in headway). Additionally, three more vehicles are integrated into the simulation initialized as uncongested traffic condition. Vehicle 2 begins with a headway deviation of -0.1 seconds, no pace deviation, a lateral deviation of 3.6 meters (positioned in the outer lane), and no angular deviation. Vehicle 3 is set with a headway deviation of 0.1 seconds, while its other states are at equilibrium. Lastly, Vehicle 4 starts with a headway deviation of 0.3 seconds, a pace deviation of $-1/200\ s/m$ (equivalent

to a starting speed of 16.5 m/s), a lateral deviation of 3.6 meters (positioned in the outer lane), and no angular deviation.

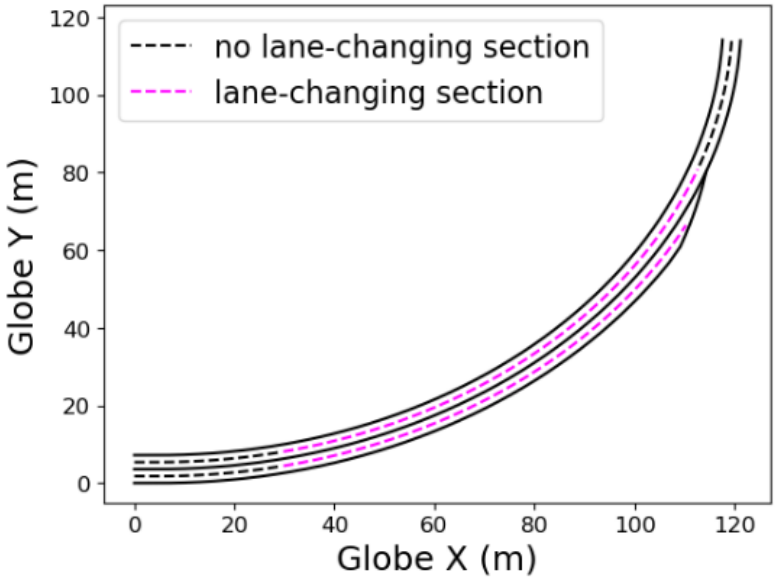

FIG. 8-1. Illustration of Road Trajectory.

To illustrate the performance of the algorithm, Fig. 6 plots the positions of the vehicles within a time frame starting from 0 seconds to 8 seconds, with a 1 second resolution. Due to the spatial formulation of the algorithm, only vehicle 1 is depicted in **FIG. 8-2** (a)-(b). This is because vehicle 2 enters the section at approximately 1.1 seconds. A closer analysis of **FIG. 8-2** (d)-(h) for vehicle 2 and vehicle 4, reveals that as vehicles enter the lane-changing section, they begin to execute lane-changing decisions. This merging process is initially unhurried, particularly when vehicles are at a considerable distance from the merging endpoint for convenience consideration. As they approach the merging endpoint, however, they accelerate to ensure safety. This transition in speed is modulated by our dynamic weighting strategy, which adeptly balances convenience and safety concerns.

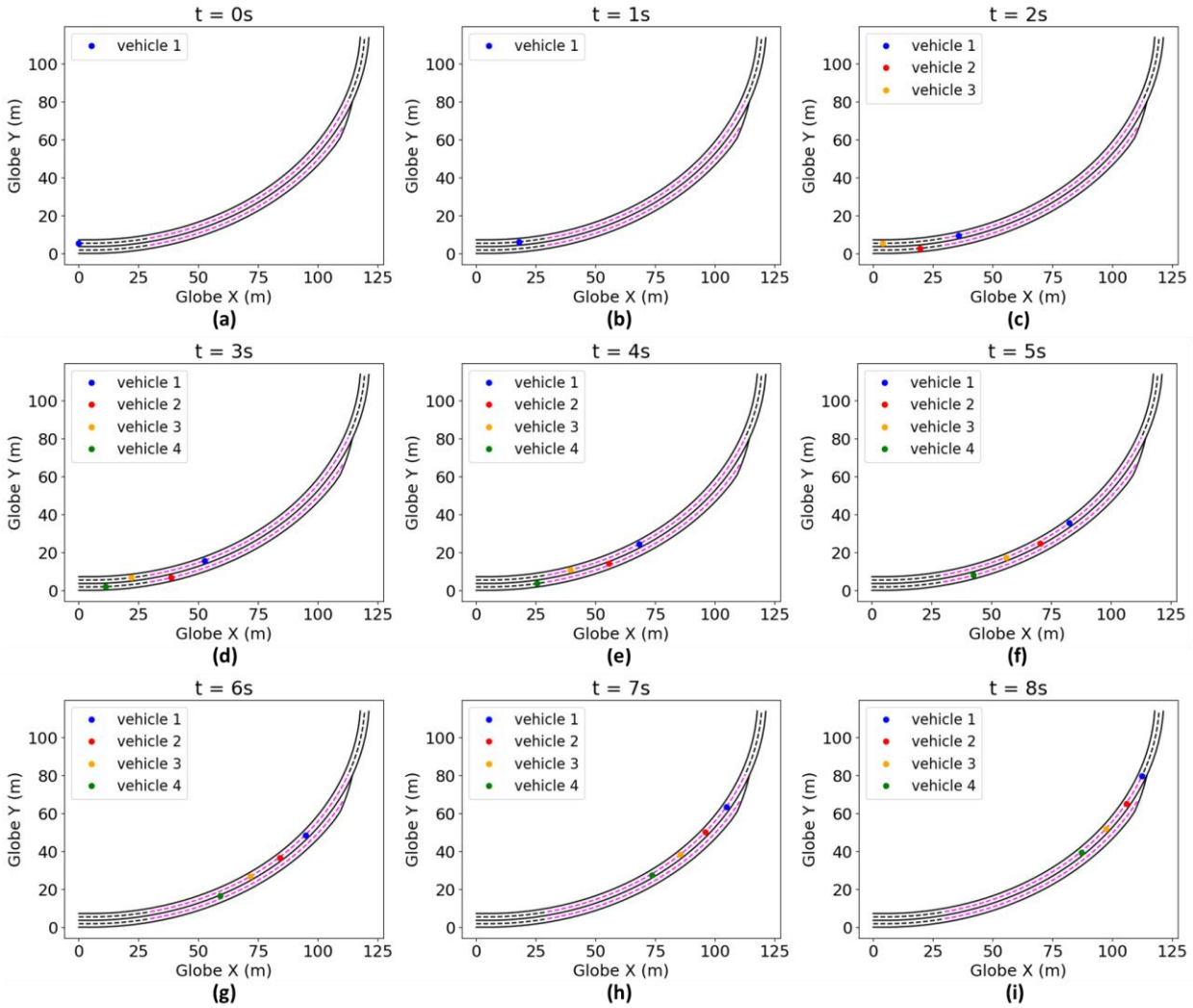

FIG. 8-2. CAVs Trajectories Snapshots.

FIG. 8-3 further illustrates the evolution of various system state parameters of the proposed planning algorithm. This graph elucidates the dynamics of headway deviation, pace deviation, lateral deviation, and angular deviation. To provide a more comprehensive comprehension of the car-following and lane-changing approach, we transposed the system states from the spatial domain to the temporal domain, and additionally transformed pace into speed for ease of understanding. Notably, vehicle 1, as the role of the lead vehicle, does not have any headway deviation. Vehicle 2, on the other hand, starts off with an initial headway deviation of -0.1 seconds, implying that the gap between vehicle 1 and vehicle 2 is initially greater than anticipated. In pursuit of attaining headway equilibrium, vehicle 2 engages in an initial acceleration phase, swiftly succeeded by a deceleration phase. Furthermore, vehicle 2 initiates a

lane-change maneuver as it enters the designated lane-changing section at 3 seconds, which leads to lateral deviation and angular deviation change. Vehicle 3 initiates with a headway deviation of 0.1 seconds, indicating that the spacing between vehicle 2 and vehicle 3 is initially tighter than expected. To achieve headway equilibrium, vehicle 3 starts with a small deceleration phase, taking into account that the speed of vehicle 2 surpasses its own. This measured deceleration is a strategic maneuver aimed at creating an optimal distance between the vehicles with the lowest cost. Vehicle 4 starts with a headway of 0.3 seconds, which is relatively close for car-following, resulting in a sharp deceleration to attain an equilibrium distance. Furthermore, vehicle 4 starts a lane-change maneuver as it navigates into the lane-changing section at 5.5 seconds, which induces fluctuations in lateral deviation and angular deviation. Moreover, the infinitesimal oscillations after vehicles achieve equilibrium also demonstrate the robustness of our proposed trajectory planning algorithm, which is achieved through the integration of road geometric characteristics and the dynamics of the leading and following vehicles.

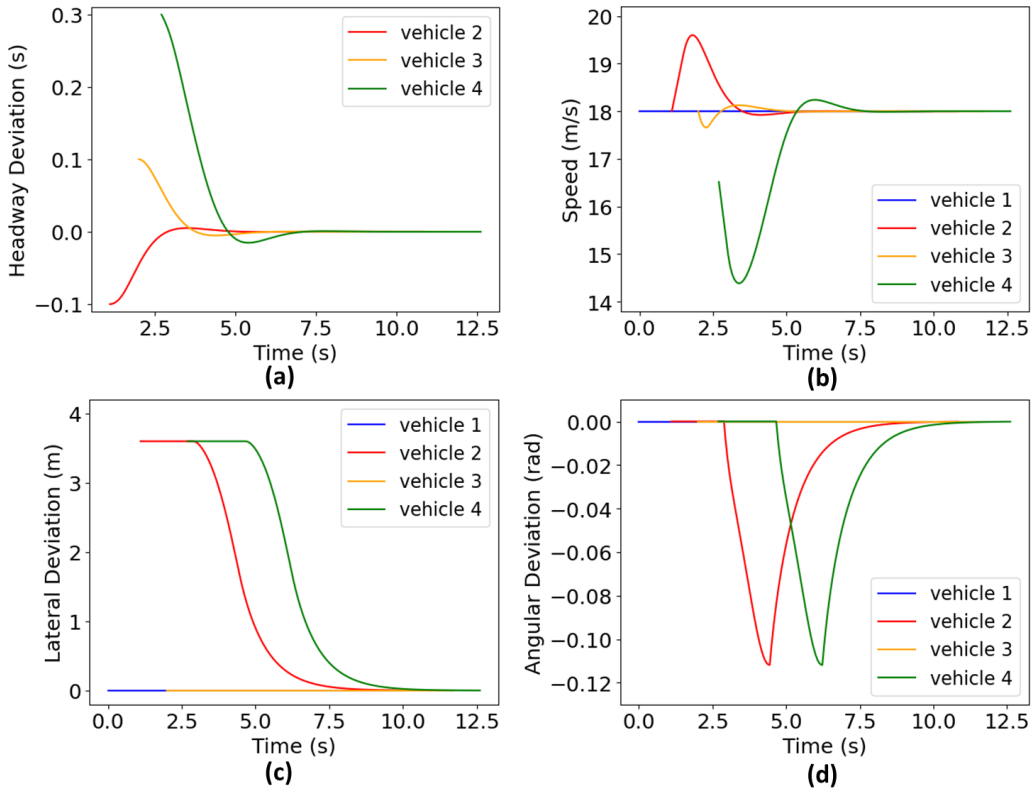

FIG. 8-3. CAVs States Results in Time Domain: (a) Headway Deviation; (b) Speed Deviation; (c) Lateral Deviation; (d) Angular Deviation.

8.2 Scenario II: Uncongested Mandatory Lane-changing with Obstacle Presence

The preceding section's results demonstrate the efficacy and stability of the proposed CAV car-following and lane-changing methodology without any obstacles. To make a more rigorous test, we executed a simulation experiment factoring in the presence of an obstacle. In this simulation, we introduced a 20 meters long obstacle situated between 60 meters and 80 meters, as depicted in **FIG. 8-4**. Within the bounds of this obstacle, the lane width is constricted to $\tilde{r}_{j,s}^{L} = 0.5$ meters. This inclusion of an obstacle is to test how the proposed CAV car-following and lane-changing strategy navigates to constrained environments, thus providing a more comprehensive evaluation of its real-world applicability.

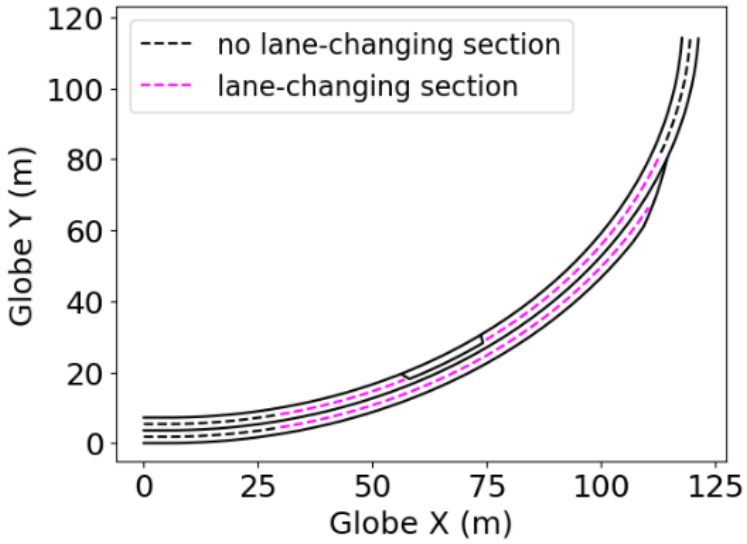

FIG. 8-4. Illustration of Road Trajectory with Obstacle Presence.

The leading vehicle is initialized with a pace deviation of $-1/180$ s/m, no lateral and no angular deviation, corresponding to an initial speed of 18 m/s (note that the leading vehicle's speed is capped at 18 m/s to avert any potential gap in headway). Both vehicle 2 and vehicle 3 begins with a headway deviation of 0.2 seconds except vehicle 2 has a lateral deviation of 3.6 meters. Vehicle 4 starts with a headway deviation of 0 seconds, a pace deviation of $-1/200\ s/m$ (equivalent to a starting speed of $16.5\ m/s$), a lateral deviation of 3.6 meters, and no angular deviation. To provide a visual

representation of the algorithm's performance, **FIG. 8-5** delineates the positions of the vehicles within a time frame of the first 8 seconds. As can be observed in **FIG. 8-5** (d)-(g), vehicles 1 and 3, occupying the inner lane, exhibit quick a response to the obstacle. They use flexible and intelligent control decisions that facilitate smooth avoidance of obstacles, ultimately guiding them to maintain a central path. This central positioning is a strategic maneuver aimed at avoiding any possible collisions with the obstacle while navigating through the obstacle section. Conversely, as seen in **FIG. 8-5** (e)-(h), vehicles 2 and 4, which are situated in the outer lane, choose a different strategy. They decide against fully merging before entering the obstacle section, demonstrating the algorithm's adaptability in facilitating diverse vehicular responses based on positioning and surrounding conditions.

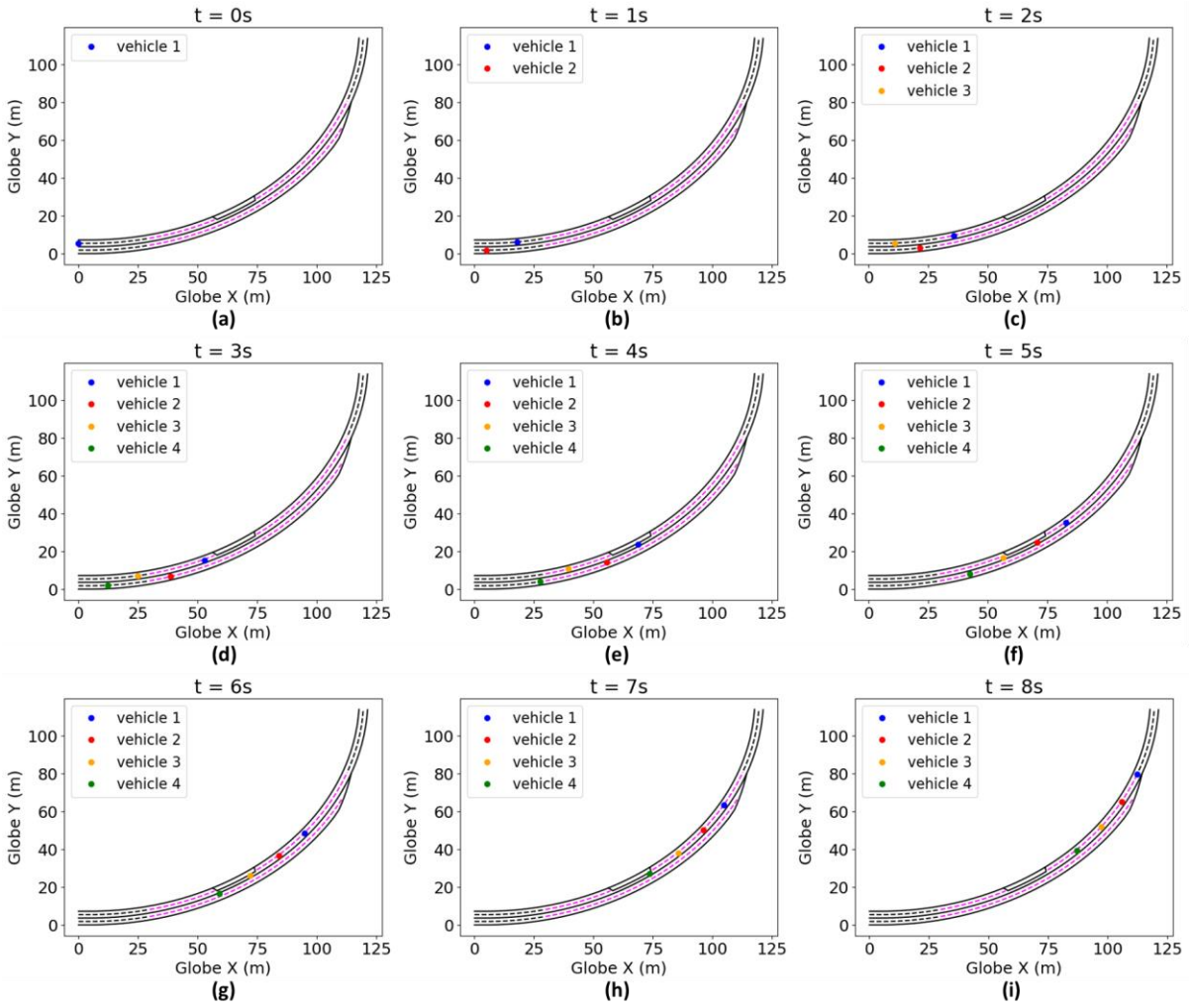

FIG. 8-5. CAVs Trajectories Snapshots with Obstacle Presence.

To validate the convergence properties of the algorithm, **FIG. 8-6** presents details of system state parameters through the performance of the proposed planning algorithm. By analyzing the trends and interactions exhibited in the intricate dynamics of headway deviation, speed deviation, lateral deviation, and angular deviation, we can garner valuable insights into how the planning algorithm operates and adapts in response to the obstacle. Because vehicles 2, 3 have an initial headway of 0.2 seconds, they both engage in an initial deceleration phase to achieve headway equilibrium which lead to a deceleration phase of vehicle 4 as can be seen in **FIG. 8-6** (b). **FIG. 8-6** (c)-(d) offer a detailed illustration of the dynamic responses of vehicles when confronted with an obstacle. Vehicles 1 and 3, as the inner lane vehicles, demonstrate an agile reaction to the obstacle. They successfully execute smooth maneuvers to evade the obstacle while ensuring that they maintain a safe clearance from it. In contrast, vehicles 2 and 4, as the outer lane vehicles, adopt a more conservative approach by moderating their merging speed which can be seen from 5.5 seconds and 7 seconds. This contrasting behavior highlights the algorithm's capacity to enable vehicles to employ different strategies based on their positions and surrounding environments, ensuring both effective navigation and safety. **FIG. 8-6** (e) illustrates the trajectories of 4 vehicles in the spatial domain where the obstacle is present. As evident in the diagram, each vehicle consistently maintains a safe distance from the obstacle.

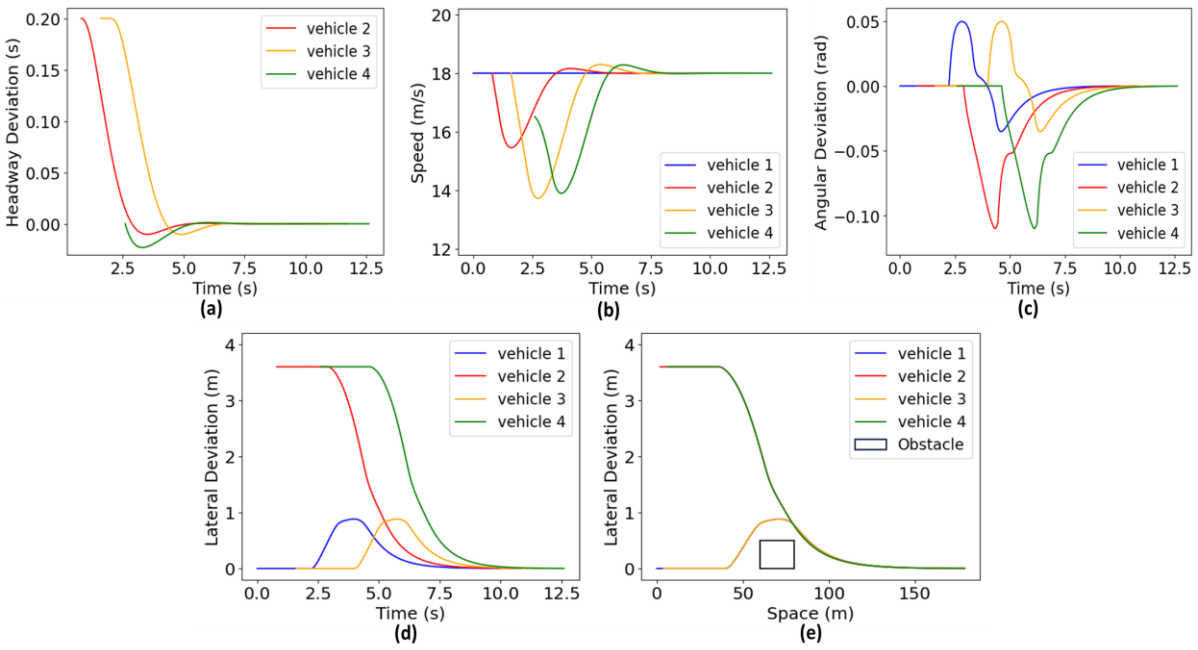

FIG. 8-6. CAVs States Results with Obstacle Presence: (a) Headway Deviation; (b) Speed Deviation; (c) Angular Deviation; (d) Lateral Deviation; (d) Lateral Deviation in Space Domain.

8.3 Scenario III: Congested Mandatory Lane-changing

To validate the effectiveness of the proposed lane-changing planning algorithm under congested environment, an extreme case is given using the same simulation environment as scenario 1. The leading vehicle is initialized with a pace deviation of $-1/180\ s/m$, no lateral and no angular deviation. Vehicle 2 begins with a headway deviation of 0.7 seconds, no pace deviation, a lateral deviation of 3.6 meters (positioned in the outer lane), and no angular deviation. Vehicle 3 is set with a headway deviation of 0.7 seconds, while its other states are at equilibrium. Lastly, Vehicle 4 starts with a headway deviation of $-0.2\ seconds$, a lateral deviation of 3.6 meters (positioned in the outer lane), and no pace and angular deviation.

FIG. 8-7 illustrates that Vehicles 1, 2, and 3 start in close proximity to each other. Initially, Vehicles 2 and 4 do not exhibit any lane-changing behavior as they enter the lane-changing section. The lane-changing behavior is influenced by the spacing between each vehicle and its neighboring vehicles, which can be clearly observed in **FIG. 8-7** (e)-(h). More specifically, lane-changing is only initiated when the distance between both the leading and following vehicles is adequately large, preventing risky mandatory lane-changing maneuvers when vehicles are too closely spaced.

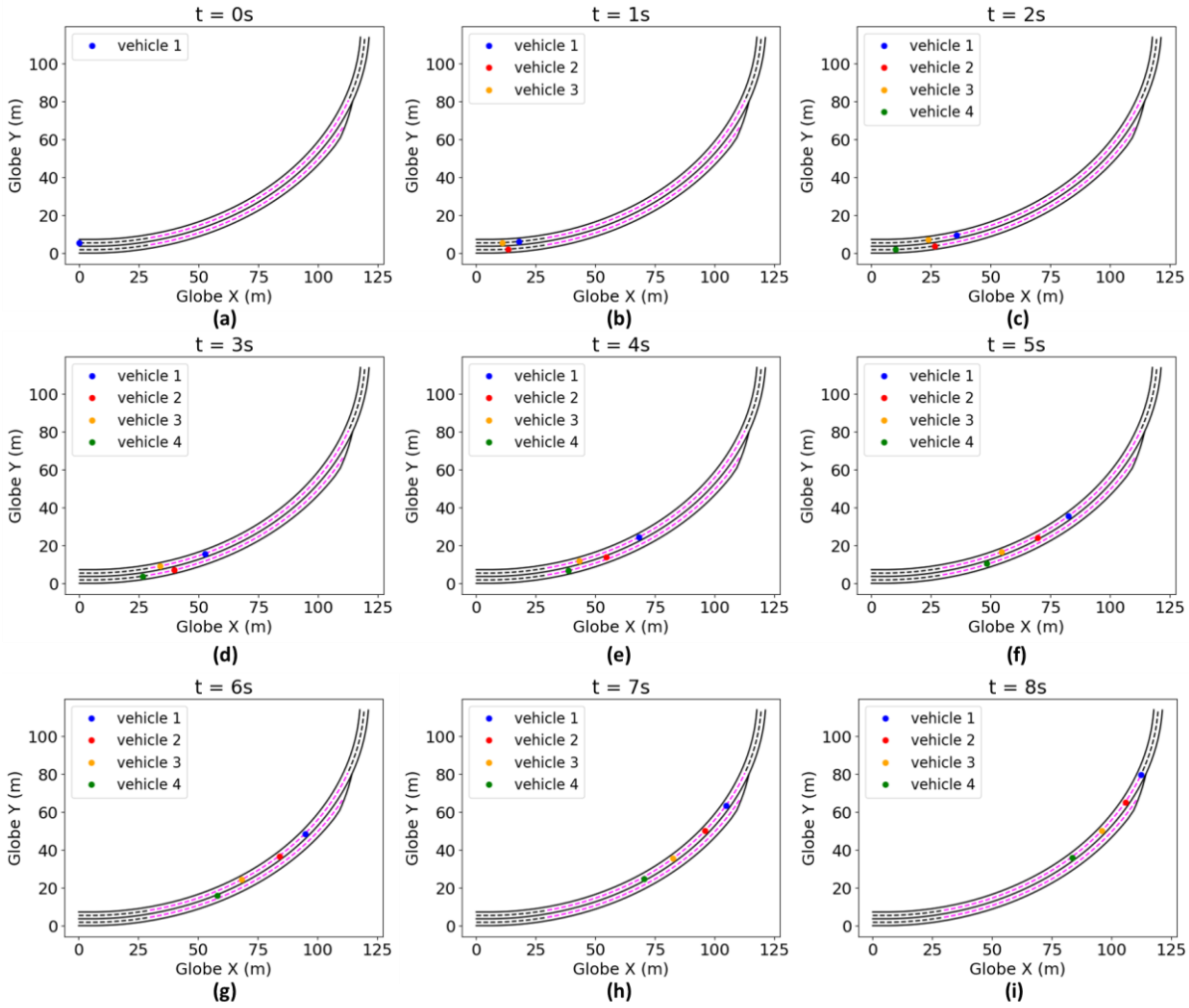

FIG. 8-7. CAVs Trajectories Snapshots.

FIG. 8-8 shows the details of system state parameters. Vehicles 2 and 3 commence their journey with an initial headway deviation of 0.7 seconds, suggesting that the spatial gap between Vehicles 1, 2, and 3 is initially significantly smaller than expected. Both vehicles 2 and 3 engage in an initial deceleration phase in pursuit of attaining headway equilibrium, which explains that the headway between vehicles 2 and 3 stays unchanged until vehicle 3's speed falls below that of vehicle 2. Meanwhile, vehicle 4 starts with a deceleration phase even though the initial headway deviation of vehicle 4 is smaller than anticipated, taking into account the fast deceleration of vehicle 3. Further, both the lateral and angular deviations maintain the same trends as observed in Scenario 1.

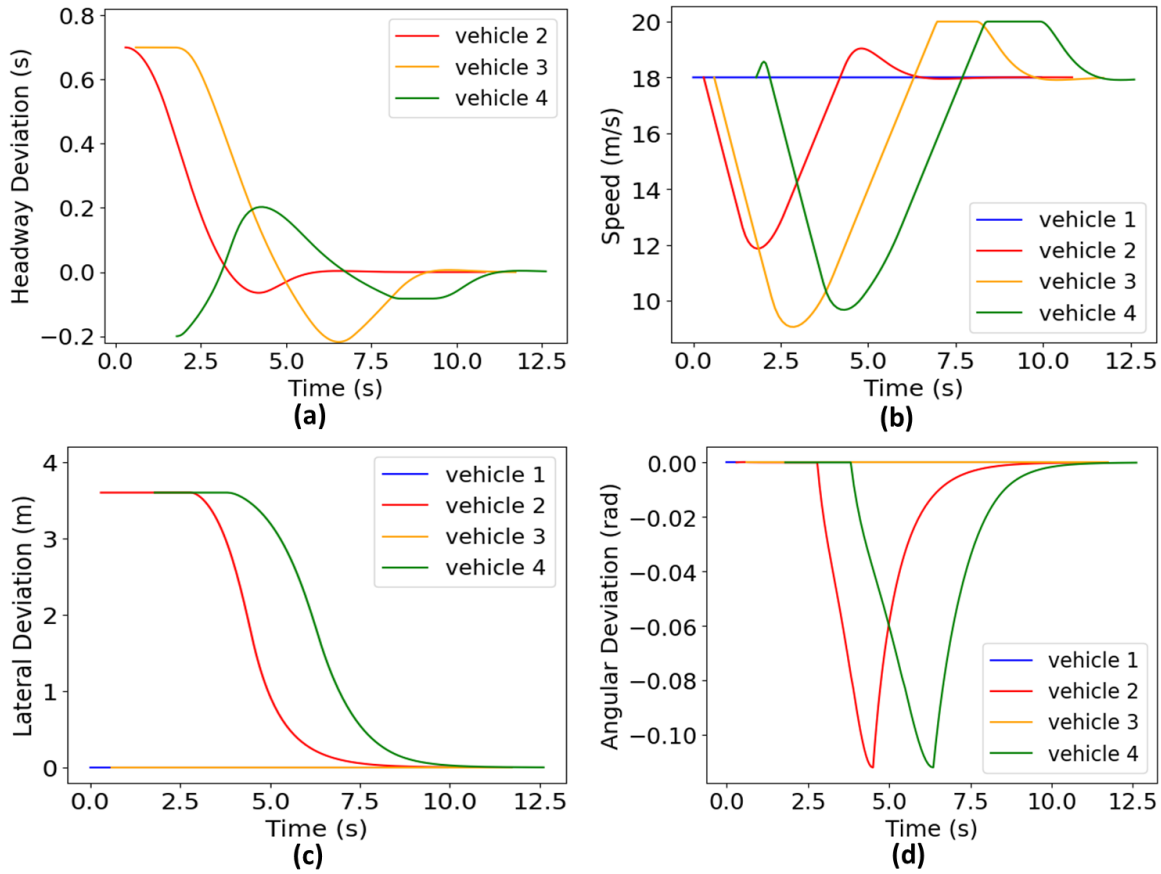

FIG. 8-8. CAVs States Results: (a) Headway Deviation; (b) Speed Deviation; (c) Lateral Deviation; (d) Angular Deviation.

To further evaluate the collision risks, we further customize a surrogate safety measure, Inverse TTC, which is the reciprocal of Time to Collision (TTC). TTC is a common safety metric used in traffic and vehicle safety studies. It represents the time that remains until a collision with an object or vehicle will occur if both continue at their current speed and along their current path. The customized Inverse TTC is given as

$$Inverse\ TTC_{j,t} = \begin{cases} \dfrac{v_{j,t} - v_{j-1,t}}{s_{j-1,t} - s_{j,t}}, & if\ \left|r_{j,t} - r_{j-1,t}\right| \le 0.5\ and\ v_{j,t} > v_{j-1,t} \\ 0, & otherwise \end{cases}, \tag{46}$$

where $v_{j,t}$ and $v_{j-1,t}$ are the speeds of vehicle j and vehicle $j-1$ at time t.

FIG. 8-9 illustrates the Inverse TTC for vehicles 2, 3, and 4. It's worth noting that the Inverse TTC is

computed based on the sequence of the vehicles in each lane prior to their entry into the lane-changing section, as well as their sequence in the virtual lane following this entry. The red, orange, and green dots displayed in **FIG. 8-9** serve as markers indicating the moments when Vehicles 2, 3, and 4 commence their transition into the lane-changing section. The performance of our algorithm, as evaluated through the Inverse TTC metric, has demonstrated commendable results. The highest Inverse TTC values are $0.02\ 1/s$, $0.10\ 1/s$, and $0.08\ 1/s$ for vehicles 2, 3, and 4, which are sufficiently small. The results show that the algorithm effectively ensures safer vehicle transitions during lane-changing, providing an ample margin for collision avoidance. The algorithm manages to keep the Inverse TTC values within a reasonable range, thereby signifying a guaranteed safety. The consistent efficiency of the algorithm in maintaining desirable Inverse TTC values serves as a strong testament to its robustness and reliability in managing vehicle sequences during lane-changing procedures, thus substantially enhancing road safety.

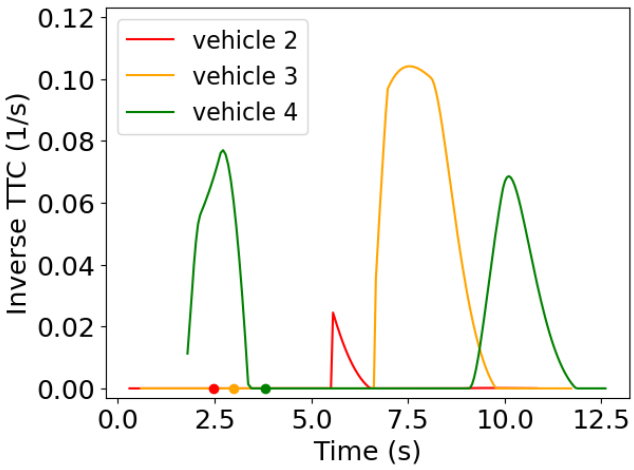

FIG. 8-9. Inverse TTC.

9. CONCLUSION

This paper proposes 2D spatially formulated trajectory optimization, car-following, and lane-changing methods of CAVs. Vehicular trajectory optimization, car-following and lane-changing strategy play an essential role in ensuring vehicles' travel safety and efficiency. Traditional trajectory planning algorithms and methods are primarily formulated in the time domain by detecting the road information with a limited range and optimizing the trajectory myopically, which cannot competently handle the spatially varying road geometric change, obstacles, and traffic regulations. To remedy that, this paper provided a new angle to plan long-term trajectories in a spatial domain with the help of infrastructure. Specifically, this paper systematically formulates trajectory optimization in a spatial domain and on a curvilinear coordinate, enabling our method to flexibly formulate spatially varying complex road geometries, traffic regulations, and road obstacles whose information can be obtained through V2I communication. Traditional car-following strategies are primarily formulated in the 1D time domain, which only focus on vehicle longitudinal control and ignore all lateral force. This paper provided a new angle to combine 1D car-following algorithm with our vehicle trajectory optimization algorithm in the spatial domain, which forms a new car-following algorithm that fills the gap of no 2D CAV car-following in the literature. For rigor, the controllability of the state space was mathematically proved by using both the linear test and the small-angle approximation. Considering vehicle travel efficiency and trajectory smoothness while satisfying the collision avoidance and vehicle kinematics constraint, a multi-objective MPC was constructed, which can be efficiently solved by the state of arts optimization methods.

To demonstrate the usefulness and wide applications of our proposed trajectory planning optimization algorithm, car-following, and lane-changing algorithm, multi-scenarios numerical simulations were conducted for our proposed trajectory planning optimization algorithm

including: (i) a continuous curvy road segment with the constant speed limit, (ii) a curved road with two different desired driving behaviors, (iii) a curved road with an obstacle, and (iv) a continuous curvy road segment with speed limit change. Moreover, (i) a continuous curvy road segment without an obstacle and (ii) a curved road with an obstacle were designed to test our car-following algorithm. Finally, (i) uncongested two-lane curved highway mandatory lane-changing, testing the algorithm's handling of the lane-merging process in curved highway conditions, (ii) uncongested two-lane curved highway mandatory lane-changing with the introduction of an obstacle, testing the algorithm's ability to adapt and respond to unexpected disruptions in the driving environment, and (iii) congested two-lane curved highway mandatory lane-changing, testing the algorithm's effectiveness in reducing collision risks during lane-changing and car-following. The simulation results show that our algorithm adeptly finds optimal control inputs to regain system equilibrium, factoring in vehicle states and upcoming obstacles. By managing vehicle sequences and gap acceptance, it enables safer, smoother lane changes, reducing potential collisions. It demonstrates resilience in handling traffic variations, including fluctuating speeds and unexpected obstacles, proving its versatility and robustness. Unlike strategies using only time-domain approaches, our method handles spatial disturbances better, leveraging precise road geometric data and leading vehicle dynamics.

Nevertheless, some directions can be extended on the current framework in the future. For example, future research could enhance realism by incorporating factors like communication delays, vehicle dynamics uncertainties, and measurement errors. Possible improvements include using a comprehensive control model, like a four-wheel vehicle model, integrating dynamics uncertainties for robustness, and examining more complex scenarios like CAV control at intersections.

REFERENCE

Acharya, S., & Mekker, M. (2022). Importance of the reputation of data manager in the acceptance of connected vehicles. *Communications in Transportation Research*, *2*. https://doi.org/10.1016/j.commtr.2022.100053

Adeli, H., & Ghosh-Dastidar, S. (2004). Mesoscopic-Wavelet Freeway Work Zone Flow and Congestion Feature Extraction Model. Journal of Transportation Engineering, 130(1), 94–103. https://doi.org/10.1061/ASCE0733-947X2004130:194

Akpakwu, G. A., Silva, B. J., Hancke, G. P., & Abu-Mahfouz, A. M. (2017). A survey on 5G networks for the Internet of Things: Communication technologies and challenges. IEEE Access, 6, 3619–3647.

Ali, Y., Bliemer, M. C. J., Zheng, Z., & Haque, M. M. (2020). Comparing the usefulness of real-time driving aids in a connected environment during mandatory and discretionary lane-changing manoeuvres. Transportation Research Part C: Emerging Technologies, 121. https://doi.org/10.1016/j.trc.2020.102871

Ali, Y., Zheng, Z., Haque, M. M., & Wang, M. (2019). A game theory-based approach for modelling mandatory lane-changing behaviour in a connected environment. Transportation Research Part C: Emerging Technologies, 106, 220–242. https://doi.org/10.1016/j.trc.2019.07.011

Attia, R., Orjuela, R., & Basset, M. (2014). Combined longitudinal and lateral control for automated vehicle guidance. Vehicle System Dynamics, 52(2), 261–279.

Balal, E., Cheu, R. L., & Sarkodie-Gyan, T. (2016). A binary decision model for discretionary lane changing move based on fuzzy inference system. Transportation Research Part C: Emerging Technologies, 67, 47–61. https://doi.org/10.1016/j.trc.2016.02.009

Barfoot, T. D., & Clark, C. M. (2004). Motion planning for formations of mobile robots. Robotics and Autonomous Systems, 46(2), 65–78.

Berglund, T., Brodnik, A., Jonsson, H., Staffanson, M., & Soderkvist, I. (2009). Planning smooth and obstacle-avoiding B-spline paths for autonomous mining vehicles. IEEE Transactions on Automation Science and Engineering, 7(1), 167–172.

Bohren, J., Foote, T., Keller, J., Kushleyev, A., Lee, D., Stewart, A., Vernaza, P., Derenick, J., Spletzer, J., & Satterfield, B. (2008). Little ben: The ben franklin racing team's entry in the 2007 DARPA urban challenge. Journal of Field Robotics, 25(9), 598–614.

Cao, D., Wu, J., Wu, J., Kulcsár, B., & Qu, X. (2021). A platoon regulation algorithm to improve the traffic performance of highway work zones. Computer-Aided Civil and Infrastructure Engineering.

Carlson, R. C., Papamichail, I., Papageorgiou, M., & Messmer, A. (2010a). Optimal mainstream traffic flow control of large-scale motorway networks. Transportation Research Part C: Emerging Technologies, 18(2), 193–212.

Carlson, R. C., Papamichail, I., Papageorgiou, M., & Messmer, A. (2010b). Optimal motorway

traffic flow control involving variable speed limits and ramp metering. Transportation Science, 44(2), 238–253.

Chen, B. C., Luan, B. C., & Lee, K. (2014). Design of lane keeping system using adaptive model predictive control. IEEE International Conference on Automation Science and Engineering (CASE), 922–926.

Chen, B. M., Lin, Z., & Shamash, Y. (2004). Linear Systems Theory. https://doi.org/10.1007/978-1-4612-2046-6

Chen, D., & Ahn, S. (2018). Capacity-drop at extended bottlenecks: Merge, diverge, and weave. Transportation Research Part B: Methodological, 108, 1–20. https://doi.org/10.1016/j.trb.2017.12.006

Chen, D., Ahn, S., & Hegyi, A. (2014). Variable speed limit control for steady and oscillatory queues at fixed freeway bottlenecks. Transportation Research Part B: Methodological, 70, 340–358.

Chen, J., Zhao, P., Mei, T., & Liang, H. (2013). Lane change path planning based on piecewise bezier curve for autonomous vehicle. Proceedings of 2013 IEEE International Conference on Vehicular Electronics and Safety, IEEE, 17–22.

Chen, N., Wang, M., Alkim, T., & van Arem, B. (2018). A robust longitudinal control strategy of platoons under model uncertainties and time delays. Journal of Advanced Transportation, 2018.

Chen, T., Wang, M., Gong, S., Zhou, Y., & Ran, B. (2021). Connected and automated vehicle distributed control for on-ramp merging scenario: A virtual rotation approach. Transportation Research Part C: Emerging Technologies, 133. https://doi.org/10.1016/j.trc.2021.103451

Chu, K., Lee, M., & Sunwoo, M. (2012). Local path planning for off-road autonomous driving with avoidance of static obstacles. IEEE Transactions on Intelligent Transportation Systems, 13(4), 1599–1616. https://doi.org/10.1109/TITS.2012.2198214

Cremean, L. B., Foote, T. B., Gillula, J. H., Hines, G. H., Kogan, D., Kriechbaum, K. L., Lamb, J. C., Leibs, J., Lindzey, L., Rasmussen, C. E., & others. (2006). Alice: An information-rich autonomous vehicle for high-speed desert navigation. Journal of Field Robotics, 23(9), 777–810.

Ding, F., Ran, B., Cheng, Y., Li, S., Zhang, Z., Zhou, Y., Tan, H., Dong, S., Chen, T., Li, X., & others. (2019). Systems and methods for driving intelligence allocation between vehicles and highways. Google Patents.

Dunbar, W. B., & Caveney, D. S. (2011). Distributed receding horizon control of vehicle platoons: Stability and string stability. IEEE Transactions on Automatic Control, 57(3), 620–633.

Elbanhawi, M., & Simic, M. (2014). Sampling-based robot motion planning: A review. Ieee Access, 2, 56–77.

Fraichard, T., & Scheuer, A. (2004). From Reeds and Shepp's to continuous-curvature paths. IEEE Transactions on Robotics, 20(6), 1025–1035.

Frazzoli, E., Dahleh, M. A., & Feron, E. (2002). Real-time motion planning for agile autonomous vehicles. Journal of Guidance, Control, and Dynamics, 25(1), 116–129.

Gong, S., Shen, J., & Du, L. (2016). Constrained optimization and distributed computation based car following control of a connected and autonomous vehicle platoon. Transportation Research Part B: Methodological, 94, 314–334. https://doi.org/10.1016/j.trb.2016.09.016

Gritschneder, F., Graichen, K., & Dietmayer, K. (2018). Fast Trajectory Planning for Automated Vehicles using Gradient-based Nonlinear Model Predictive Control. 2018 IEEE/RSJ International Conference on Intelligent Robots and Systems (IROS), 7369–7374.

Guo, H., Shen, C., Zhang, H., Chen, H., & Jia, R. (2018). Simultaneous trajectory planning and tracking using an MPC method for cyber-physical systems: A case study of obstacle avoidance for an intelligent vehicle. IEEE Transactions on Industrial Informatics, 14(9), 4273–4283.

Gutjahr, B., Gröll, L., & Werling, M. (2016). Lateral vehicle trajectory optimization using constrained linear time-varying MPC. IEEE Transactions on Intelligent Transportation Systems, 18(6), 1586–1595.

Han, Y., & Ahn, S. (2018). Stochastic modeling of breakdown at freeway merge bottleneck and traffic control method using connected automated vehicle. Transportation Research Part B: Methodological, 107, 146–166.

Heilmeier, A., Wischnewski, A., Hermansdorfer, L., Betz, J., Lienkamp, M., & Lohmann, B. (2019). Minimum curvature trajectory planning and control for an autonomous race car. Vehicle System Dynamics, 1–31.

Héry, E., Masi, S., Xu, P., & Bonnifait, P. (2017). Map-based curvilinear coordinates for autonomous vehicles. 2017 IEEE 20th International Conference on Intelligent Transportation Systems (ITSC), 1–7.

Hoogendoorn, S., Hoogendoorn, R., Wang, M., & Daamen, W. (2012). Modeling driver, driver support, and cooperative systems with dynamic optimal control. Transportation Research Record, 2316(1), 20–30.

Hooshdar, S., & Adeli, H. (2004). Toward Intelligent Variable Message Signs in Freeway Work Zones: Neural Network Model. Journal of Transportation Engineering, 130(1), 83–93. https://doi.org/10.1061/ASCE0733-947X2004130:183

International, S. A. E. (2014). Automated Driving Levels of Driving Automation are Defined in New SAE International Standard J3016. SAE International Troy, MI.

Jiang, X., & Adeli, H. (2003). Freeway Work Zone Traffic Delay and Cost Optimization Model. Journal of Transportation Engineering, 129(3), 230–241. https://doi.org/10.1061/ASCE0733-947X2003129:3230

Jiang, X., & Adeli, H. (2004a). Clustering-neural network models for freeway work zone capacity estimation. International Journal of Neural Systems, 14(03), 147–163.

Jiang, X., & Adeli, H. (2004b). Object-oriented model for freeway work zone capacity and queue delay estimation. Computer-Aided Civil and Infrastructure Engineering, 19(2), 144–156. https://doi.org/10.1111/j.1467-8667.2004.00344.x

Kala, R., & Warwick, K. (2013). Multi-level planning for semi-autonomous vehicles in traffic scenarios based on separation maximization. Journal of Intelligent & Robotic Systems, 72(3–4), 559–590.

Karaman, S., Walter, M. R., Perez, A., Frazzoli, E., & Teller, S. (2011). Anytime motion planning using the RRT. 2011 IEEE International Conference on Robotics and Automation, 1478–1483.

Karim, A., & Adeli, H. (2003). Fast Automatic Incident Detection on Urban and Rural Freeways Using Wavelet Energy Algorithm. Journal of Transportation Engineering, 129(1), 57–68. https://doi.org/10.1061/ASCE0733-947X2003129:157

Karim, A., & Adeli, H. (2003). CBR Model for Freeway Work Zone Traffic Management. Journal of Transportation Engineering, 129(2), 134–145. https://doi.org/10.1061/ASCE0733-947X2003129:2134

Kesting, A., Treiber, M., & Helbing, D. (2007). General lane-changing model MOBIL for car-following models. Transportation Research Record, 1999, 86–94. https://doi.org/10.3141/1999-10

Khalifa, A., Kermorgant, O., Dominguez, S., & Martinet, P. (2019). An Observer-based Longitudinal Control of Car-like Vehicles Platoon Navigating in an Urban Environment. 2019 IEEE 58th Conference on Decision and Control (CDC), 5735–5741.

Kianfar, R., Falcone, P., & Fredriksson, J. (2015). A control matching model predictive control approach to string stable vehicle platooning. Control Engineering Practice, 45, 163–173.

Kogan, D., & Murray, R. (2006). Optimization-based navigation for the DARPA Grand Challenge. Conference on Decision and Control (CDC).

Kuwata, Y., Teo, J., Fiore, G., Karaman, S., Frazzoli, E., & How, J. P. (2009). Real-time motion planning with applications to autonomous urban driving. IEEE Transactions on Control Systems Technology, 17(5), 1105–1118.

Labakhua, L., Nunes, U., Rodrigues, R., & Leite, F. S. (2008). Smooth trajectory planning for fully automated passengers vehicles: Spline and clothoid based methods and its simulation. In Informatics in control automation and robotics (pp. 169–182). Springer.

Laval, J. A., & Leclercq, L. (2010). A mechanism to describe the formation and propagation of stop-and-go waves in congested freeway traffic. Philosophical Transactions of the Royal Society A: Mathematical, Physical and Engineering Sciences, 368(1928), 4519–4541.

Leclercq, L., Knoop, V. L., Marczak, F., & Hoogendoorn, S. P. (2016). Capacity drops at

merges: New analytical investigations. Transportation Research Part C: Emerging Technologies, 62, 171–181. https://doi.org/10.1016/j.trc.2015.06.025

Leclercq, L., Laval, J. A., & Chiabaut, N. (2011). Capacity drops at merges: An endogenous model. Procedia - Social and Behavioral Sciences, 17, 12–26. https://doi.org/10.1016/j.sbspro.2011.04.505

Li, H., Zhang, J., Zhang, Z., & Huang, Z. (2021). Active lane management for intelligent connected vehicles in weaving areas of urban expressway. Journal of Intelligent and Connected Vehicles, 4(2), 52–67. https://doi.org/10.1108/JICV-08-2020-0009

Liu, Y., Zhou, Y., Su, S., Xun, J., & Tang, T. (2021). An analytical optimal control approach for virtually coupled high-speed trains with local and string stability. Transportation Research Part C: Emerging Technologies, 125, 102886.

Lu, C., & Liu, C. (2021). Ecological control strategy for cooperative autonomous vehicle in mixed traffic considering linear stability. Journal of Intelligent and Connected Vehicles, 4(3), 115–124. https://doi.org/10.1108/JICV-08-2021-0012

Lu, X.-Y., Tan, H.-S., Shladover, S. E., & Hedrick, J. K. (2004). Automated vehicle merging maneuver implementation for AHS. Vehicle System Dynamics, 41(2), 85–107.

Luo, Y., Xiang, Y., Cao, K., & Li, K. (2016). A dynamic automated lane change maneuver based on vehicle-to-vehicle communication. Transportation Research Part C: Emerging Technologies, 62, 87–102. https://doi.org/10.1016/j.trc.2015.11.011

Mahmoud, M. S. (2018). Advanced Control Design with Application to Electromechanical Systems. Butterworth-Heinemann.

Manzinger, S., Pek, C., & Althoff, M. (2020). Using reachable sets for trajectory planning of automated vehicles. IEEE Transactions on Intelligent Vehicles.

Mensing, F., Trigui, R., & Bideaux, E. (2011). Vehicle trajectory optimization for application in ECO-driving. 2011 IEEE Vehicle Power and Propulsion Conference, 1–6.

Morbidi, F., Colaneri, P., & Stanger, T. (2013). Decentralized optimal control of a car platoon with guaranteed string stability. 2013 European Control Conference (ECC), 3494–3499.

Nie, J., Zhang, J., Ding, W., Wan, X., Chen, X., & Ran, B. (2016). Decentralized Cooperative Lane-Changing Decision-Making for Connected Autonomous Vehicles∗. IEEE Access, 4, 9413–9420. https://doi.org/10.1109/ACCESS.2017.2649567

Nolte, M., Rose, M., Stolte, T., & Maurer, M. (2017). Model predictive control based trajectory generation for autonomous vehicles—an architectural approach. 2017 IEEE Intelligent Vehicles Symposium (IV), 798–805.

Pan, T. L., Lam, W. H. K., Sumalee, A., & Zhong, R. X. (2016). Modeling the impacts of mandatory and discretionary lane-changing maneuvers. Transportation Research Part C: Emerging Technologies, 68, 403–424. https://doi.org/10.1016/j.trc.2016.05.002

Papadimitriou, I., & Tomizuka, M. (2003). Fast Lane Changing Computations using Polynomials. Proceedings of the 2003 American Control Conference, 1(IEEE), 48–53.

Pérez, J., Godoy, J., Villagrá, J., & Onieva, E. (2013). Trajectory generator for autonomous vehicles in urban environments. 2013 IEEE International Conference on Robotics and Automation, 409–414.

Pilutti, T., & Ulsoy, A. G. (1999). Identification of driver state for lane keeping tasks. IEEE Transactions on Systems, Man, and Cybernetics-Part A: Systems and Humans, 20, 486–502.

Plessen, M. G. (2017). Trajectory planning of automated vehicles in tube-like road segments. 2017 IEEE 20th International Conference on Intelligent Transportation Systems (ITSC), 1–6.

Pohl, J., Birk, W., & Westervall, L. (2007). A driver-distraction-based lane-keeping assistance system. Proceedings of the Institution of Mechanical Engineers. Part I: Journal of Systems and Control Engineering, 221(4), 541–552. https://doi.org/10.1243/09596518JSCE218

Qu, X., Yu, Y., Zhou, M., Lin, C. T., & Wang, X. (2020a). Jointly dampening traffic oscillations and improving energy consumption with electric, connected and automated vehicles: A reinforcement learning based approach. Applied Energy, 257. https://doi.org/10.1016/j.apenergy.2019.114030

Qu, X., Yu, Y., Zhou, M., Lin, C.-T., & Wang, X. (2020b). Jointly dampening traffic oscillations and improving energy consumption with electric, connected and automated vehicles: a reinforcement learning based approach. Applied Energy, 257, 114030.

Raksincharoensak, P., Mizushima, T., & Nagai, M. (2008). Direct yaw moment control system based on driver behaviour recognition. Vehicle System Dynamics, 46(SUPPL.1), 911–921. https://doi.org/10.1080/00423110802037156

Ran, B., Cheng, Y., Chen, T., Zhou, Y., Zhang, Z., Li, X., Li, S., Dong, S., & Shi, K. (2020). System and methods for partially instrumented connected automated vehicle highway systems. Google Patents.

Reeds, J., & Shepp, L. (1990). Optimal paths for a car that goes both forwards and backwards. Pacific Journal of Mathematics, 145(2), 367–393.

Ren, D. B., Zhang, J. Y., Zhang, J. M., & Cui, S. M. (2011). Trajectory planning and yaw rate tracking control for lane changing of intelligent vehicle on curved road. Science China Technological Sciences, 54(3), 630–642. https://doi.org/10.1007/s11431-010-4227-6

Risack, R., Moehler, N., & Enkelmann, W. (2000). Video-based lane keeping assistant. IEEE Intelligent Vehicles Symposium, Proceedings, Mi, 356–361. https://doi.org/10.1109/ivs.2000.898369

Shi, H., Zhou, Y., Wu, K., Wang, X., Lin, Y., & Ran, B. (2020). Partially Connected Automated Vehicle Cooperative Control Strategy with a Deep Reinforcement Learning Approach. ArXiv Preprint ArXiv:2012.01841.

Shi, K., Wu, Y., Shi, H., Zhou, Y., & Ran, B. (2022). An integrated car-following and lane changing vehicle trajectory prediction algorithm based on a deep neural network. Physica A: Statistical Mechanics and Its Applications, 599.

https://doi.org/10.1016/j.physa.2022.127303

Shi, X., Wang, Z., Li, X., & Pei, M. (2021). The effect of ride experience on changing opinions toward autonomous vehicle safety. Communications in Transportation Research, 1. https://doi.org/10.1016/j.commtr.2021.100003

Sun, D., & Elefteriadou, L. (2010). Research and implementation of lane-changing model based on driver behavior. Transportation Research Record, 2161, 1–10. https://doi.org/10.3141/2161-01

Sun, K., Gong, S., Zhou, Y., Chen, Z., Zhao, X., & Wu, X. (2023). A Cooperative Smooth Lane Change Control Strategy for Multi-Connected and Autonomous Vehicle with Traffic Flow Efficiency. https://ssrn.com/abstract=4243830

Tajalli, M., Niroumand, R., & Hajbabaie, A. (2022). Distributed cooperative trajectory and lane changing optimization of connected automated vehicles: Freeway segments with lane drop. Transportation Research Part C: Emerging Technologies, 143. https://doi.org/10.1016/j.trc.2022.103761

Treiber, M., & Kesting, A. (2009). Modeling lane-changing decisions with MOBIL.

Wang, H., Lai, J., Zhang, X., Zhou, Y., Li, S., & Hu, J. (2022). Make space to change lane: A cooperative adaptive cruise control lane change controller. Transportation Research Part C: Emerging Technologies, 143. https://doi.org/10.1016/j.trc.2022.103847

Wang, J., Gong, S., Peeta, S., & Lu, L. (2019). A real-time deployable model predictive control-based cooperative platooning approach for connected and autonomous vehicles. Transportation Research Part B: Methodological, 128, 271–301.

Wang, M., Daamen, W., Hoogendoorn, S. P., & van Arem, B. (2014a). Rolling horizon control framework for driver assistance systems. Part I: Mathematical formulation and non-cooperative systems. Transportation Research Part C: Emerging Technologies, 40, 271–289.

Wang, M., Daamen, W., Hoogendoorn, S. P., & van Arem, B. (2014b). Rolling horizon control framework for driver assistance systems. Part II: Cooperative sensing and cooperative control. Transportation Research Part C: Emerging Technologies, 40, 290–311.

Wang, M., Daamen, W., Hoogendoorn, S. P., & van Arem, B. (2015). Cooperative car-following control: Distributed algorithm and impact on moving jam features. IEEE Transactions on Intelligent Transportation Systems, 17(5), 1459–1471.

Wang, M., Hoogendoorn, S. P., Daamen, W., van Arem, B., & Happee, R. (2015). Game theoretic approach for predictive lane-changing and car-following control. Transportation Research Part C: Emerging Technologies, 58, 73–92. https://doi.org/10.1016/j.trc.2015.07.009

Wang, P., Chan, C.-Y., & de La Fortelle, A. (2018). A reinforcement learning based approach for automated lane change maneuvers. 2018 IEEE Intelligent Vehicles Symposium (IV), IEEE, 1379–1384.

Wang, Y., Hou, S., & Wang, X. (2020). Reinforcement learning-based bird-view automated vehicle control to avoid crossing traffic. Computer-Aided Civil and Infrastructure Engineering.

Wang, Z., Zhao, X., Xu, Z., Li, X., & Qu, X. (2020). Modeling and field experiments on autonomous vehicle lane changing with surrounding human-driven vehicles. Computer-Aided Civil and Infrastructure Engineering.

Wei, S., Zou, Y., Zhang, X., Zhang, T., & Li, X. (2019). An Integrated Longitudinal and Lateral Vehicle Following Control System with Radar and Vehicle-to-Vehicle Communication. IEEE Transactions on Vehicular Technology, 68(2), 1116–1127. https://doi.org/10.1109/TVT.2018.2890418

Werling, M., Ziegler, J., Kammel, S., & Thrun, S. (2010). Optimal trajectory generation for dynamic street scenarios in a frenet frame. 2010 IEEE International Conference on Robotics and Automation, 987–993.

Wu, J., Ah, S., Zhou, Y., Liu, P., & Qu, X. (2020). The Cooperative Sorting Strategy for Connected and Automated Vehicle Platoons. ArXiv Preprint ArXiv:2003.06481.

Wu, J., Kulcsár, B., Ahn, S., & Qu, X. (2020). Emergency vehicle lane pre-clearing: From microscopic cooperation to routing decision making. Transportation Research Part B: Methodological, 141, 223–239.

Xu, X., Zuo, L., Li, X., Qian, L., Ren, J., & Sun, Z. (2020). A Reinforcement Learning Approach to Autonomous Decision Making of Intelligent Vehicles on Highways. IEEE Transactions on Systems, Man, and Cybernetics: Systems, 50(10), 3884–3897. https://doi.org/10.1109/TSMC.2018.2870983

Yang, D., Zheng, S., Wen, C., Jin, P. J., & Ran, B. (2018). A dynamic lane-changing trajectory planning model for automated vehicles. Transportation Research Part C: Emerging Technologies, 95, 228–247. https://doi.org/10.1016/j.trc.2018.06.007

Yuan, K., Knoop, V. L., & Hoogendoorn, S. P. (2017). A microscopic investigation into the capacity drop: Impacts of longitudinal behavior on the queue discharge rate. Transportation Science, 51(3), 852–862. https://doi.org/10.1287/trsc.2017.0745

Zeng, Y., Wang, M., & Rajan, R. T. (2022). Decentralized coordination for truck platooning. Computer-Aided Civil and Infrastructure Engineering, 37(15), 1997–2015. https://doi.org/10.1111/mice.12899

Zhang, L., & Orosz, G. (2016). Motif-based design for connected vehicle systems in presence of heterogeneous connectivity structures and time delays. IEEE Transactions on Intelligent Transportation Systems, 17(6), 1638–1651.

Zhang, L., & Orosz, G. (2017). Consensus and disturbance attenuation in multi-agent chains with nonlinear control and time delays. International Journal of Robust and Nonlinear Control, 27(5), 781–803.

Zhang, S., Deng, W., Zhao, Q., Sun, H., & Litkouhi, B. (2012). An intelligent driver model with trajectory planning. 2012 15th International IEEE Conference on Intelligent

Transportation Systems, IEEE, 876–881.

Zhang, Y., Bai, Y., Wang, M., & Hu, J. (2020). Cooperative Adaptive Cruise Control With Robustness Against Communication Delay: An Approach in the Space Domain. IEEE Transactions on Intelligent Transportation Systems.

Zhang, Y., Bai, Y., Wang, M., & Hu, J. (2021). Cooperative Adaptive Cruise Control with Robustness against Communication Delay: An Approach in the Space Domain. IEEE Transactions on Intelligent Transportation Systems, 22(9), 5496–5507. https://doi.org/10.1109/TITS.2020.2987746

Zhao, J., Knoop, V. L., & Wang, M. (2020). Two-dimensional vehicular movement modelling at intersections based on optimal control. Transportation Research Part B: Methodological, 138, 1–22. https://doi.org/10.1016/j.trb.2020.04.001

Zheng, Y., Li, S. E., Li, K., Borrelli, F., & Hedrick, J. K. (2016). Distributed model predictive control for heterogeneous vehicle platoons under unidirectional topologies. IEEE Transactions on Control Systems Technology, 25(3), 899–910.

Zheng, Y., Ran, B., Qu, X., Zhang, J., & Lin, Y. (2020). Cooperative Lane Changing Strategies to Improve Traffic Operation and Safety Nearby Freeway Off-Ramps in a Connected and Automated Vehicles Environment. IEEE Transactions on Intelligent Transportation Systems, 21(11), 4605–4614. https://doi.org/10.1109/TITS.2019.2942050

Zheng, Z. (2014). Recent developments and research needs in modeling lane changing. Transportation Research Part B: Methodological, 60, 16–32. https://doi.org/10.1016/j.trb.2013.11.009

Zheng, Z., Ahn, S., Chen, D., & Laval, J. (2013). The effects of lane-changing on the immediate follower: Anticipation, relaxation, and change in driver characteristics. Transportation Research Part C: Emerging Technologies, 26, 367–379. https://doi.org/10.1016/j.trc.2012.10.007

Zheng, Z., Ahn, S., & Monsere, C. M. (2010). Impact of traffic oscillations on freeway crash occurrences. Accident Analysis and Prevention, 42(2), 626–636. https://doi.org/10.1016/j.aap.2009.10.009

Zhou, Y., & Ahn, S. (2019). Robust local and string stability for a decentralized car following control strategy for connected automated vehicles. Transportation Research Part B: Methodological, 125, 175–196. https://doi.org/10.1016/j.trb.2019.05.003

Zhou, Y., Ahn, S., Chitturi, M., & Noyce, D. A. (2017a). Rolling horizon stochastic optimal control strategy for ACC and CACC under uncertainty. Transportation Research Part C: Emerging Technologies, 83, 61–76. https://doi.org/10.1016/j.trc.2017.07.011

Zhou, Y., Ahn, S., Chitturi, M., & Noyce, D. A. (2017b). Rolling horizon stochastic optimal control strategy for ACC and CACC under uncertainty. Transportation Research Part C: Emerging Technologies, 83, 61–76.

Zhou, Y., Ahn, S., Chitturi, M., & Noyce, D. A. (2017c). Rolling horizon stochastic optimal control strategy for ACC and CACC under uncertainty. Transportation Research Part C:

Emerging Technologies, 83, 61–76. https://doi.org/10.1016/j.trc.2017.07.011

Zhou, Y., Ahn, S., Wang, M., & Hoogendoorn, S. (2020). Stabilizing mixed vehicular platoons with connected automated vehicles: An H-infinity approach. Transportation Research Part B: Methodological, 132, 152–170.

Zhou, Y., Wang, M., & Ahn, S. (2019a). Distributed model predictive control approach for cooperative car-following with guaranteed local and string stability. Transportation Research Part B: Methodological, 128, 69–86.

Zhou, Y., Wang, M., & Ahn, S. (2019b). Distributed model predictive control approach for cooperative car-following with guaranteed local and string stability. Transportation Research Part B: Methodological, 128, 69–86. https://doi.org/10.1016/j.trb.2019.07.001